4

RESULTS AND DISCUSSION

The results pertaining to the study, "**Eco-friendly Chitosan Schiff bases for Enhanced Corrosion Resistance of Mild Steel in Acid Medium and Calcium Carbonate Scale Inhibition"** are being presented and discussed in the backdrop of the objectives set forth. The study attempted to synthesize eco-friendly biodegradable Chitosan Schiff bases and to analyze their inhibitive properties on mild steel in 1M HCl medium. The efficacy of the Chitosan Schiff bases as anti-scalants for calcium carbonate, antiscalant tests were carried out using EDTA titration.

The results are being discussed in the following phased manner:

Phase I: Synthesis and Characterization of Chitosan Schiff bases

Phase II: Evaluation of Chitosan Schiff bases as corrosion inhibitors- Using Weight loss methods and electrochemical measurements

Phase III: Adsorption monitoring technique, Adsorption properties of the inhibitors and protective layer characterization of the metal surface using surface analytical techniques

Phase IV: Theoretical investigation of Chitosan Schiff bases, Mechanism and supporting evidences for adsorption of Chitosan Schiff bases on metal surface

Phase V: Evaluation of Chitosan Schiff bases as anti-scalants for calcium carbonate scale

Phase I

4.1 Synthesis of Chitosan Schiff bases

A set of four Chitosan Schiff bases was synthesized using selected aldehydes by following the procedure mentioned earlier in materials and methods. The schematic representation of the synthesis procedure is shown in Figure 6 and the photographic images of Chitosan and its synthesized Schiff bases are shown in Figure 7. The abbreviations and chemical structure of the Chitosan Schiff bases are given in the Table 6. The photographic images depict that all the four Chitosan Schiff bases appear to be yellow fibrous flakes. The change of colour of the Chitosan to yellow itself suggests the preliminary indication for the formation of Schiff bases in the Chitosan matrix.

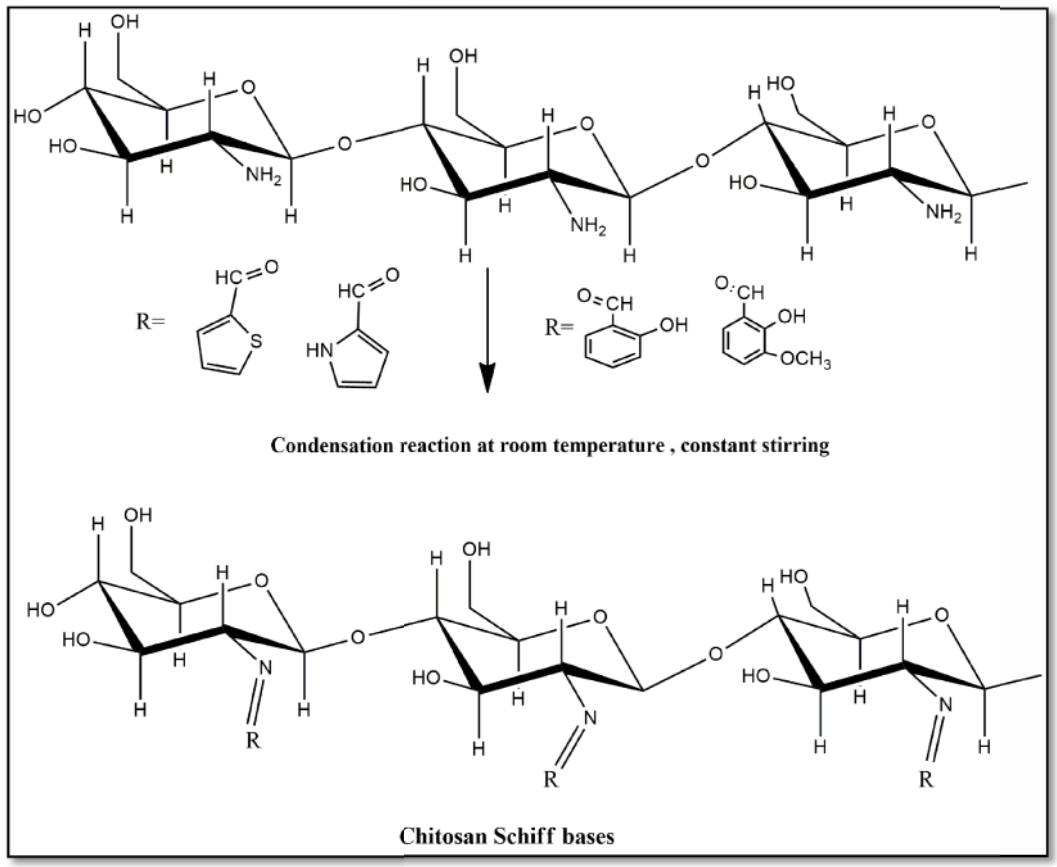

Figure 6 – Schematic representation for the synthesis of Chitosan Schiff base

Table 6 – Chemical Structure and abbrevations of the Chitosan Schiff bases

Synthesized compounds	Abbrevation	Chemical Structure
Chitosan salicylaldehyde Schiff base	**ChSSB**	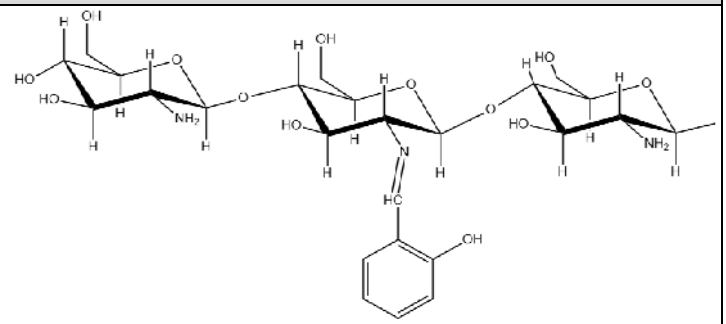
Chitosan Vanillin Schiff base	**ChVSB**	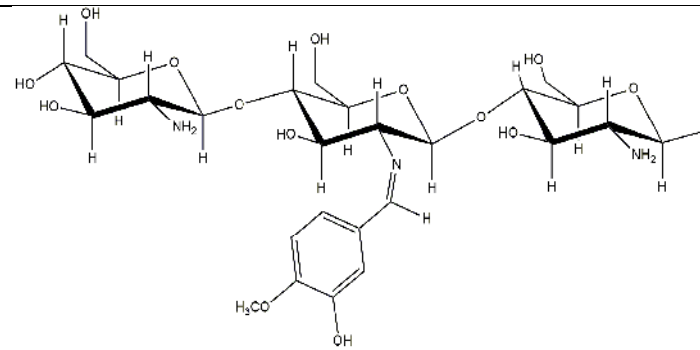
Chitosan Thiophene 2-carboxaldehyde Schiff base	**ChTSB**	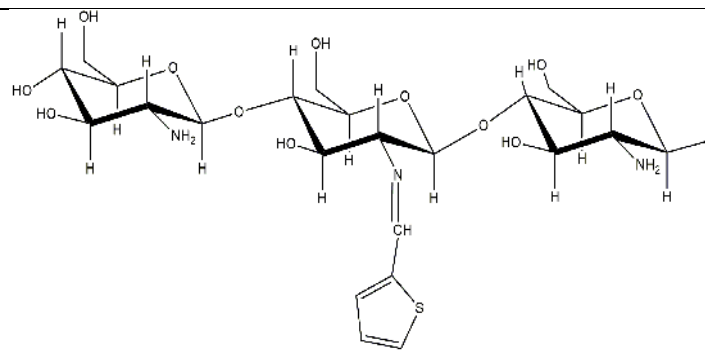
Chitosan pyrrole 2-carboxalbehyde Schiff base	**ChPSB**	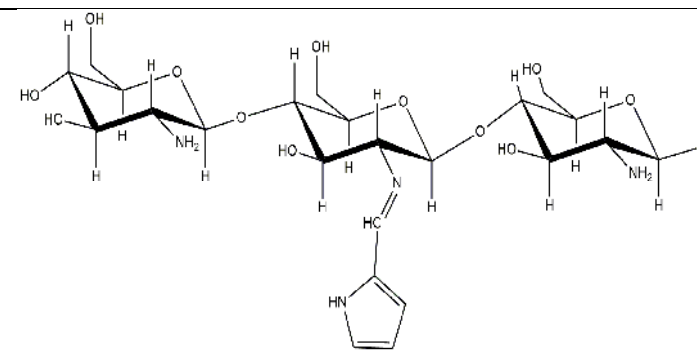

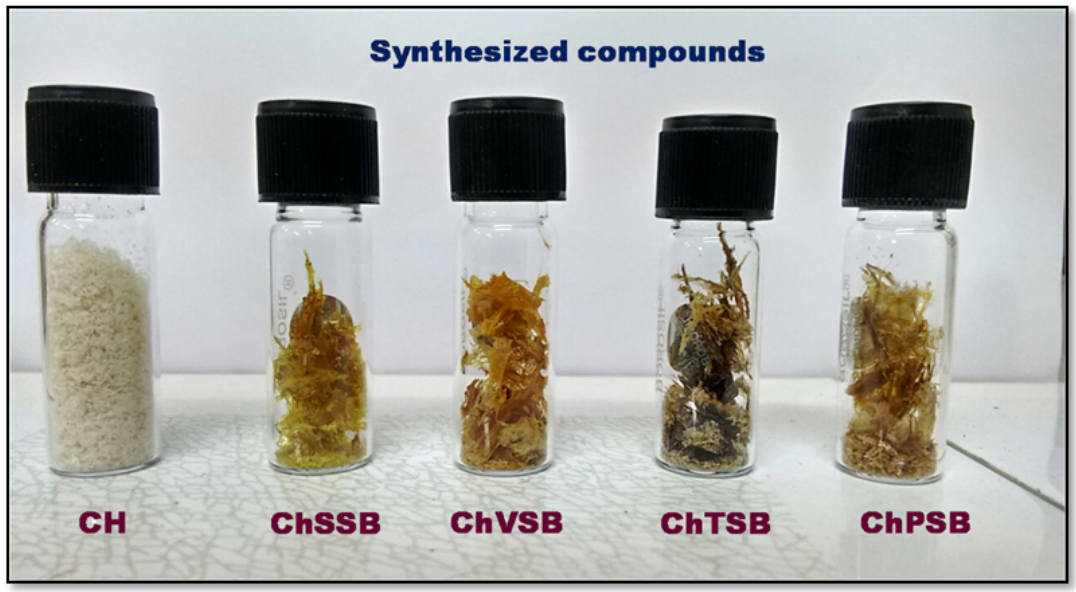

Figure 7 - Photographic images of the synthesized Chitosan Schiff bases

4.1.1. Evaluation of degree of deacetylation of Chitosan, Yield and solubility of Chitosan Schiff bases:

The degree of deacetylation (DD) of the commercial Chitosan used in the synthesis was evaluated by using the equation (2). Due to the low solubility of Chitosan in most of the solvents, it is difficult to obtain NMR data so as to find the degree of deacetylation and degree of substitution. Hence elemental analysis was used to overcome the difficulty. From the values of C/N ratio of Chitosan obtained from elemental analysis the degree of deactylation was calculated. The value of DD of Chitosan was found to be 76.99%.

Yield of the Chitosan Schiff bases was calculated using the equation (1) given in Materials and method and the same are presented in Table 7. As 100% substitution is not possible with Chitosan matrix due to its DD%, still a favorable yield has been obtained using the standardized procedure. The solubility of Chitosan Schiff bases in different solvents was determined and the results are presented in Table 7. Chitosan polymer backbone is hydrophobic in nature. Chitosan is soluble only in aqueous acidic solution due to its conversion into an ionic structure. The insolubility of Chitosan in aqueous and organic solvents has been attributed to extensive intramolecular and intermolecular hydrogen bonding between the chain and sheets respectively in crystalline structure. The solubility depends on the substituent used for the modification of Chitosan. The synthesized Chitosan Schiff bases were insoluble in water due to the extent of substitution contributing to an increase in hydrophobicity (**Kumar and Koh, 2012**).

Table 7 – Yield, Physical property and Solubility of Chitosan Schiff bases in different solvents

Sample	Colour	Yield (%)	Solvents					
			Water	Methanol	DMSO	DMF	Acetone	Acetic acid
ChSSB	Yellow	64	-	-	+/-	+/-	-	+
ChVSB	Yellow	62	-	-	+/-	+/-	-	+
ChTSB	Brownish yellow	58	-	-	+/-	+/-	-	+
ChPSB	Light yellow	59	-	-	+/-	+/-	-	+

(* - indicates the insoluble nature, +/- indicates the swelling nature, + indicates the soluble nature in the appropriate solvents)

4.1.2 Characterization of Chitosan Schiff bases:

4.1.2.1 Elemental Analysis:

To confirm the formation of Schiff base on the Chitosan matrix, the elemental composition of Chitosan and synthesized Chitosan Schiff bases were determined using CHNS analyzer (instrument Vario EL III CHNS serial number 11035060). The percentage composition of carbon, hydrogen, nitrogen and sulphur are being presented in Table 8.

Table 8 - Elemental analysis of Chitosan and Synthesized Chitosan Schiff bases

S.No	Sample Name	Element (%)				C/N ratio
		C	H	N	S	
1.	CH	39.71	7.48	7.16	-	5.548106
2.	ChSSB	52.02	8.25	6.04	-	8.618647
3.	ChVSB	40.33	9.13	5.83	-	6.916637
4.	ChPSB	39.81	8.25	6.97	-	5.709204
5.	ChTSB	38.47	8.01	5.96	1.10	6.452513
Degree of deactylation of Chitosan – 76.99%						

The results have been as expected for partial condensation substitution, implying that all NH_2 groups in Chitosan are not modified into its Schiff base derivatives completely. The C, H, N contents of Schiff base polymers increased after substitution compared to the “native” Chitosan. This indicates the substitution of aldehydes onto the Chitosan chain. The increase

in the C/N ratio after modification of Chitosan indicates the successful anchoring of aldehyde molecule into Chitosan chain through –HC=N linkage (**Anthony *et al.*, 2013a, Dos Santos *et al.*, 2005).** The presence of 'S' content in the Chitosan Thiophene carboxaldehyde derivative strongly confirms the substitution of thiophene moiety into the Chitosan. Thus, the elemental analysis strongly indicates the formation of Schiff bases onto the Chitosan backbone.

4.1.2.2 Ultraviolet Visible Spectroscopy:

When the polymer is subjected to some modification or change, by having the UV-Vis spectra of the base matrix and the modified sample, it can be analyzed for the change if any one of the cases is active to this range. The UV visible absorption spectra of Chitosan Schiff bases were recorded in the wavelength region of 200-600nm.

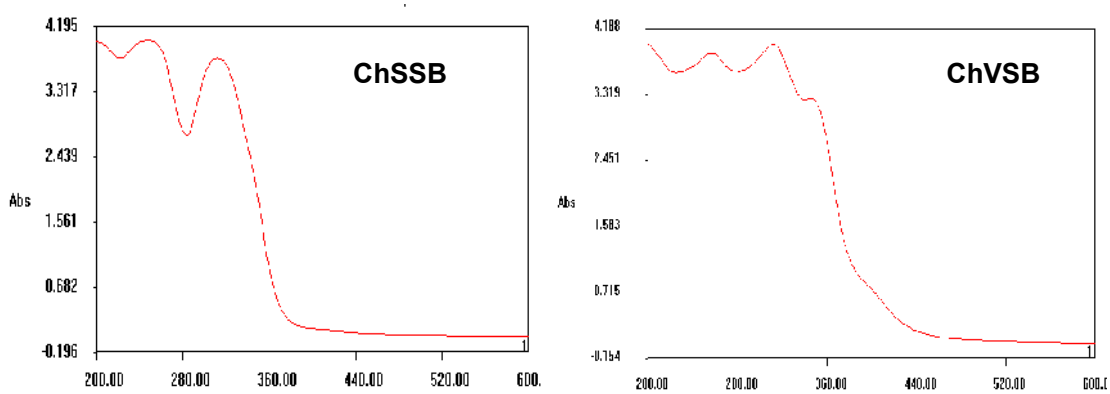

Figure 8 – UV spectra of ChSSB and ChVSB

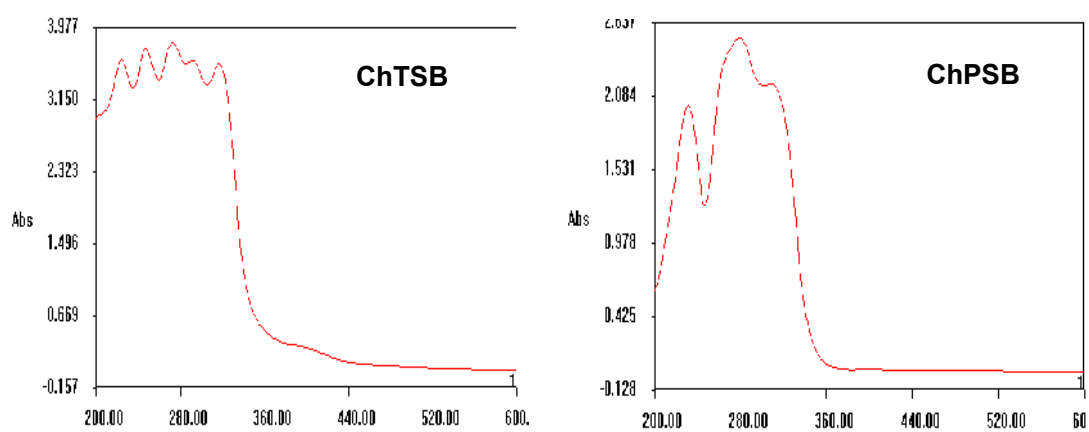

Figure 9 – UV spectra of ChTSB and ChPSB

Chitosan is transparent in the UV and visible region, so it is hard to characterize it by UV spectroscopy. Chitosan exhibited no characteristic peaks in the examined UV-visible range of the absorption spectrum. On the contrary, all the four modified Chitosan Schiff bases showed the characteristics peaks in the examined region. The electronic spectra of Chitosan Schiff bases show significant absorption bands below the region, 400 nm.

The UV spectral scans of the Chitosan Schiff bases are shown in Figure 8 & 9. The spectral data corresponds to the particular transition have been classified and briefed in Table 9. These transitions below 400 nm are generally assigned to π -π* and n- π* bonds.

Table 9 – UV spectral transitions corresponding to the Chitosan Schiff bases

S.No	Sample	Absorption bands (nm)	
		π -π*	n- π*
1.	CH	-	-
2.	ChSSB	222,248	283,312
3.	ChVSB	225,254	280,312,339
4.	ChTSB	224,235,248	272,284,305,316
5.	ChPSB	232,246	280,300

π -π* transition

π -π* transition as a high energy transition occurs due to the presence of unsaturated groups in the investigating compounds. In the Schiff base polymers, π -π* transition occurs due to the presence of the azomethine (-HC=N) groups and the C=C bonds present in the aromatic system of the aldehydes. Thus the absorption band in the region 220-250 nm is assigned to the π -π* transition of azomethine chromophore group.The presence of the broad peak in the region around 300-320 nm in the Schiff base polymers is an indication of presence of aromatic rings in their structure (**Chethan *et al*., 2013**). These transitions indicate the incorporation of aldehydeic groups into Chitosan backbone (**Koutroumanis *et al*., 2010, Kumar *et al.,* 2010, Kumar and Koh, 2012, Antony *et al*., 2013a, Antony *et al*., 2013b)**

n -π* transition

Generally, n-π* is a forbidden transition since it requires high energy for excitation and appears as a low intensity signal. This transition is very slightly affected by substitution or conjugation. Chitosan Schiff bases have undergone this type of transition in the region

270-280 nm. This absorption band can be attributed to the n-π* transition generated by the lone pair of electrons present on the O, N and S atoms in the incorporated aldehydes.

From the above results of UV spectra analysis, it is clear that the aldehydeic groups are successfully anchored onto the Chitosan matrix by the condensation reaction between Chitosan and aldehydes.

4.1.2.3 Fourier Transform Infra red spectroscopy:

FTIR spectra of Chitosan and Chitosan Schiff bases are analyzed to identify the functional groups present in them. The spectra and the spectral data are presented in Figures 10-13 and Tables 10-12 respectively.

Characteristic Vibrations of Chitosan:

The FTIR spectrum of Chitosan exhibit a sharp characteristic absorption peak for the presence of free –OH groups in the region 3751 and 3637 cm^{-1} and for the presence of $–NH_2$ groups in the region 3371.63, 3100.50 and 3012 cm^{-1}. The peak at 3459 cm^{-1} can be assigned to the axial vibration of O-H that may be superimposed with the N-H stretching band (**Antony *et al*., 2013a)**. Thus the peaks in the region 3000-3800 cm^{-1} can be reported to the vibrations of –OH and $–NH_2$ groups present in the Chitosan chain (**Kocak *et al*., 2012)**. The peaks at 2887.25 and 2828.49 cm^{-1} can be assigned to the axial stretching of aliphatic C-H groups in the Chitosan molecule (**Kumar *et al.,* 2010, Anan *et al*., 2011)**. Additional peak around 1425.34 cm^{-1} can be assigned to CH_2 scissoring vibration.

A cluster of peaks being observed in the region of 1510 - 1570 cm^{-1} that can be resolved into two peaks viz., 1574.65 and 1536.54 cm^{-1}. The former peak can be due to the amine groups ($-NH_2$) present in Chitosan matrix (**Feng and Xia, 2011**). The latter peak (1536.54 cm^{-1}) can be attributed to the amide II (**Costa- Junior *et al*., 2009**). Moreover, the strong peaks at 1656.29 and 1367.80 cm^{-1} can be attributed to the N-H bending vibrations of secondary amide linkage band (I) and amide III formed due to acetylation of Chitosan. These four peaks have been reported earlier as the characteristic peaks of Chitosan to prove that Chitosan possess both free amine group and acetylated amide group in the matrix (**DD=76.99%**)

The peak observed at 1739.53 cm^{-1} corresponds to the carbonyl stretching in the secondary amides. The band at 1010.88 cm^{-1} is due to the characteristic asymmetric C-O-C bridge stretching and the skeletal vibrations of C-O stretching. The bands of the ß(1–4) glycoside bridge observed at 1216.17 and 895.02 cm^{-1} are the characteristics of Chitosan saccharide structure (**Antony *et al*., 2013b)** .

Table 10 - FTIR spectral assignments of Chitosan

Frequency (cm^{-1})	Assignment
3751, 3637	O-H stretching
3371.63, 3100.50 and 3012	-NH_2 groups (symmetric and antisymmetric NH stretching)
3459	axial vibration of O-H superimposed with NH stretching
2887.25 and 2828.49, 1425.34	CH_2 symmetric and asymmetric stretching
1574.65	Amine –NH_2 group
1536.54	Amide II region
1656.29, 1367.80	Amide I, Amide III
1739.53	C=O stretching in secondary amide
1010.88	Ring, C-O-C bridge stretching
1216, 895	ß(1–4) glycoside bridge

Characteristic Vibrations of Chitosan Schiff bases - ChSSB:

From the FTIR spectrum of Chitosan Schiff base (ChSSB), presence of strong absorption band at 1646.12 cm^{-1} is being attributed to the C=N vibrations of azomethine group which is a characteristic band of imines (**Chethan *et al*., 2013, Dos Santos *et al*., 2005**).This characteristic band is not observed in the FTIR spectrum of Chitosan. Thus the presence of this band reveals the formation of Schiff base in the Chitosan matrix. Also, there is no peak observed in the region 1660-1730 cm^{-1} related to the free aldehyde group indicating that the salicylaldehyde has been successfully anchored onto the chitosan backbone to obtain chitosan salicylaldehyde Schiff base (ChSSB) (**Anan *et al*., 2011)**. The imine formation was also confirmed by the absorption peak at 1552.93 cm^{-1}, which is due to the C=C stretching in the aromatic ring of the aldehyde. In the Chitosan spectrum, this peak was part of the cluster being observed due to amine and amide group of Chitosan. The formation of strong peak at 1552.93 cm^{-1} clearly confirms the formation of Schiff base by the reaction of amine and active carbonyl group of the salicylaldehyde and also suggests the successful anchoring of aromatic system onto the Chitosan backbone (**Menaka and Subhashini, 2016a**).

Table 11 - FTIR spectral assignments of Chitosan Schiff bases

Frequency (cm^{-1})				Assignment
ChSSB	**ChVSB**	**ChTSB**	**ChPSB**	
3793, 3713,3547	3600-3200	3300-3700	3300-3700	O-H stretching
2927.98 and 2870.02,	2922.11, 2870.02	2883.22, 2828.93	2881.01, 2828.80	CH_2 symmetric and asymmetric stretching
1422		1415.01	1431.86	C-N axial deformation
1552.93	**1527.25**	**1544.11**	**1552.20**	**C=C stretching of aromatic sysytem**
1646.12	**1683.78**	**1631.59**	**1649.71**	**C=N vibrations of azomethine group**
-	-	1744.44	1745.88	C=O stretching in secondary amide
1383.27	-	1369.86	1365.82	CH_3 symmetrical angular deformation
1323.27	-	-	-	C-N amino groups
784.69, 657.75	643.8	701.06,645.32	639.41	C-H stretching of aromatic ring
1023.16	1018.02	1020.64,	1014.36	Ring, C-O-C bridge stretching
1156.70, 841.19	1156.97,1290.25, 891.82	1218.88, 1149.75, 897.18	1216.14, 1150.10, 895.49	ß(1–4) glycoside bridge, Chitosan peaks

Also, absorption peaks around 784.69 and 657.75 cm^{-1} can be assigned to the skeletal vibration of C-H stretching of benzene ring which suggests the presence of aromatic system in the polymer matrix. The absorption peak at 1383.43 can be due to CH_3 symmetrical angular deformation and the peaks at 1422.1 and 1323.27 cm^{-1} can be due to C–N axial deformation and C–N amino groups of Chitosan respectively suggests that 100% substitution did not occur. The characteristic polysaccharide bands, 1156.70 and 1023.6 cm^{-1} are also present in the FTIR of ChSSB.

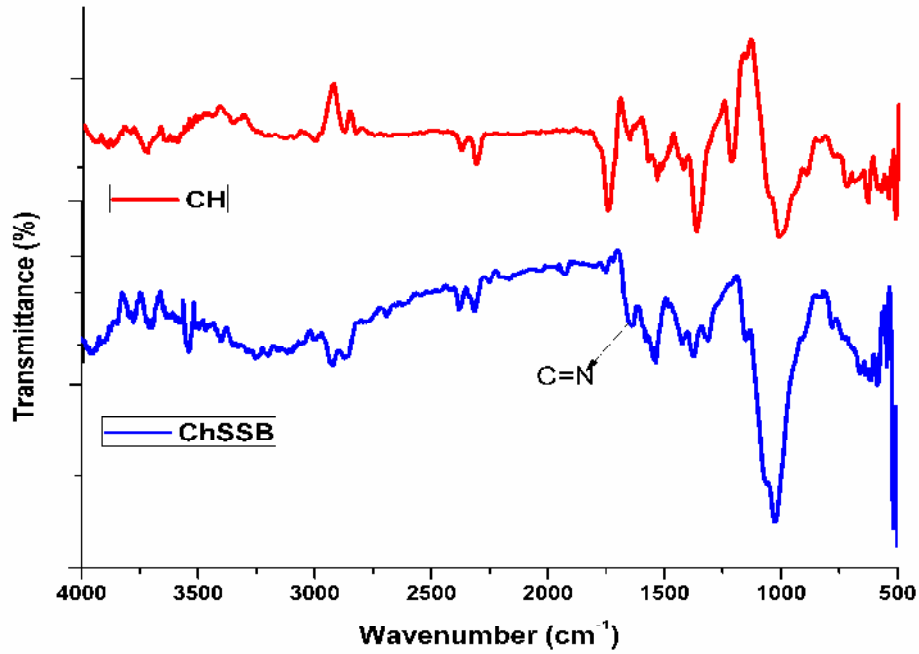

Figure 10 - FTIR spectrum of Chitosan and Chitosan Schiff base (ChSSB)

Characteristic Vibrations of Chitosan Schiff base- ChVSB:

FTIR spectrum of ChVSB show similar peaks that are present in the Chitosan spectrum. The three stage peaks at 1155.97, 1018.02, 891.82 cm^{-1} that are the characteristic peaks of Chitosan polysaccharide structure are present in the ChVSB spectrum. The very strong broad peak around 3600-3200 cm^{-1} observed can be assigned to the stretching vibration of the O-H groups and the intermolecular hydrogen bonds of the polysaccharide. The peaks responsible for primary amines i.e., 1656.29 and 1574.65 cm^{-1} are absent and the new strong absorption band at 1638.78 cm^{-1} is observed. This characteristic band can be assigned to the C=N stretching vibrations of imines. On the other hand, the absence of characteristic band in the region 1660-1730 cm^{-1} that correspond to the free aldehyde groups reveal the successful anchoring of vanillin onto the Chitosan backbone to obtain biopolymeric Schiff base. The characteristic bands of stretching and bending vibrations of the C=C bond of the aromatic ring can be observed at 1531.65 cm^{-1}. The peak at 643.8 cm^{-1} can be assigned to the C-H bending vibrations of aromatic aldehydes. This also confirms the substitution of vanillin in the Chitosan matrix. The absence of peaks pertaining to the amino groups of Chitosan viz., CH_3 symmetrical angular deformation (1383.43), C–N axial deformation (1422.1 cm^{-1}) and C–N amino groups (1323.27 cm^{-1}) suggest higher rate of substitution.

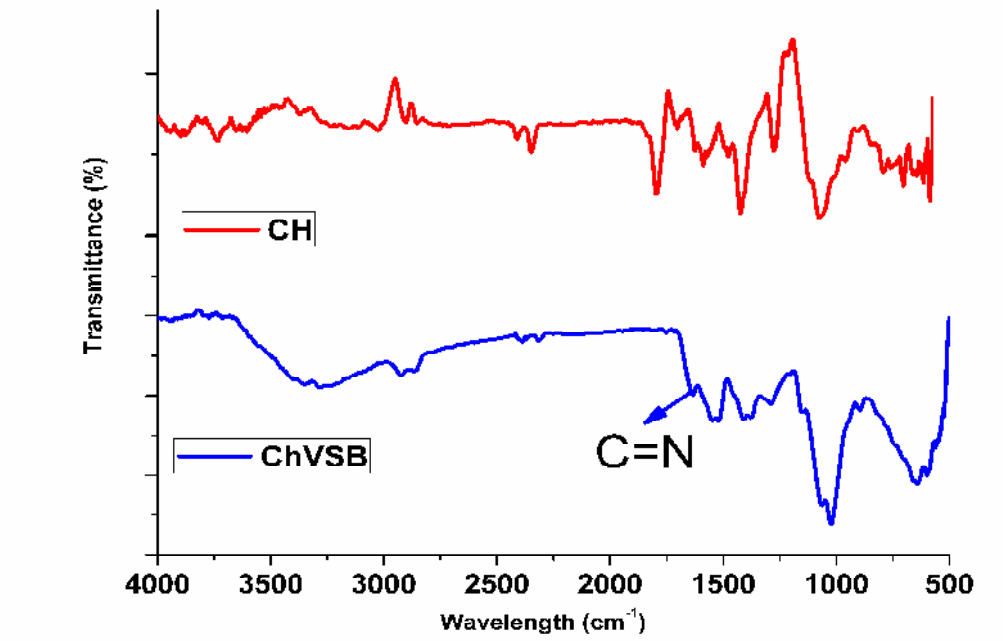

Figure 11 - FTIR spectrum of Chitosan and Chitosan Schiff base (ChVSB)

Characteristic Vibrations of Chitosan Schiff base - ChTSB and ChPSB:

The FTIR spectrum of Chitosan and Chitosan Schiff bases ChTSB and ChPSB are shown in Figure 12 &13 and their spectral assignments are given in Table 11. Both the derivatives of Chitosan exhibit the similar type of vibrations. For comparison purposes, they can be discussed simultaneously. The Chitosan and Chitosan derivatives (ChTSB and ChPSB) exhibit the characteristics peaks concerning to the Chitosan absorptions. The absorption bands for O-H and N-H stretching vibrations can be observed by both the Schiff base derivatives in the region of 3300-3700cm^{-1}. The presence of peak at 1658.8 cm^{-1} in Chitosan is due to the NC=O stretching vibrations in the acetamide moiety, vanished in the Chitosan derivatives and a new absorption peak at 1631.59 cm^{-1} (ChTSB), 1649.71 cm^{-1} (ChPSB) was observed. This characteristic peak has been attributed to the (HC=N) azomethine stretching vibrations (**Dos Santos *et al.*, 2005**, **Menaka and Subhashini, 2016b**). Moreover the absence of vibrations related to free aldehyde in the region 1660-1730 cm^{-1} reveals that the condensation reaction between the amino group of Chitosan and carbonyl group of aldehydes have successfully taken place and thereby introducing the imine anchoring groups in the Chitosan matrix.

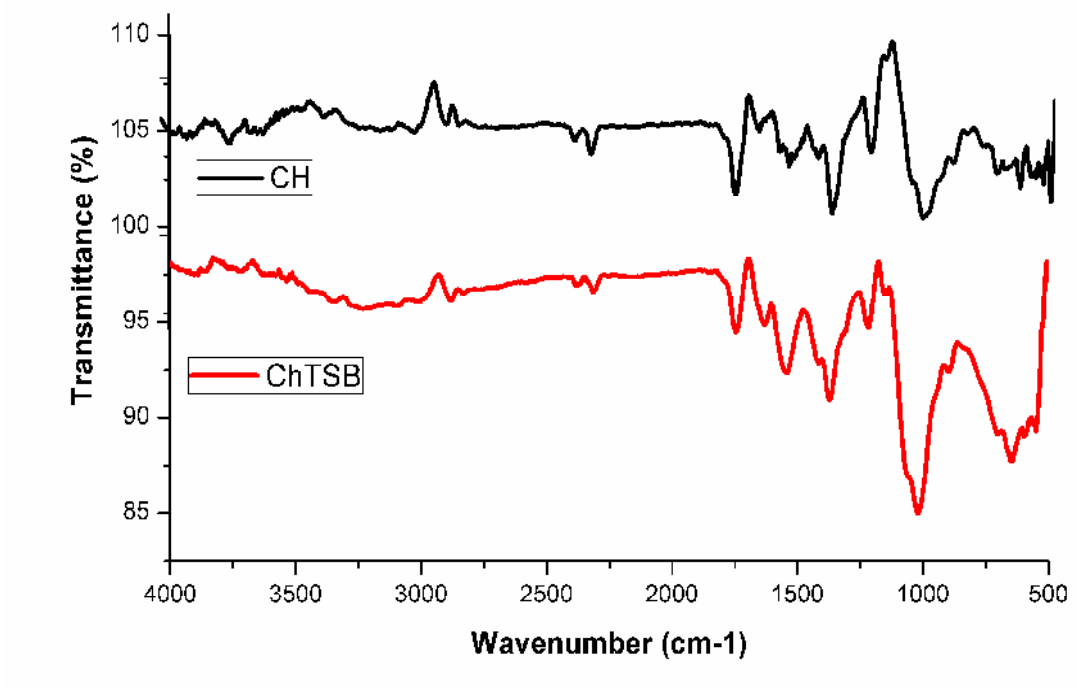

Figure 12 - FTIR spectrum of Chitosan and Chitosan Schiff base (ChTSB)

The characteristic peak at 1544.11 cm^{-1} (ChTSB) and 1552.20 cm^{-1} (ChPSB) observed, can be assigned to the stretching and bending vibrations of the C=C bond of the aromatic ring. This peak is yet another confirmation for the successful anchoring of aldehydeic groups onto Chitosan backbone. The peaks for C-H vibrations of aromatic ring are also observed in both the derivatives of Chitosan – ChTSB (701.06 and 645.32 cm^{-1}) and ChPSB(639.41 cm^{-1}). The absence of C-N axial deformation peaks of Chitosan (around 1323.50 cm^{-1}) in the chitosan derivatives supports the substitution reaction of aldehydes. Also, the shift in the intensity of the vibrations due to C-N axial deformation, CH_3 symmetrical angular deformation that is observed may be attributed to the distortion in the polymeric chain during the substitution reaction. The peaks pertaining to the C=O stretching in secondary amide are observed in ChTSB and ChPSB derivatives in the region 1744.44 and 1745.88 cm^{-1} respectively. These characteristic peaks reveal that 100% substitution is difficult.

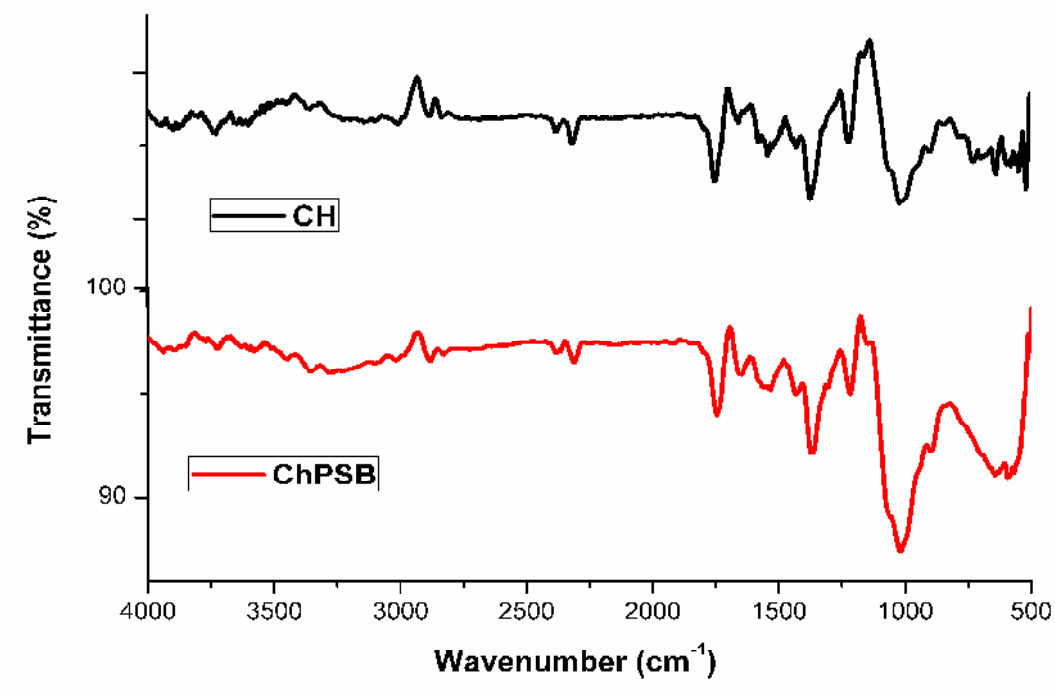

Figure 13 - FTIR spectrum of Chitosan and Chitosan Schiff base (ChPSB)

Inference from FTIR spectroscopy of Chitosan and Chitosan Schiff bases:

Based on the above discussions, it can be inferred that Chitosan have been successfully modified into its Schiff base by condensation reaction. The main absorption bands confirming the formation of Schiff base are being summarized and given in the Table 12.

Table 12 - FTIR spectral assignments corresponding to the confirmation of Chitosan Schiff bases

Sample name	Frequency (cm^{-1})						
	C=O Amide I	N-H Amide II	C=N Imine	$-NH_2$ amine	C-H Aromatic ring	C=C Aromatic ring	C-O-C bridging
CH	1656.29	1536.54	-	1574.65	-	-	1010.88
ChSSB	-	-	1646.12	-	657.75	1552.93	1023.16
ChVSB	-	-	1638.78	-	643.8	1527.25	1018.02
ChTSB	1744.44*	-	1631.59	-	645.32	1544.11	1020.64
ChPSB	1745.88*	-	1649.71	-	639.41	1552.20	1014.36

*- The shift in the intensity due to the distortion of polymeric molecules and also suggest 100% substitution is difficult.

From the table, the successful anchoring of aldehydeic groups onto the Chitosan backbone have been confirmed by the results of FTIR spectrum of Chitosan and Chitosan Schiff bases.

4.1.2.4 Surface Morphology- SEM Analysis:

The surface morphology of the Chitosan and Chitosan Schiff bases was examined using scanning electron microscope. The difference in structural morphology between "native" Chitosan and its Schiff base derivative is supported by their SEM photographs. The scanning electron micrographs of Chitosan and Chitosan Schiff base derivatives are shown in Figure 14, 15 (a, b) & 16 (a, b).

The SEM image of Chitosan exhibits a non-porous, smooth membranous phases and flat lamellar phases. The surface of the Chitosan contains some microfibrils and crystallite like particles.

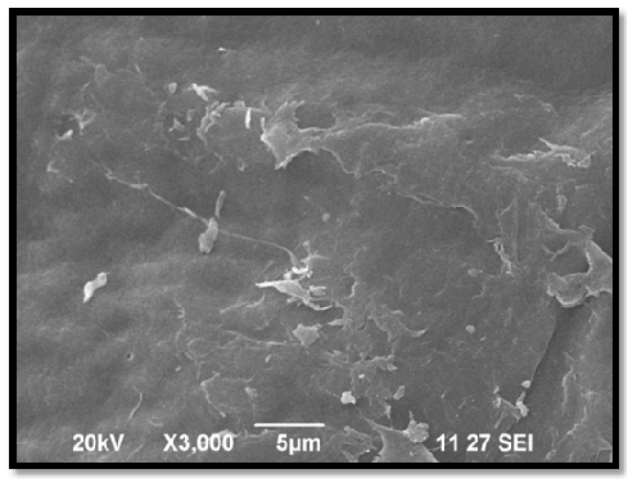

Figure 14 – SEM image of Chitosan

The surface morphology of the Chitosan Schiff bases was totally different from the smooth and flat nature of the Chitosan. This difference might be due to the chemical modification of Chitosan through condensation reaction with aldehydes. Moreover, the surface morphology of all the prepared Chitosan Schiff bases shows variation to each other. Thus it can be concluded that condensation reactions of Chitosan have given rise a complete alteration in the surface morphology of the prepared derivatives.

SEM micrograph of ChSSB (Figure 15a) shows a noticeable wrinkles and porous structure which is different from the flaky nature of the Chitosan. The highly porous structure with holes and openings on the surface of the derivative can be seen. The significant

morphological change that is noticed in ChSSB can be attributed to the formation of imine linkages in the Chitosan matrix. The SEM image of ChVSB is shown in Figure 15b exhibits polymorphic porous and layered structure. On observing the surface features of ChTSB (Figure 16a), a completely changed morphology with wrinkles and irregular structure with some pores on the surface can be seen. A typical layered morphology with extensive floral texture is displayed in the electron micrograph of ChPSB (Figure 16b).

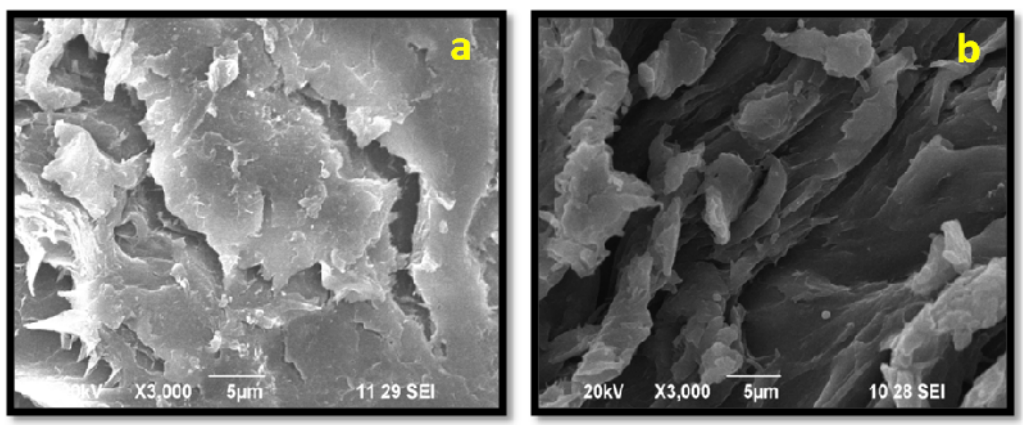

Figure 15 – SEM image of a) ChSSB b) ChVSB

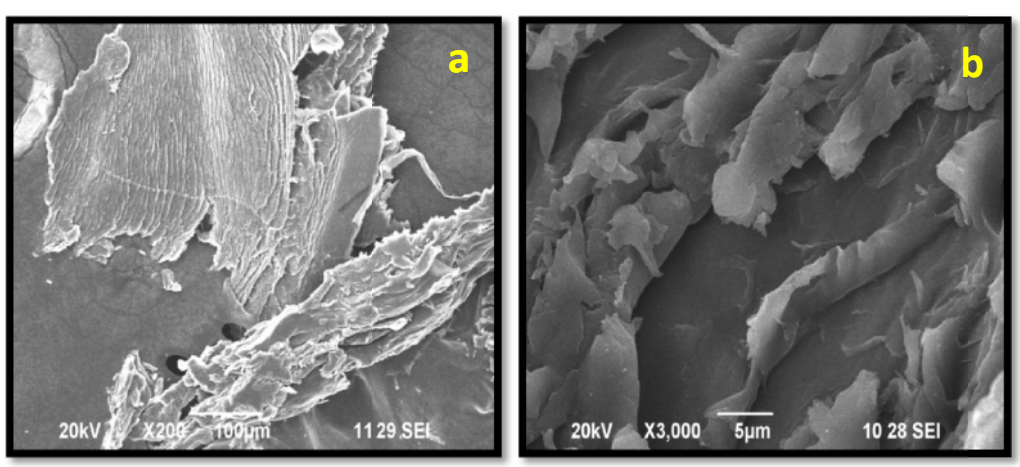

Figure 16 – SEM image of a) ChTSB b) ChPSB

The morphological changes occuring in the Chitosan Schiff base derivatives can be attributed to the alternation of inter and intra-molecular interactions. Incorporation of aromatic moieties of aldehyde molecules between Chitosan polymeric chains leads to weakening of the internal forces between polysaccharide chains including hydrogen bonding and subsequently its arrangement within the polymeric matrix (**Kumar *et al*., 2014, Anthony *et al*., 2013a, Monier *et al*., 2012, Menaka and Subhashini, 2016b**). The smooth surface of the Chitosan is altered to more extensive three dimensional network structures in derivatives

of Chitosan. This might be due to the modification of Chitosan by the formation of Schiff base in the matrix. Because of the modification, the anchored aldehyde moieties leave the footprints on the surface of the matrix and thereby the irregularity in the morphology increases.

4.1.2.5 Thermo gravimetric analysis of Chitosan Schiff bases

Thermogravimetric analysis (TGA) is being used to determine the thermal stability of the compounds by measuring the amount and rate of change in the weight of the compounds as a function of temperature in a controlled atmosphere. TGA technique has been mainly used to explore the thermal degradation, phase transition and crystallization of the polymers.

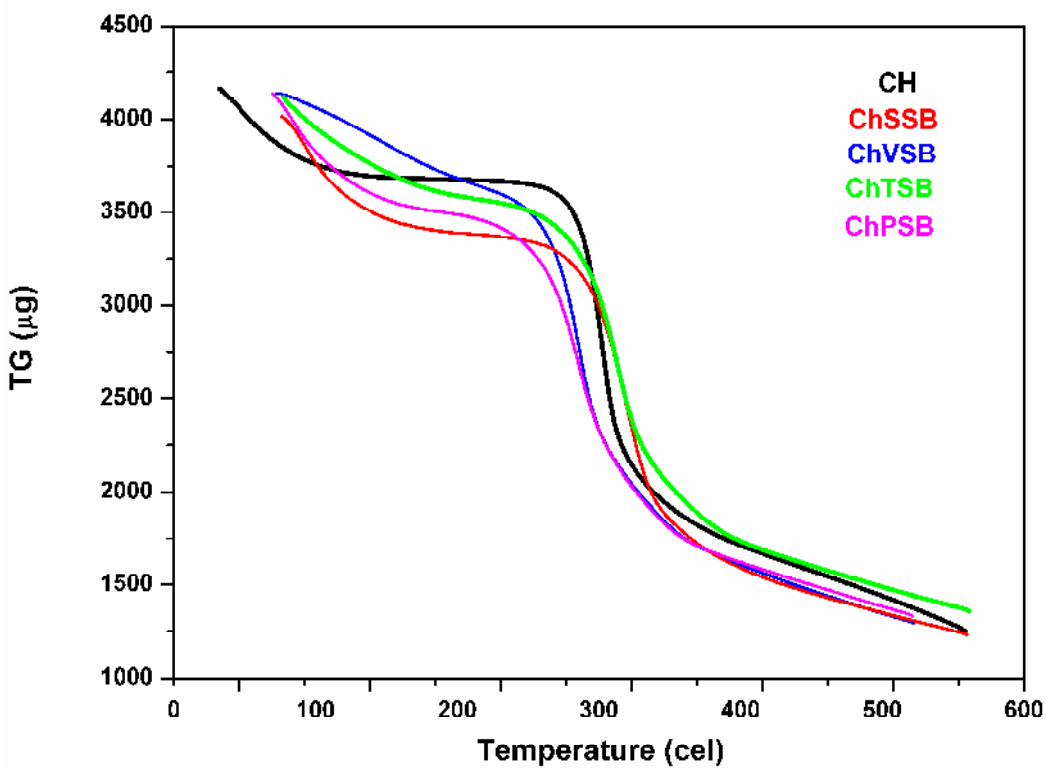

Figure 17 – TGA curves of Chitosan Schiff bases

The thermal stability of Chitosan and Chitosan Schiff base derivatives were studied by thermogravimetric analyzer (Exstar SII TG/DTA 6300). TG curves of Chitosan and its Schiff base derivatives are shown in Figure 17. The degradation temperature with corresponding weight loss percentage obtained from TGA analysis is presented in Table 13. An observation of the thermograph of Chitosan reveals the first thermal degradation step started in the region 50-100 ^{o}C with the weight loss of about 11%. This degradation step was assigned to the loss of water molecules bounded to the polymeric structure of hydroxyl and

amino groups (**Pereira *et al*., 2013**). According to the literature, the loss of water molecules occurring at the temperature below 100 ^{o}C gives rise to the view that these water molecules may be physically adsorbed onto the Chitosan matrix. The second degradation step starts at 270 ^{o}C and reaches a maximum at 390 ^{o}C with a weight loss of about 48%. This is the main degradation step and corresponds to the decomposition of the Chitosan matrix. Also, the presence of residual mass of about 20% till the temperature of 550 ^{o}C shows the stability of the Chitosan which is not completely decomposed. The thermal degradation steps of Chitosan are in good agreement with the results reported by the earlier studies (**Tirkistani,1998**, **Diab *et al*., 2011**, **Tameer *et al*., 2016, Kocak *et al*., 2012, Gavalyan, 2016).** The main degradation step in the region 270-390 ^{o}C may be due to the thermal degradation of the pyranose ring with rupture of the glycosidic linkages between the glucosamine and N-acetylglucosamine rings.

Table 13 - Stepwise thermal degradation with corresponding Weight loss % from TGA and DTG

Polymer	First stage		Second stage		DTG maxima/ ^{o}C	Residual mass (%) at 550^{o}C
	Temperature range/ ^{o}C	Weight loss (%)	Temperature range/^{o}C	Weight loss (%)		
Chitosan	50-110	11	270-390	48	302.3	20
ChSSB	65-120	12	250-330	45	297.6	17
ChVSB	60-110	10	240-330	46	284	15
ChTSB	40-100	10	220-350	50	282.2	21
ChPSB	30-120	14	220-360	46	288.2	20

The thermal graphs of Chitosan Schiff bases (ChSSB, ChVSB, ChTSB, ChPSB) are presented in Figure 17. In this thermal analysis, thermal degradation behaviour and stability of Chitosan show changes after the formation of Schiff bases. All the Schiff base derivatives of Chitosan have the first degradation step of elimination of water molecules below 120 ^{o}C with the weight loss of about 12%.The TG curves of all the Schiff base derivatives seem to be exhibiting similar degradation process.

The second degradation step of the Chitosan Schiff bases (Table 13) occurs in the temperature range of 220-360 ^{o}C. This main degradation process of the Schiff base derivatives occurs at lower temperature range than the temperature range of second degradation process of native Chitosan. These slight variations in the thermal stability of the Schiff bases may probably be due to the presence of new functional groups (-N=CH) which

degrades under the applied experimental conditions. The introduction of functional groups in the Chitosan matrix may obstruct the closed packing nature of the Chitosan and thus loosens the packing structure wherein the main degradation temperature range of the Schiff bases decreases.

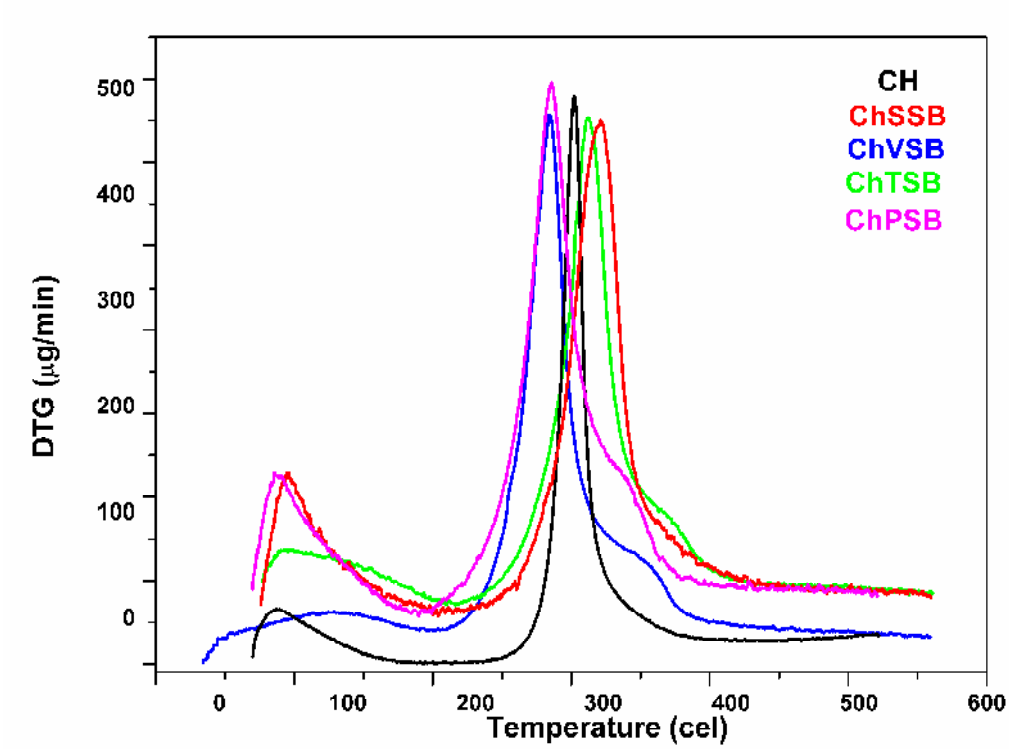

Figure 18 – DTG curves of Chitosan Schiff bases

The variation in the temperature range also indicates that Chitosan is more stable than the prepared Chitosan Schiff bases. The instability of Chitosan Schiff bases compared to Chitosan may due to the replacement of amino groups by aromatic aldehydes with the formation of imine group in the Chitosan matrix. The stability order of the Schiff bases can be arranged according to the onset degradation temperature of second thermal process and the order is as follows: ChSSB>ChVSB>ChPSB>ChTSB.

According to DTG curves of Chitosan and its Schiff base derivatives (Figure 18), the maximum thermal decay temperature (DTG_{max}) of Chitosan is found to be 302.3 ^{o}C which is in good agreement with the reported values of Chitosan DTG_{max} (**Baran *et al.*, 2015**). The DTG_{max} values for Chitosan Schiff bases ChSSB, ChVSB, ChPSB, ChTSB are 297.6 ^{o}C,284 ^{o}C,282.2 ^{o}C, 288.2 ^{o}C respectively. The decrease in the maximum thermal decay temperature may be due to the reduction in the number of amino groups in the Chitosan matrix after the modification into Schiff base formation.

Phase II

4.2 Corrosion Monitoring Techniques - Weight loss Method:

The weight loss method of monitoring corrosion rate is useful because of its simplicity and reliability. Weight loss experiments are carried out for desired time and temperature depending upon the type of application. Thus the method helps us to find out the most influencing factors viz. concentration of the inhibitor, effect of exposure time and temperature on corrosion inhibition. Weight loss experiments have a number of attractive advantages that account such as **Simple** – no sophisticated instrumentation is required to obtain the results, **Direct** – a direct measurement is obtained, with no theoretical assumptions or approximations and **Versatile** – it is applicable to all corrosive environments, and gives information about all forms of corrosion, that accounts for its sustained popularity.

To assess the effectiveness of the inhibitors ChSSB, ChVSB, ChTSB and ChPSB, the weight loss experiments were carried on the basis of the three parameters:

- Effect of concentration
- Effect of time
- Effect of temperature

4.2.1 Chitosan Schiff bases as corrosion inhibitor – Weight loss results as a function of Concentration and time:

Concentration of the corrosion inhibitor plays a major role in the acid corrosion of mild steel. The weight loss of MS was determined; in 1M HCl at room temperature (30 ^{o}C) at different time periods in the absence and presence of different concentrations (100-1500 ppm) of Chitosan Schiff bases (ChSSB, ChVSB, ChTSB and ChPSB). The behaviour of Chitosan Schiff bases and their inhibition efficiencies IE (%) will be discussed in the following sections.

Performance of Chitosan Salicylaldehyde Schiff base (ChSSB):

Corrosion rates and Inhibition efficiencies calculated for MS in 1M HCl from weight loss data in the presence of different concentration of the ChSSB at room temperature for different immersion periods are listed in Table 14. Inspection of the data in this table reveals that the IE increases with increasing concentration and the maximum inhibition performance of the inhibitor was observed with 1500 ppm.

The corrosion rate of MS in 1M HCl decreases with the increase of inhibitor concentration. The increase in the inhibitor concentration resulted in the increase in surface coverage, thus the metal surface becomes efficiently separated from the acid medium. The

results indicate that the presence of ChSSB inhibits the mild steel corrosion in 1M HCl and the extent of inhibition is dependent on concentration of the inhibitor.

Table 14- Corrosion rates and IE obtained for various concentrations of ChSSB at various immersion periods

S.No.	Conc (ppm)	1 hour		3 hours		6 hours		12hours		24 hours	
		CR (mpy)	IE (%)	CR (mpy)	IE (%)	CR (mpy)	IE (%)	CR (mpy)	IE (%)	CR (mpy)	IE (%)
1	**Blank**	780.44	-	1027.11	-	1859.18	-	1984.9	-	1672.1	-
2	**100**	331.56	57.52	278.18	72.92	330.17	82.24	431.41	78.27	303.16	81.87
3	**300**	321.36	58.82	254.40	75.23	288.58	84.48	328.56	83.45	253.93	84.81
4	**600**	239.75	69.28	221.12	75.23	233.13	87.46	273.56	86.22	212.53	87.29
5	**900**	204.04	73.86	194.96	81.02	220.53	88.14	259.99	86.9	197.25	88.2
6	**1200**	198.94	74.51	185.45	81.94	187.77	89.9	246.42	87.59	167.39	89.98
7	**1500**	132.63	83.01	178.32	82.64	165.08	91.12	223.56	88.74	149.62	91.05

In Figure 19, the IE as a function of immersion period is presented for all the concentrations studied. The IE pertaining to 1500 ppm of inhibitor gradually increases upto 6 hours of immersion to 91.12%, slightly decreases to 88.74 % at 12th hour and again increases to 91.05 % at 24th hour. The best performance in the immersion time experiments is given by 1500ppm of inhibitor at 24 hours of immersion. This shows the stability of the adsorbed inhibitor on the metal (**Ajmal *et al*., 2000**).

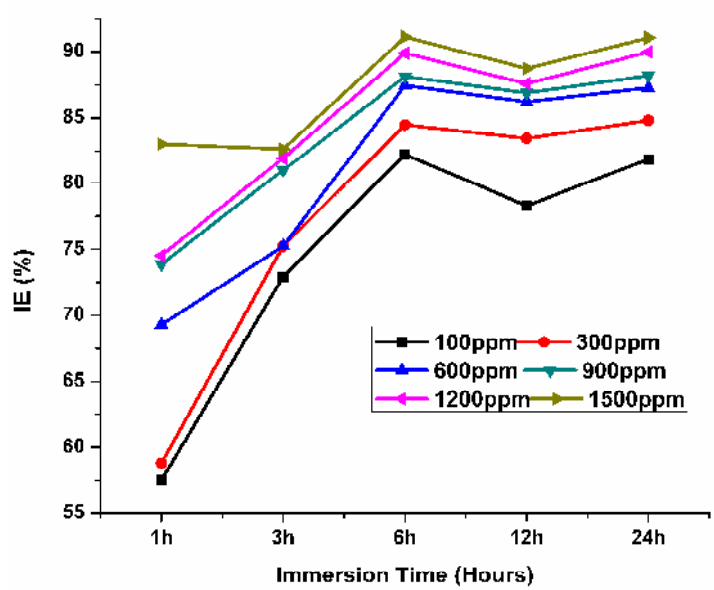

Figure 19 - Variation of IE at different immersion periods for various concentrations of ChSSB

Performance of other investigated Chitosan Schiff bases :

The behavior of Chitosan Schiff bases (ChVSB, ChTSB, ChPSB) were investigated with different immersion time (1-24 h) to monitor the metal dissolution process and the results are given in Appendix – A1. The variation of IE with different immersion period for different concentration of Chitosan Schiff bases viz ChVSB, ChTSB, ChPSB is shown in Figures 20 a, b & c respectively.

In ChVSB, the inhibition efficiency increases with immersion time till 6 h and slight decline was observed at 12 hour of immersion (Figure 20a). At immersion time of 24 h, inhibition efficiency of the system was increased as same as 6 h immersion. This ensures the stability of the film formed on the metal surface. The higher inhibition may be attributed to the film forming capability of the Chitosan derivative and also its greater stability towards the acid attack.

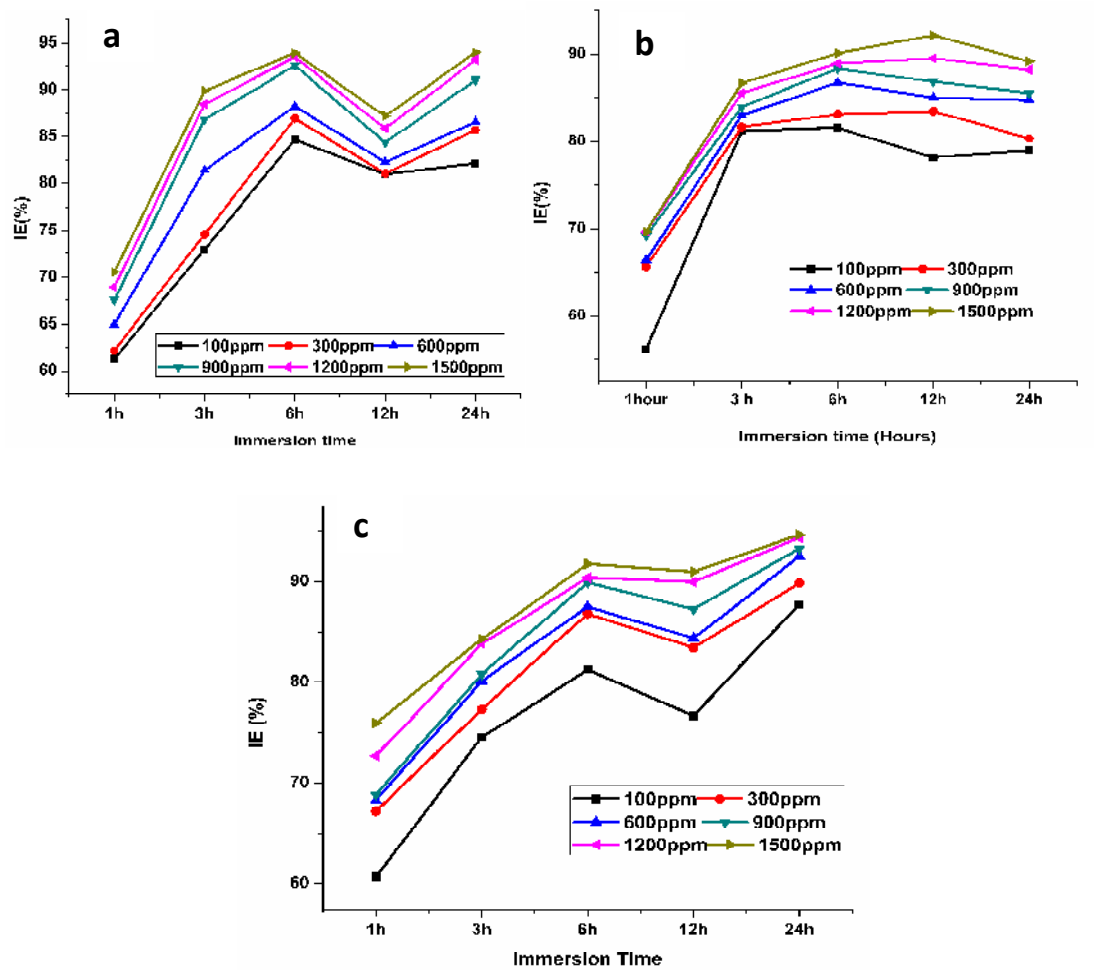

Figure 20 - Variation of IE with different concentration of a) ChVSB b) ChTSB c) ChPSB at different immersion periods

In the case of inhibitor system ChTSB (Figure 20b), the trend was quite different from the other two systems. The inhibition efficiency increases with immersion period upto 6 hours and then there is decrease in the efficiency on increasing the immersion time to 12 h and 24 h. The decrease in the IE at these immersion periods may be attributed to the stabilization period taken by the film to adsorb strongly onto the metal surface.

A steady trend of increase in inhibition efficiency with immersion time is seen in the case of ChPSB (Figure 20c). The maximum inhibition efficiency was obtained for 24 hours of immersion with the optimum concentration of 1500 ppm. The inhibition effect is due to the formation of adsorption layer on the metal surface. Generally, the inhibition efficiency of the investigated inhibitor systems increases with increase in immersion time.

4.2.1.1 Analysis of results obtained by weight loss technique – Effect of concentration and time:

The behaviour of Chitosan Schiff bases for mild steel dissolution in 1 M HCl can be understood by considering the adsorption of inhibitor molecules, the stability of adsorbed molecules and tendency to form chemical bonding with the metal.

Effect of Concentration:

From the results of weight loss technique, a better inhibiting behaviour of Chitosan Schiff bases was seen in positive manner with respect to concentration. The inhibition efficiency increases as the concentration increases from 100 to 1500 ppm weight by volume. Further increase in the inhibitor concentration was not possible because of the limited solubility of these polymers in acidic medium. The Schiff base polymers show a steady and stable IE at higher concentration of 1500 ppm. The reason for inhibition may be argued as follows: Generally, Cationics are quite stable in acid media and they can retain their structure in strong acids (**Negm *et al*., 2011**). Since Chitosan is a cationic polymer and its Schiff base polymers can also form stable cations in the acid medium which can form a tight and well arranged stable adsorbed layer especially at higher concentration exhibiting high inhibition efficiency.

Generally, the inhibitive action of inhibitors is due to the adsorption of the molecules on the metal surface. The increase in inhibition efficiency with increasing concentrations of the Schiff base polymers can also be related to increase in the number of molecules adsorbed on the mild steel surface by blocking the corrosive sites of the acid attack and thereby protecting the metal from corrosion (**Umoren *et al*., 2006, Sayyah *et al*., 2014**). This is also an evidence for the maximum surface coverage on the metal surface owing to multiple adsorption centers which makes the adsorption process favourable **(Ali *et al*., 2012)**.

Obviously, the corrosion rate of mild steel is more in presence of 1M hydrochloric acid due to the aggressiveness of acid solution. The anodic dissolution of mild steel in acidic media and the corresponding cathodic reaction has been reported to proceed as follows (**Solomon *et al*., 2010**).

$$Fe \rightarrow Fe^{2+} + 2e^-$$

$$2H^+ + 2e^- \rightarrow 2H_{ads} \rightarrow H_2$$

As a result of these reactions, including the high solubility of the corrosion products, the metal loses weight in the solution and the corrosion rate is more. From the results obtained, the corrosion rate decreases with increasing the concentration of Schiff base polymers. The degree of inhibition depends upon the nature and the concentration of the polymers. These polymers inhibit the acid dissolution of mild steel by adsorption of Schiff base polymers at mild steel/acid interface (**El-Haddad, 2013**). The increase in inhibition efficiency as the concentration of Schiff bases increased and reaching a stable IE, indicating the formation of protective layer at the surface of the mild steel.

The data reveals that the inhibition efficiency for all the Chitosan Schiff bases increases with increase in concentration. The inhibition efficiency of these inhibitors increases in the order:

ChPSB> ChVSB> ChSSB>ChTSB

It is clear that these Chitosan Schiff base compounds are good inhibitors for mild steel in acid medium.

Effect of Immersion Time:

The behaviour of Chitosan Schiff bases with immersion time was explained by **Atta *et al*. (2008)** as follows: increase in IE with time is due to initial electrostatic interaction by charged groups, and as the time proceeds formation of multiple layers and/or complex formation with Fe orbital can occur. In other words, the adsorption of the inhibitor molecules on the metal surface initially takes place at some sites, and later as the time proceeds the inhibitor form adsorbed layers by forming complex with iron. The same trend was reported by **Quarishi and Shukla (2009)** for poly (aniline-formaldehyde) with exposure time in weight loss measurements. The IE decreased at 12 h of immersion and it seems to increase at 24 h of exposure to inhibited solution. This was attributed to the removal of the adsorbed layer owing to the weaker interaction between inhibitor and MS surface. But in present study, a slight decrease in 12^{th} hour may not be pertained to desorption instead it may be attributed to the stabilization period for the Schiff base polymers to form a highly adherent

stable film. The formation of stable film on the metal surface results in increase in IE after 24 hours of exposure, showing the persistency of inhibitor film on the MS surface. The high inhibition efficiency with longer immersion time is an indication of the formation of a time-dependant protective film on the MS surface **(Mu and Li, 2005)**. The increase in inhibition efficiency with increasing immersion time is due to increase in surface coverage with time and also indicates the stability of adsorbed layer on mild steel surface.

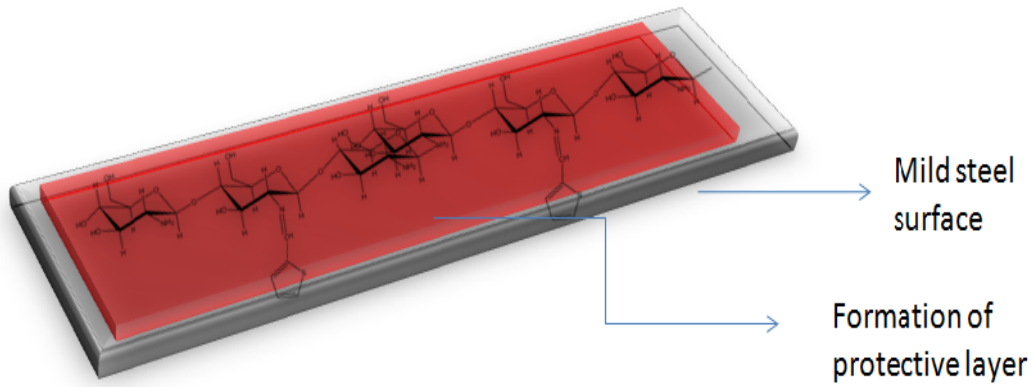

Figure 21 – Pictorial representation of adsorption of Chitosan Schiff bases on MS Surface

4.2.2 Chitosan Schiff bases as corrosion inhibitor – Weight loss results as a function of temperature

Temperature has a great effect on the rate of metal electrochemical corrosion. In acidic corrosion (hydrogen depolarization), the corrosion rate increases exponentially with increase in temperature because the hydrogen evolution over potential decreases (**Popova *et al.*, 2003**). The effect of temperature on the inhibited acid–metal reaction is highly complex because many changes occur on the metal surface such as rapid etching and inhibitor desorption or decomposition (**Fekry and Mohamed, 2010**). Temperature sometimes used as a gauge to determine whether an inhibitor is physically or chemically adsorbed on a metal surface to inhibit corrosion; as increase in inhibition efficiency with increase in temperature is often associated with chemisorption phenomenon while the reverse signifies physisorption (**Umoren *et al.*, 2015**).

To study the effect of temperature on the corrosion inhibition of mild steel in the acid medium, weight loss experiments were carried out at various temperatures (303-343 K) in presence and absence of different concentrations of Chitosan Schiff bases (100-1500 ppm). The behaviour of the Schiff base polymers in the studied temperature and temperature dependence on the inhibition efficiency and corrosion rate are discussed in the following section:

Performance of Chitosan salicylaldehyde Schiff base (ChSSB):

Table 15 gathers the values of CR of MS/1M HCl in different concentrations of ChSSB, determined by weight loss measurement at various temperatures (303-343 K) and the corresponding inhibitor efficiencies. The variation of both CR and IE for different concentrations of ChSSB is depicted in Figure 22. At each temperature, the inhibition of corrosion increases with inhibitor concentration. At a given inhibitor concentration, the inhibition effect increases more and more to jump from 66.1% at 303 K to 81.04% at 323 K. After 323 K the inhibition efficiency found to decrease but stabilized to 75% at 343 K for highest concentration (1500 ppm). In the presence of ChSSB, IE slightly decreases at higher temperature which suggests that the efficiency of ChSSB is stable in the studied range of temperature and effectively protects the mild steel even at high temperature (**Cheng *et al*., 2007**).

Table 15- Corrosion rates and IE obtained for various concentrations of ChSSB at various immersion temperatures

S.No.	Conc (ppm)	303 K		313 K		323 K		333 K		343 K	
		CR (mpy)	IE (%)	CR (mpy)	IE (%)	CR (mpy)	IE (%)	CR (mpy)	IE (%)	CR(mpy)	IE (%)
1	**Blank**	503.24	-	2217.67	-	4230.63	-	7727.72	-	11651.3	-
2	**100**	238.82	52.54	707.94	68.07	1287.95	69.55	2413.84	68.76	3411.8	70.71
3	**300**	213.23	57.62	537.35	75.76	1134.42	73.18	2157.96	72.07	3275.32	71.88
4	**600**	204.7	59.32	528.82	76.15	1066.18	74.79	2098.25	72.84	3190.03	72.62
5	**900**	196.17	61.01	503.24	77.3	972.36	77.01	1833.84	76.26	3138.85	73.06
6	**1200**	187.64	62.71	477.65	78.46	912.65	78.42	1791.19	76.82	2959.73	74.59
7	**1500**	170.59	66.1	469.12	78.84	801.77	81.04	1680.31	78.25	2900.03	75.1

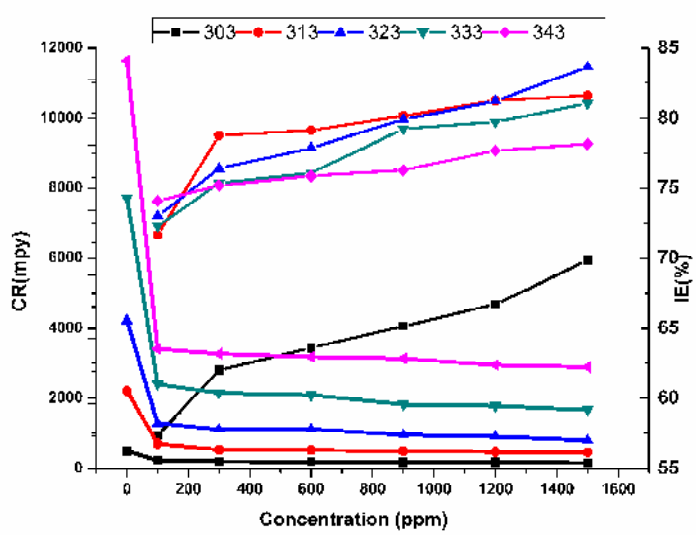

Figure 22 - Variation of CR and IE with various concentrations of ChSSB at 303-343K

Performance of other investigated Chitosan Schiff bases:

To assess the effect of temperature on the corrosion and corrosion inhibition of mild steel without and with Chitosan Schiff bases (ChVSB, ChTSB, ChPSB) were studied by conducting weight loss measurements at 303–343 K containing different concentrations (100-1500 ppm). The results are given in the Appendix - A2 and corresponding Figures are presented in Figures 23 - 25. The data reveal that the inhibition efficiency increases till the temperature of 323 K for almost all the concentration.

In case of ChVSB, the maximum IE of 82.56% was obtained for the highest concentration of 1500 ppm. At temperatures 333 K and 343 K, the efficiency of 77.15% and 75.58% are observed respectively. The decrease in the IE can be attributed to low stability of the inhibitor film formed on the metal surface. Moreover the dissolution of metal predominates at higher temperature.

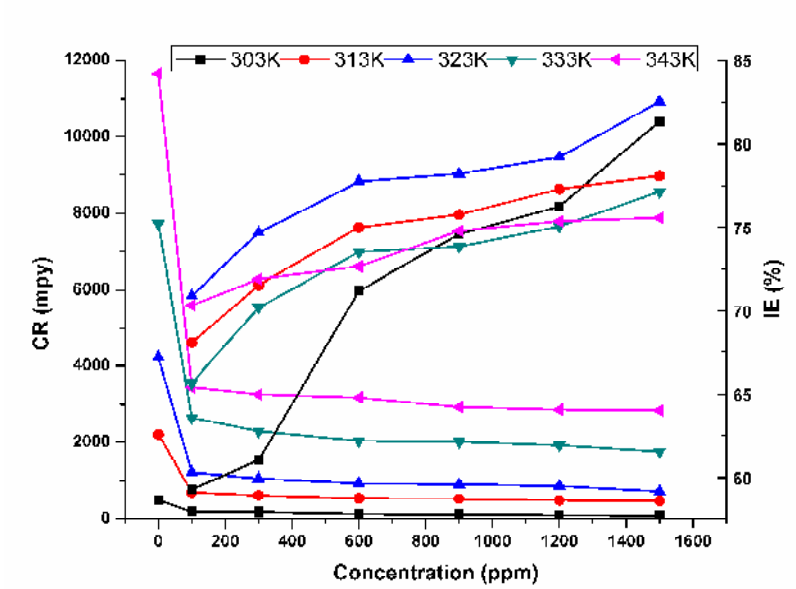

Figure 23 - Variation of CR and IE with various concentrations of ChVSB at 303-343 K

In the inhibitor system (ChTSB), the results show that the inhibition efficiency increases with increase in temperature till 333 K with the values from 63.15% to 86.94% for the maximum concentration of 1500 ppm. This indicates that the higher temperature favors the adsorption of inhibitor molecules on the metal surface. At 343 K, the slight decline in the inhibition efficiency is seen but still provides a better efficiency of 81.6% which ensures the protectiveness of the inhibitor film.

In the case of ChPSB, the values of inhibition efficiency increases upto 323 K affording an efficiency of 80.46%. Above 323 K, the inhibition efficiency decreases slightly to 77.92% but found to be steady and stable at 343 K. This may be due to the strong adsorption and high stability of the film formed on the metal surface even at high temperatures.

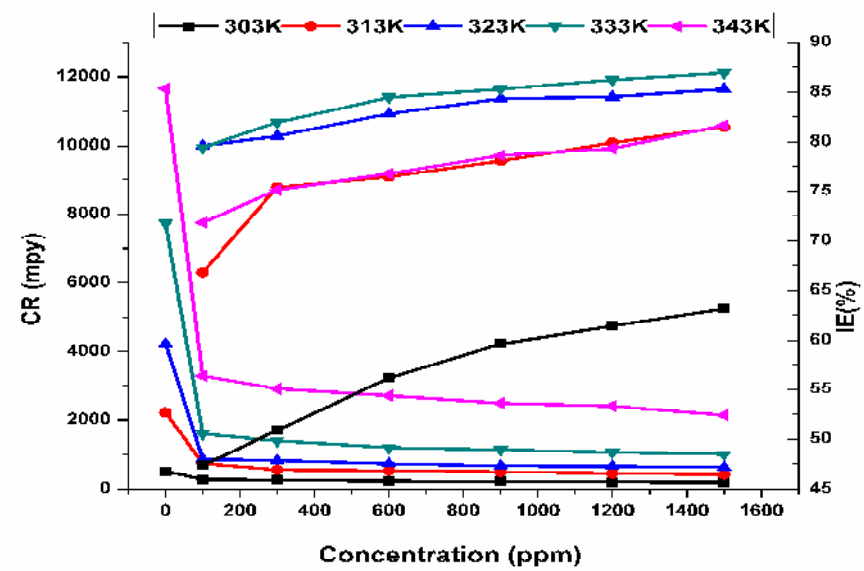

Figure 24 - Variation of CR and IE with various concentrations of ChTSB at 303-343 K

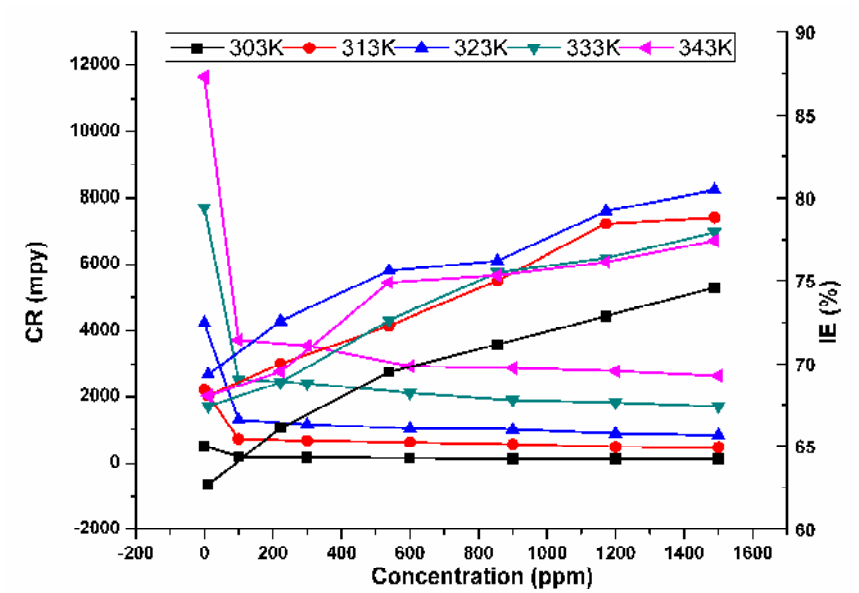

Figure 25 - Variation of CR and IE with various concentrations of ChPSB at 303-343 K

4.2.2.1 Analysis of results by weight loss technique- Effect of temperature:

On scrutinizing the Tables (Table 15 and Appendix A2), we could find that all the Schiff base polymers were found to behave in the same manner except ChTSB. All the Schiff base polymers except ChTSB were found to provide better IE upto 323 K, whereas the latter provides upto 333 K. Thus it can be concluded that the Schiff base polymers inhibit the mild steel dissolution by the formation of protective layer on the metal surface at all the studied temperatures.

The influence of temperature increases the values of corrosion rate with rise in temperature. The increase in corrosion rate with temperature is reasonable and is well concurrence with report given by Ebenso, that a doubling in reaction rate is expected with a 10 ^{o}C rise in temperature (**Ebenso (2001)**, **Obot and Obi-egbedi, 2010**).The increase in trend of IE is observed with temperature upto 333 K and a decrease of less than 5% at 343 K. The higher IE at higher temperature indicates the formation of stable inhibitor layer on the metal surface. The increase in the IE with temperature also suggests the chemical adsorption mode between the inhibitor molecule and metal surface.

The trend of IE with temperature suggests that Schiff base polymers were chemically adsorbed onto the mild steel surface. Chemisorption involves charge sharing or charge transfer from the inhibitor molecules to the metal surface to form a coordinate-type bond. This may be facilitated by the presence of vacant d- orbitals of the iron atom. Although it could not be rationalize the decrease in inhibition efficiency values obtained for mild steel at higher temperatures, however, the effectiveness of a particular inhibitor on a given metal depends on so many factors including number of adsorption sites and their charge density, molecular size, heat of hydrogenation, mode of interaction with the metal surface, and formation of metallic complexes (**Bilgic and Caliskan, 1999**).

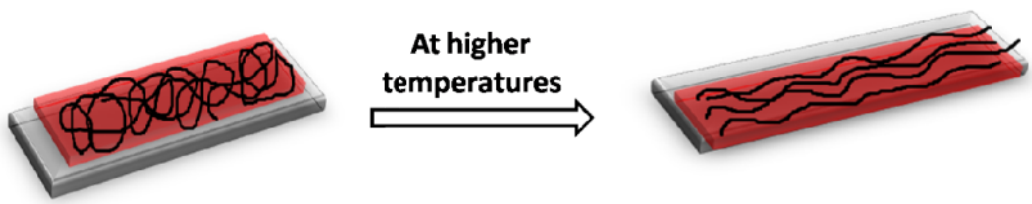

Figure 26 - Pictorial representation of plausible changes of the Chitosan Schiff bases on mild steel surface at higher temperatures

According to **Fares *et al*. 2012a, Geethanjali and Subhashini, 2015,** the coiled long chain structure of the Schiff base polymers may adsorb on the metal surface at a larger

surface area thereby preventing the metal dissolution. Hence better inhibition efficiencies were obtained in the temperature range of 303-323 K. But at higher temperatures (333-343 K), these coiled polymers may be uncoiled in to long chains which are more feasible to adhere onto the metal surface forming well oriented protective layer and hence a stable film at higher temperature is obtained.

4.2.3. Activation energy and Kinetic parameters:

Temperature is an important parameter in considering the metal dissolution process. Temperature influences the corrosion rate and is capable of modifying the interaction between the mild steel surface and acidic medium. The effect of temperature on the inhibited acid–metal reaction is very complex, because many changes occur on the metal surface such as rapid etching and desorption of inhibitor and the inhibitor itself may undergo decomposition (**Fekry *et al*., 2010**). To understand the dependence of temperature on the corrosion reaction of mild steel, Arrhenius equation (9) was used,

$$\log(CR) = \frac{-Ea}{2.303RT} + \lambda \qquad (9)$$

where Ea is the activation energy, λ is the Arrhenius pre-exponential factor, CR is the corrosion rate obtained from weight loss techniques.

The activation energy (E_a) and the pre- exponential factor (λ) were determined by using the Arrhenius plot of log CR vs 1/T. The slope ($-E_a$ /R) of the Arrhenius plot gives the value of activation energy.

Popova *et al*., 2003, Dehri and Ozcan, 2006 have reported the relation between the temperature, inhibition efficiency and the activation energy of the inhibitor as follows:

- If the inhibition efficiency of the inhibitor increases with the rise in temperature, the value of activation energy of the inhibitor will be less compared to blank solution.
- If the inhibition efficiency of the inhibitor decreases with the rise in temperature, the value of activation energy will be more for the inhibited solution than the blank.
- If the inhibition efficiency of the inhibitor does not change with temperature, the value of activation energy does not change in the presence or absence of the inhibitor.

The change in activation energy in the presence of inhibitor suggests the type of interaction between the inhibitor molecules and the metal surface.

1. The higher values of activation energy in presence of inhibitor can be attributed to the physical adsorption of the inhibitor on the metal surface (**Herrag *et al*., 2010**)

2. While, unchanged or the lower values of activation energy compared to the blank solution can be attributed to the chemisorption of the inhibitor (**Varsha and Singh, 2010).**

The thermodynamic parameters (ΔH*, ΔS*) of the corrosion process were determined using the transition state equation (10),

$$CR = \frac{RT}{Nh} exp\left(\frac{\Delta S*}{R}\right) exp\left(-\frac{\Delta H*}{RT}\right) \quad (10)$$

where R the universal gas constant and T the absolute temperature, N is the Avagadro's number, ΔH* is the enthalpy of activation, ΔS* is the entropy of activation.

The transition plot of log (CR/T) versus 1/T gives the straight line with the slope of (-ΔH*/R) and an intercept of (log (R/Nh) + ΔS*/R) from which the values of ΔH* and ΔS* were calculated respectively.

4.2.3.1 Thermodynamic activation parameters for corrosion process in presence of Chitosan Schiff bases:

Arrhenius plot of log CR vs 1/T for the corrosion process of the mild steel in the presence and absence of Chitosan Schiff base polymers are shown in Figure 27. From the linear plots obtained, the values of E_a and λ for mild steel were calculated and are summarized in Table 16. The obtained activation energy for blank (65.64 kJ mol^{-1}) lies in the range of 57.7-87.8 kJ mol^{-1} as reported in the literature (**Popova *et al*., 2003, Riggs *et al*., 1967**).

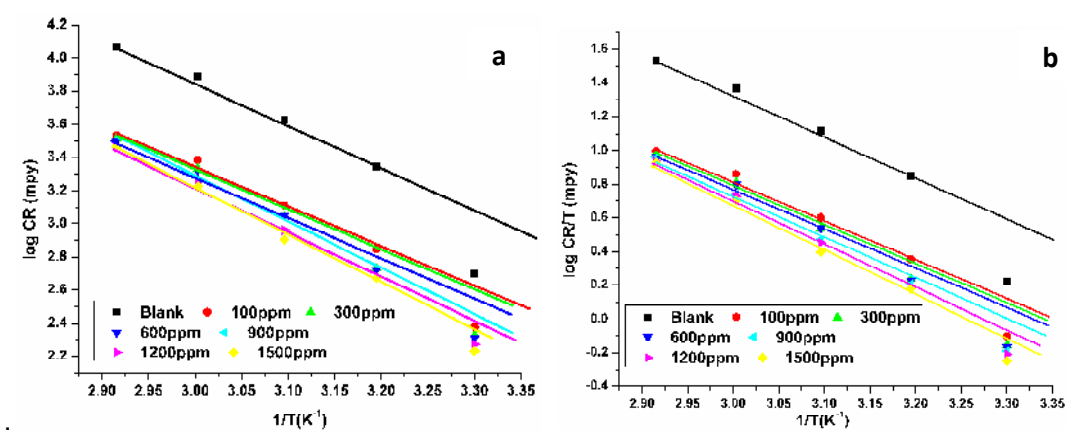

Figure 27 – a) Arrhenius plot and b) Transition plot of ChSSB

The values of λ and E_a decreased in the presence of Chitosan Schiff base derivatives compared to the blank solution. The modification in the values of E_a may be attributed to the chemical blocking effect of the adsorbed inhibitor molecules on the metal surface. The pre-exponential factor λ is related to the number of active centres in the heterogenous chemical reaction. In presence of adsorbed inhibitor molecules, blocking of active sites on the metal surface takes place which is energetically non-homogenous. Generally, the adsorbed inhibitor species block the more active sites i.e. sites with lower E_a value. Also, the sites with higher E_a which are in greater number take part in subsequent corrosion process. The λ value obtained for 1M HCl was found to be $1.44*10^{14}$. The trend of λ values is same as the activation energy (E_a). The significant decrease of λ value with increase in concentration of inhibitors shows less number of active centres leading to the reduction of CR of mild steel (**Mohana and Badiea, 2008; Morad, 2007**).

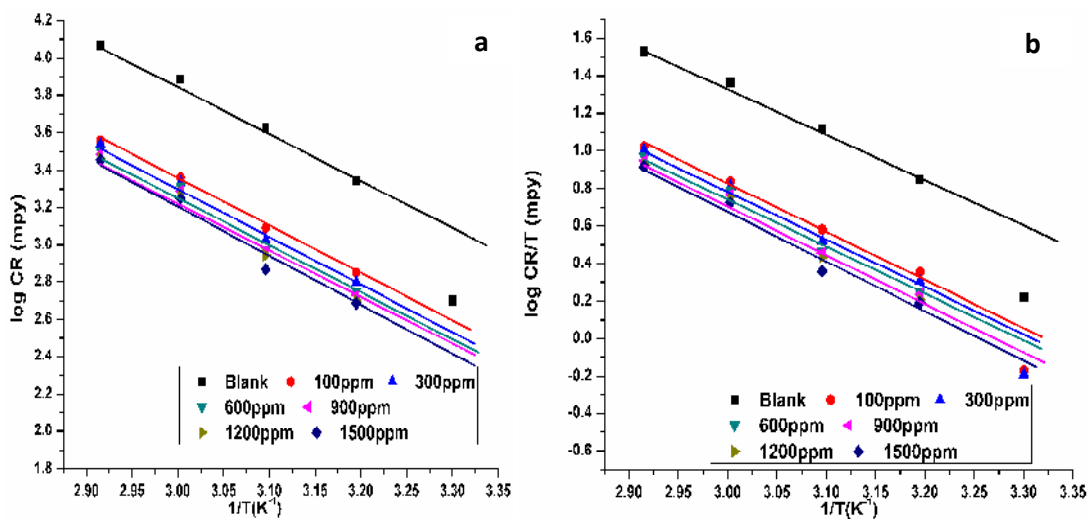

Figure 28 – a) Arrhenius plot b) Transition plot of ChVSB

The lower values of E_a obtained in the presence of Chitosan Schiff base derivatives indicates the formation of chemisorbed layer of the inhibitor on mild steel surface (**Fouda and Badr, 2013**).The decrease in the activation energy by increasing the concentration of the inhibitor may be due to the shift of net corrosion reaction from that on the uncovered portion on the metal surface to the covered portion (**Riggs *et al.*, 1967**). **Hoar and holliday (1953)** explained this fact as a slower rate of inhibitor adsorption with the resultant approach to equilibrium during the experiments at elevated temperatures. (**Oguzie (2004)** had reported that the lower values of E_a is an indicative of chemisorption of the corrosion inhibitor. **Szauer and brandt (1981)** also associates this behaviour with the chemisorption nature of the

inhibitor molecule to the metal surface. By taking these references into consideration, the inhibition of Chitosan Schiff base derivatives in 1M HCl solution can be attributed to the strong chemisorptive nature of adsorption involving charge sharing or charge transfer from the chitosan Schiff base derivatives to the mild steel surface to form a coordinate bond (**De Souza and Spinelli, 2009**).

The E_a values found to decrease on increasing the inhibitor concentration in all the investigated systems except Chitosan vanillin Schiff base. The observed results in the particular system can be explained by the mechanism proposed by Riggs and Hurd. The author suggested that the corrosion rate, -d(Fe)/dt can be expressed by sum of two rates: -

$$d(Fe)/dt=k1[1-\theta]+ k2\theta$$

where k1 and k2 are rate constants of the uninhibited reaction and completely covered reaction respectively, θ is the fraction of the surface covered by the adsorbed inhibitor. The inhibition mechanism can be explained by following equation,

$$Fe + Inh \longrightarrow Fe(Inh)_{ads} + Fe^{n+} + ne^{-} + Inh$$

At first when the inhibitor concentration is low, there will be lack of $Fe(Inh)_{ads}$ to cover the metal surface or the rate of adsorption will be slow so that the dissolution of metal takes place on the uncovered portion of mild steel surface. At higher inhibitor concentration, the compact and coherent inhibitor layer is formed on the mild steel which reduces the acid attack of the metal. In many cases, k2 may be so small that the term k2θ can be neglected. When θ becomes quite large (>0.9), a small increase in k2 makes the term k1[1-θ] to decrease markedly, hence the ratio of k1/k2 will be large and the term k2θ can be neglected at high coverage. The corrosion rates of many inhibited systems at high coverage do not suggest simply the high degree of adsorption but rather a new expression, k2θ is considered. In such cases, the term k1[1-θ] will be neglected and the corrosion mechanism involves the direct reaction of the reaction intermediate $Fe(Inh)_{ads}$. Thus, the activation energy in $\ln k2 = \ln A - E_a/RT$ probably different from that in the uninhibited rate constant k1. Thus it is possible that the activation energy of the inhibited reaction at high coverage can be either larger or smaller than that of the uninhibited reaction. So this trend of activation energy is applicable for the Chitosan vanillin Schiff base system (**Singh and Quraishi ,2010a**).

From the data (Table 16), the values of ΔH^* decreases with the increase in the concentration of inhibitor. The positive values of the enthalpy (ΔH^*) reflects the endothermic

nature of the dissolution process and the difficult dissolution of mild steel (**Fontana, 1986**, **Tebbji *et al.*, 2007, Benabdellah *et al.*, 2006**). The values of E_a and ΔH^* are close to each other and varies in same trend on the addition of different inhibitor concentration. This result permits to verify the known thermodynamic relation between the E_a and ΔH^* ie., E_a-ΔH^* = RT. The calculated RT value for all the investigated inhibitors was found to be 2.68 kJ mol^{-1} which is approximately around the theoretical average value of RT (2.69 kJ mol^{-1}). Higher inhibition efficiency at elevated temperature suggests chemisorptive nature of the inhibitor. Since heat released during the chemisorption is utilized for the corrosion process, the observed activation energy obviously becomes smaller. But the larger value of activation energy at higher concentrations of inhibitor indicates that the corrosion process is governed by the pre-exponential factor at higher concentrations and it is controlled by kinetic parameters of activation at lower concentrations (**Varsha and Singh, 2010**).

On comparing the values of entropy of activation (ΔS^*), the positive entropy value is obtained for inhibitor free solution. The lower positive and negative values of (ΔS^*) were obtained in presence of Chitosan Schiff base derivatives (Table 16). Such variation can be attributed to the phenomenon of ordering and disordering of inhibitor molecules at the metal surface. Moreover the steric factors may be assigned to the presence of linear or branched polymer molecules at the metal surface **Elmorsi (1999)**. The negative values of entropies imply that the activated complex in the rate determining step represents an association rather than a dissociation step, which means a decrease in disordering takes place on going from reactants to the activated complex (**Martinez and Stern, 2002**). The shifting of ΔS^* to more negative values with increase in inhibitor concentration can be explained that the inhibitor species involved in the activated complex of the corrosion reaction leading to more ordered systems **Noor (2007**).The activated complex could be described as Fe-H^+ which on decomposition gives Fe^{2+} and H_2. The decrease in the entropy of the activation on addition of inhibitor is attributed to the formation of Fe- inhibitor complex which results in the reduction of acid attack on the metal.

Table 16 - Thermodynamic activation parameters for mild steel in 1M HCl in presence and absence of different concentrations of Chitosan Schiff base derivatives

Inhibitor	Concentration (ppm)	A (pre exponential factor)	Ea kJmol^{-1}	ΔH* kJmol $^{-1}$	ΔS* Jmol $^{-1}$	Ea-ΔH*=RT
ChSSB	**Blank (1MHCl)**	1.44×10^{14}	**65.64**	**62.96**	**17.20**	2.68
	100	1.86×10^{12}	56.91	54.23	-18.97	
	300	4.22×10^{12}	59.47	56.80	-12.17	
	600	4.41×10^{12}	59.65	56.97	-11.81	
	900	3.53×10^{12}	59.27	56.59	-13.65	
	1200	3.39×10^{12}	59.28	56.60	-13.99	
	1500	4.39×10^{12}	60.15	57.47	-11.83	
ChVSB	**100**	5.98×10^{12}	60.14	57.46	-9.28	2.68
	300	6.63×10^{12}	60.63	57.95	-8.42	
	600	3.03×10^{13}	65.07	62.39	4.20	
	900	4.64×10^{13}	66.36	63.68	7.75	
	1200	5.82×10^{13}	67.11	64.43	9.64	
	1500	1.9×10^{13}	70.58	67.90	19.50	
ChTSB	**100**	1.30×10^{11}	50.17	47.49	-41.08	2.68
	300	1.36×10^{11}	50.64	47.96	-40.74	
	600	1.15×10^{11}	50.46	47.78	-42.12	
	900	1.12×10^{11}	50.61	47.93	-42.30	
	1200	1.24×10^{11}	50.99	48.31	-41.51	
	1500	8.00×10^{10}	50.01	47.33	-45.15	
ChPSB	**100**	1.79×10^{13}	63.03	60.35	-0.16	2.68
	300	2.11×10^{13}	63.69	61.01	1.22	
	600	1.33×10^{13}	62.77	60.09	-2.62	
	900	1.22×10^{13}	62.69	60.01	-3.38	
	1200	1.86×10^{13}	64.05	61.38	0.16	
	1500	1.6×10^{13}	63.79	61.11	-1.12	

4.2.4 Spectrophotometric investigation of the Chitosan Schiff bases:

The changes occurred in the electrolyte solution after immersing the mild steel samples for a particular immersion period can be determined by Atomic absorption spectroscopy and UV spectroscopic studies. Both AAS and UV results can provide some preliminary information about the complex formation in the solution phase and also the protective layer formation on the metal surface.

4.2.4.1 Atomic absorption spectroscopy:

In acid solution, the iron atoms of the metal are oxidized and Fe^{2+} ions are diffused into the electrolyte solution. The concentration of Fe^{2+} ions increases with the concentration of the acid and the temperature of the medium. Inhibitors prevent the attack on the metal and decrease the concentration of Fe^{2+} ions in the solution. AAS studies were carried out to determine the amount of Fe^{2+} ions in the bulk solution in the presence and absence of highest concentration of Chitosan Schiff bases after 6 h of immersion period. The IE was calculated using the equation (12) substituting the experimental results.

$$IE = \frac{\text{Amount of iron in blank - Amount of iron in sample}}{\text{Amount of iron in blank}} \times 100 \qquad (12)$$

Table 17 – IE from Atomic absorption spectroscopy obtained for higher concentration of Chitosan Schiff bases

Sample	Amount of iron content (mg/L)	IE (%)
Blank	1846	-
ChSSB	600	67.50
ChVSB	862	63.30
ChPSB	477	74.16
ChTSB	621	66.36

It can be seen that there is a decrease in the amount of the dissolved iron in the presence of the inhibitors compared to the blank solution. In the blank HCl solution the concentration of the dissolved Fe^{2+} is found to be 1846mg/L. Fe^{2+} concentration was reduced on the introduction of 1500 ppm of Chitosan Schiff bases. This may be attributed to the adsorption of the Chitosan Schiff bases on the mild steel surface thus preventing the

oxidation and diffusion of iron ions into the electrolytic solution (**Alaneme *et al*., 2016, Abboud *et al*., 2012**). The result is consistent with the trend observed with the weight loss technique.

4.2.4.2 UV-Visible spectroscopy Analysis:

UV-Visible absorption spectra were recorded for optimum concentration of Chitosan Schiff base polymers before and after 6 hours of immersion of mild steel specimens. The electronic absorption spectrum of Chitosan Schiff base polymers before the steels immersion shows broad bands in UV-region as depicted in Figure 29. These bands may arise due to π-π* and n- π* transitions with a considerable charge transfer character. After 6 hours immersion of steel samples change in the position of absorption maximum or change in the values of absorbance indicates the absence of Schiff bases in the solution.

The absence may be due to

i) the adsorption of schiff bases on the metal surface

ii) the complex formation with the metal cations in solution that is first dissolved from the metal surface (**Obi-Egbedi and Obot, 2013**)

The spectra of Chitosan Schiff base polymers before immersion showed the characteristic peak of n- π* due to the excitation of lone of pair of electrons on nitrogen and oxygen of the Schiff bases. The peak due to the transition of -HC=N π electrons to π* was also observed (Phase I). The spectra obtained after immersion reveals that the absorbance peaks in the region (220-250 nm and 280-320 nm) occurred for π- π* and n- π* respectively are decreased or disappeared. The decrease is well pronounced for n- π* transition compared to π- π* transition. This may be due to the donation of non- bonded electrons to the metal atom and sharing of π- electrons with the d-orbitals of iron. At the same time there are some significant new peaks at different wavelength after addition of Chitosan Schiff bases have been observed. This may indicate a new structure formation or degradation of original structure of Schiff bases.

These observations suggest the interaction between the Schiff bases and Fe^{2+} ions in the solution. Thus UV spectral findings give a strong evidence for the possibility of the formation of a complex between Fe^{2+} cation and Schiff bases in 1M HCl solution on the metal surface.

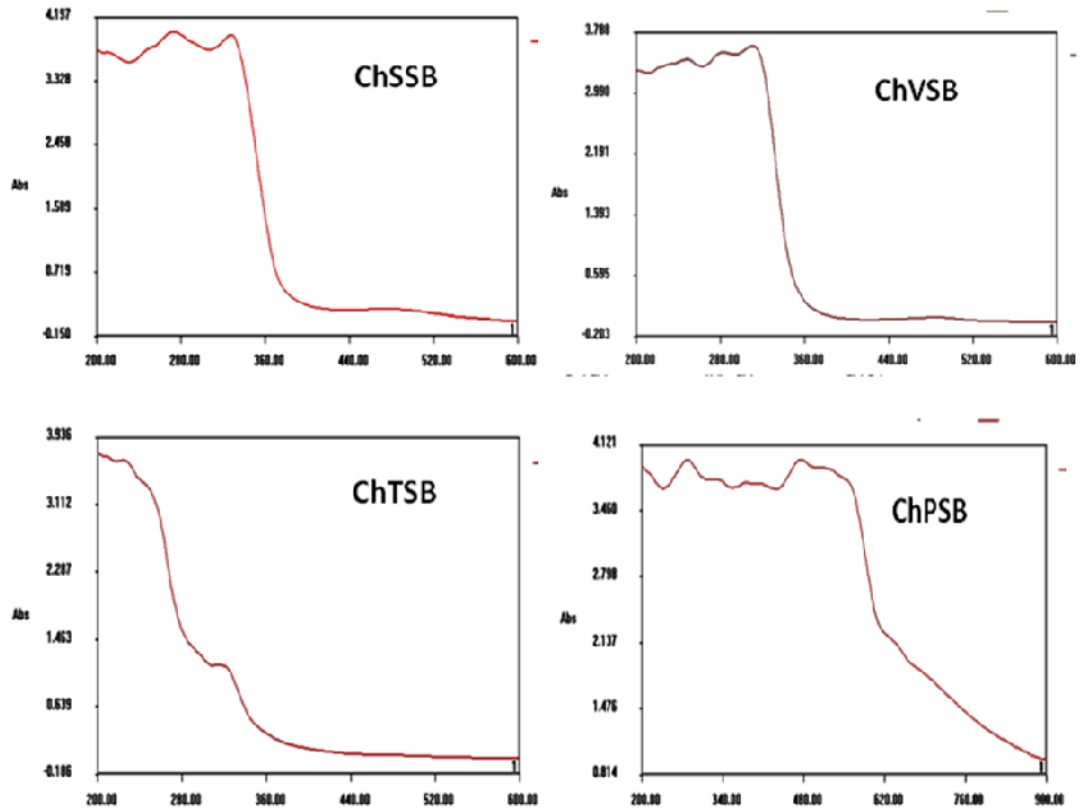

Figure 29 – UV spectra for chitosan schiff base solutions after immersing mild steel samples for 6 h of immersion

4.2.5 Corrosion monitoring techniques- Electrochemical method:

Corrosion phenomenon in aqueous environments is generally of electrochemical nature, they are dominated by the corrosion potential of the metal. Electrochemical methods in corrosion monitoring have been used ever since the electrochemical nature of the corrosion processes was discovered. Electrochemical techniques rely on the measuring of electrochemical potentials and/or currents to monitor corrosion damage. The electrochemical potential is related to thermodynamics of corrosion reaction while currents are related to reaction kinetics (corrosion rate). One of the most important applications of the electrochemical method has been the estimation of corrosion rate instantaneously by means of polarization resistance and potentiodynamic parameter (I_{corr}). Electrochemical techniques have been employed for speed data development and to understand corrosion mechanisms. Main advantages of these methods are short measuring time, high measurement accuracy, and the possibility of continuous corrosion monitoring.

Potentiodynamic polarization method:

A complete current-potential plot of a specimen can be measured in a few hours or in some cases in a few minutes. When a steel electrode is dipped in 1M HCl, both hydrogen reduction and iron oxidation processes occur on its surface. Typically the steel corrodes and the acid is reduced. The steel electrode can function as both anode and cathode, and both anodic and cathodic currents occur on the steel surface. Any corrosion processes that occur are usually a result of anodic currents. When a steel electrode is in contact with 1M HCl and the steel is not connected to the potentiostat, the steel assume a potential (relative to a SCE electrode) termed as corrosion potential, E_{corr}. A steel electrode at E_{corr} has both anodic and cathodic currents present on its surface. However, these currents are exactly equal in magnitude so there is no net current to be measured ie., the steel electrode is at equilibrium with the acid solution (even though it may be visibly corroding). E_{corr} can be defined as the potential at which the rate of oxidation is exactly equal to the rate of reduction. Experimentally one measures polarization characteristics by plotting the external current response as a function of the applied potential. Since the measured current can vary over several orders of magnitude, usually the log current function is plotted vs. potential on a semi-log chart. This plot is termed as a potentiodynamic polarization plot. The corrosion current density, I_{corr}, is obtained from Tafel plot by extrapolating the linear portion of the curve to E_{corr}. (**Khaled and Abdel-Shafi, 2013).**

Potentiodynamic polarization studies in presence of inhibitor are carried out to study the nature of the inhibitor by analyzing the cathodic and anodic curves. The changes occurred in the current-potential characteristics resulting from the polarization curves of the MS in 1M HCl in presence of Chitosan Schiff bases are evaluated. The corrosion kinetic parameters obtained from the polarization curves for the studied inhibitors were also discussed.

4.2.5.1 Chitosan Schiff bases as corrosion inhibitor – Potentiodynamic polarization measurements:

Polarization measurements are suitable for monitoring the progress and mechanism of the anodic ($Fe \rightarrow Fe^{2+} + 2e^-$) and cathodic ($2H^+ + 2e^- \rightarrow H_2$) partial reactions as well as identifying the effect of Chitosan Schiff bases on either partial reaction. The polarization behaviour of the Chitosan Schiff bases viz ChSSB, ChVSB, ChTSB and ChPSB of different concentrations (100-1500 ppm) at 303 K was studied. The polarization curves in the absence and presence of the Chitosan Schiff bases were obtained and by extrapolation method, the polarization parameters like corrosion potential (E_{corr}), corrosion current density (I_{corr}), anodic

and cathodic slopes were also determined. The IE was calculated from the polarization measurements according to the equation (5).

4.2.5.2 Polarization behaviour of Chitosan Pyrrole carboxaldehyde Schiff base (ChPSB)- Effect of concentration:

The changes observed in the polarization curves after the addition of the inhibitor are usually used as criteria to classify inhibitors as cathodic, anodic or mixed type **(Rosliza and Nik, 2010**). Figure 30 shows the results of the effect of different concentrations of ChPSB on the cathodic and anodic polarization curves of MS in 1M HCl solutions at 303 K.

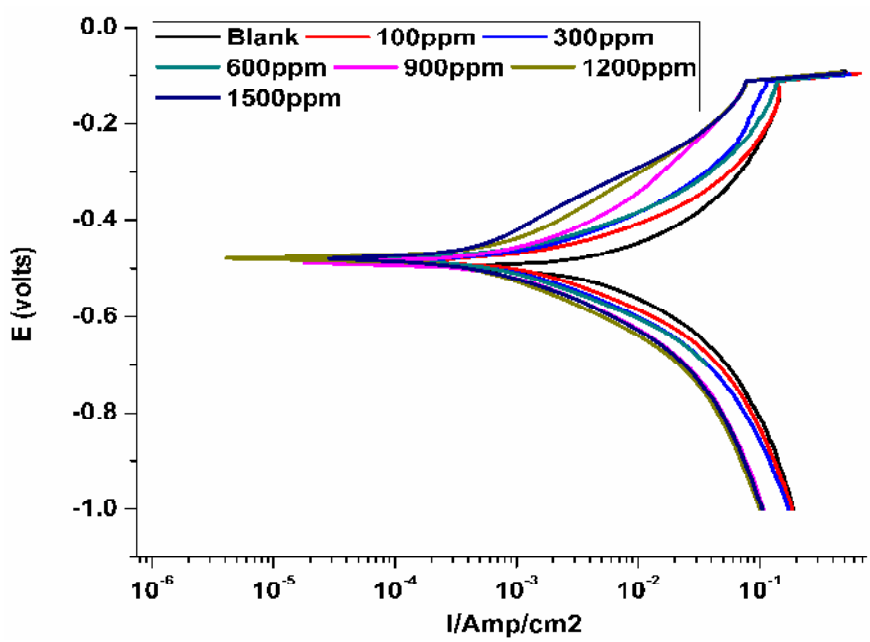

Figure 30 - Potentiodynamic polarization curves of MS in 1 M HCl in the absence and in the presence of ChPSB at various concentrations

The polarization curves at its first sight demonstrates that in presence of ChPSB, the cathodic and anodic branches of the polarization curves are shifted towards lower current to very similar extent probably as a consequence of the blocking effect of the adsorbed inhibitor molecules (**Amin *et al*., 2010**). Figure 30 clearly suggests that both the cathodic and anodic curves were affected by the addition of ChPSB thereby reducing the cathodic hydrogen evolution reaction and anodic dissolution of iron respectively. This indicates that the inhibitor has controlled both the cathodic and anodic reactions without affecting the reaction mechanism (**Zhang *et al*., 2011**). Also, the parallel nature of the cathodic polarization curves and Tafel lines with nearly equal slopes indicates that hydrogen evolution reaction is

activation controlled and the presence of the inhibitor does not affect the hydrogen- reduction mechanism through charge transfer (**Senthil kumar *et al*., 2010, Qian *et al*., 2013, Deng *et al*., 2014).**

The electrochemical parameters such as corrosion potential (E_{corr}), corrosion current density (I_{corr}), cathodic and anodic Tafel slopes (b_c, b_a) obtained from polarisation curves by Tafel extrapolation method, and corresponding inhibition efficiency (IE) values at different inhibitor concentrations are given in Table 18.

Table 18 - Polarization parameters of the MS in 1M HCl containing various concentration of ChPSB at room temperature (303 K)

Concentration (ppm)	b_a (V/dec)	b_c (V/dec)	I_{corr} (mA/cm^2)	IE I_{corr} (%)	Rp Ωcm^2	IE Rp (%)	E_{corr} (mV/SCE)
Blank	0.163	0.132	4.175		6.509		-495.45
100	0.144	0.12	1.365	67.31	15.132	56.98	-476.17
300	0.132	0.116	0.806	80.7	21.532	69.77	-476.23
600	0.108	0.085	0.631	84.88	27.163	76.03	-476.92
900	0.145	0.150	0.681	83.68	50.252	87.05	-478.73
1200	0.108	0.127	0.414	90.09	51.287	87.31	-476.92
1500	0.103	0.136	0.391	90.64	52.955	87.71	-477.29

It is evident from the table that the value of b_c changed with the addition of inhibitor, indicating the influence of the inhibitor on the kinetics of the hydrogen evolution. The gradual change in cathodic Tafel slope (b_c) upon increasing the inhibitor concentrations is the reason for the parallel nature of the Tafel lines. This implies that the hydrogen evolution reaction is activation-controlled and the addition of ChPSB inhibits the hydrogen evolution reaction (**Amin *et al*., 2010, Jeyaprabha *et al.,* 2005, Abd El Rehim *et al*., 2001, Moretti *et al*., 1996**). The shift in the anodic Tafel slope b_a may be due to the adsorption of inhibitor molecules or chloride ions on the metal surface. The adsorbed inhibitor may form a surface film on the metal surface thereby acting as a physical barrier to restrict diffusion of ions to or from the metal surface and hence retard the corrosion process (**Saliyan and Adhikari, 2008, Tourabi *et al*., 2013**). The interaction between the adsorbed inhibitor film and metal atoms on the metal surface may act as a simple blocking effect to prevent the corrosion process.

No significant changes were observed in E_{corr} values in presence of inhibitor. From the literature it is stated that, if the displacement in (E_{corr}) values is greater than 85 mV in inhibited system with respect to uninhibited system, the investigated inhibitor could be categorized as cathodic or anodic type and if displacement in E_{corr} is less than 85 mV, it could be categorized as mixed-type **(Riggs (1973), Ferreira *et al.,* 2004 and Li *et al.,* 2008)**. For the inhibitor ChPSB, the minimal change in E_{corr} values is seen towards positive direction in presence of inhibitor compared to the E_{corr} value in the blank solution. Therefore the inhibitor inhibits corrosion by controlling both anodic and cathodic reactions (mixed-type inhibitor). The displacement value was found to be less than 85 mV supporting the mixed type behaviour of the inhibitor (**Yurt *et al*., 2007**).

The corrosion rate is directly proportional to the value of the corrosion current density, which is a measure of rate of the reaction in electrochemistry. For all the inhibitor concentrations studied, lower current density (I_{corr}) values were observed with respect to the inhibitor free solution (blank). This behavior confirms the increase in the energy barrier of mild steel dissolution process (**Xometl *et al*., 2008, Migahed *et al*., 2005**) and the increase of the relative ability of a material to resist corrosion (**Kerkouche *et al*., 2008, Alsabagh *et al*., 2014**). The decrease in the current density with increase in concentration of inhibitor confirmed the corrosion inhibition activity of ChPSB.

The corrosion inhibition efficiency (IE %) of ChPSB was evaluated from the measured I_{corr} values using the equation (5). It is apparent that the IE increases with the concentration of ChPSB. This may be attributed to the increase in surface coverage of steel surface due to adsorption of more number of inhibitor molecules on the metal surface thus providing high protection from the acid attack (**Alsabagh *et al*., 2014, Atta *et al*., 2015a).**

The polarization resistance (Rp) is calculated based on the Stern-Geary kinetics equation (**Stern and Geary, 1957**),

$$Rp = \frac{b_a b_c}{2.303 Icorr(b_a + b_c)} \qquad (13)$$

where, b_a and b_c are the slopes of the anodic and the cathodic Tafel lines, respectively. From the equation, it is clear that I_{corr} and Rp is inversely proportional to each other. Obtained results show that the addition of inhibitors causes increase in the polarization resistance. IE was calculated using the equation,

$$IE(\%) = \frac{Rp - Rpcorr}{Rp} X\,100 \qquad (14)$$

where Rp_{corr} and Rp are the polarization resistance of MS in the uninhibited and inhibited solutions, respectively. The Rp value increased with the increase in concentration ChPSB (Table 18). The increase in Rp values suggest that the inhibition efficiency increases with inhibitor concentration. The increase in the resistance and IE indicated the adsorption of inhibitor molecules which imparts higher protection of the interface against reactions associated with metal dissolution. Inhibition efficiency values calculated from potentiodynamic polarization and linear polarization methods were found to follow the same trend.

In acidic solutions, Chitosan Schiff bases exist as protonated species. These protonated species may adsorb on the cathodic sites of the steel, inhibiting hydrogen evolution reaction. The adsorption on anodic sites may occur through lone pair of electrons of unprotonated nitrogen atom in imine group and oxygen atoms of –OH groups of Chitosan Schiff bases, which retards anodic dissolution of steel. The changes occurred in the anodic and cathodic Tafel curves after the addition of inhibitor also support the behavior of mixed type nature of the inhibitor.

4.2.5.3 Effect of temperature on the Polarization behaviour of Chitosan Pyrrole carboxaldehyde Schiff base (ChPSB):

In order to gain more information about the type of adsorption and the effectiveness of ChPSB at higher temperature, polarization experiments were conducted in the range of 313-343 K in absence and presence of different concentrations of ChPSB. Temperature can modify the interaction between the steel electrode and the corrosive environment with and without the inhibitor. Figure 31 & 32 represents the effect of ChPSB (100 ppm and 1500 ppm respectively) on the cathodic and anodic regions of polarization curves in the temperature range of 313-343 K. The shapes of the polarization plots, in all cases, for ChPSB solutions are not substantially different from those of blank solution. This means that the inhibitor does not alter the electrochemical reactions responsible for corrosion process. The polarization curves show that the inhibitor ChPSB modifies both the anodic and cathodic current density and there is no definite trend in the shift of E_{corr} values is observed for all the studied temperatures.

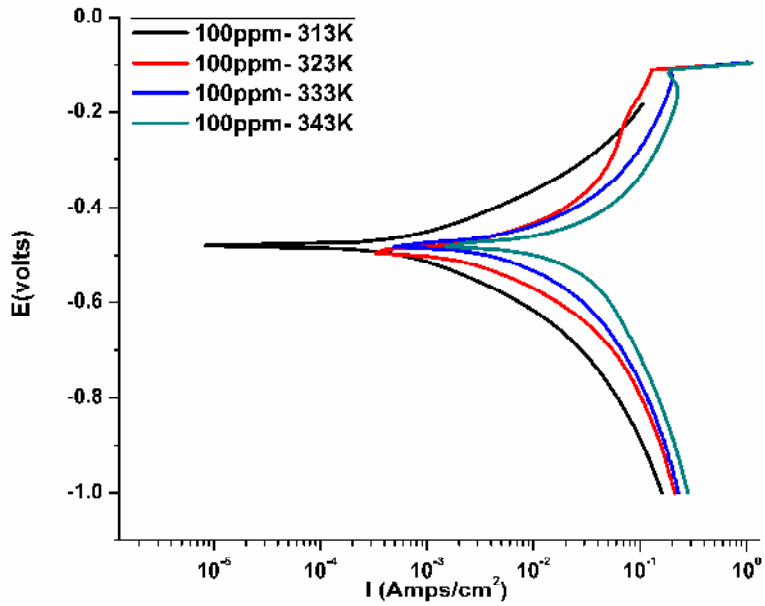

Figure 31 - Potentiodynamic Polarization curves of MS in 1 M HCl in the presence of 100 ppm of ChPSB at various temperatures

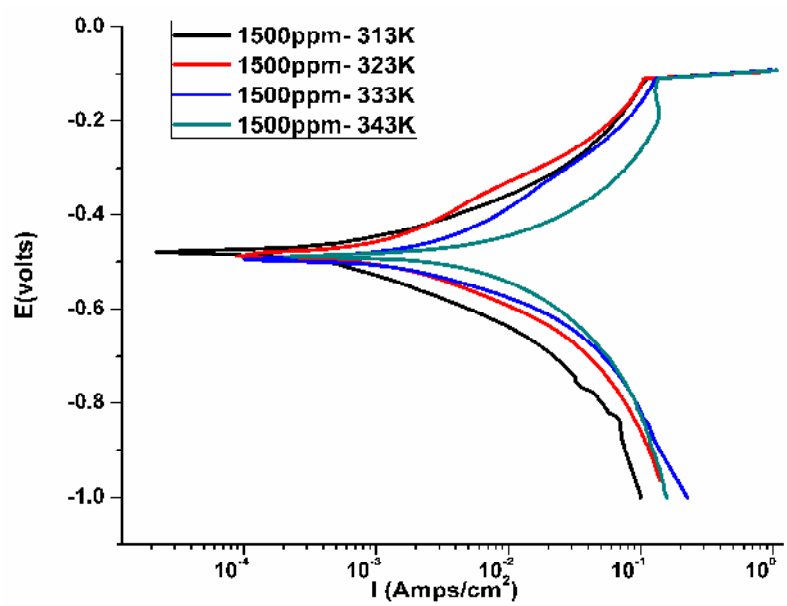

Figure 32 - Potentiodynamic Polarization curves of MS in 1 M HCl in the presence of 1500 ppm of ChPSB at various temperatures

The polarization behaviour of MS in 1M HCl in absence and presence of lower (100 ppm) and optimum concentration (1500 ppm) is given in Table 19 & 20. For convenience the results obtained for other concentrations are given in Appendix A7.

Table 19 - Polarization parameters of the MS in 1M HCl containing 100ppm and 1500ppm of ChPSB at 313-343 K

Temp (K)	b_a (V/dec)			b_c (V/dec)			E_{corr} (mV/SCE)		
	Blank	100	1500	Blank	100	1500	Blank	100	1500
313	0.214	0.202	0.125	0.151	0.178	0.150	-491.91	-485.68	-479.43
323	0.245	0.173	0.090	0.158	0.161	0.105	-478.70	-485.26	-478.07
333	0.205	0.134	0.119	0.143	0.101	0.124	-472.24	-471.75	-485.19
343	0.267	0.221	0.158	0.161	0.148	0.111	-469.91	-471.45	-478.19

Table 20 - IE obtained from Polarization parameters of the MS in 1M HCl containing 100 ppm and 1500 ppm of ChPSB at 313-343 K

Temp (K)	I_{corr} (μA/cm^2)			IE I_{corr} (%)		Rp Ωcm^2			IE Rp (%)	
	Blank	100	1500	100	1500	Blank	100	1500	100	1500
313	7.91	2.81	0.75	64.42	90.53	4.313	15.481	41.699	72.13	89.65
323	12.08	3.20	0.45	73.48	96.21	3.124	9.321	26.360	66.49	88.15
333	12.38	3.07	0.83	75.16	93.27	2.092	5.025	14.459	58.36	85.53
343	21.09	13.68	2.00	35.14	90.49	1.412	1.928	5.168	26.73	72.66

The Anodic current densities (b_a) in presence of ChPSB decreases with increase in temperature compared to their respective anodic current density in blank solution. This behaviour suggests that the inhibitor suppressed anodic reaction by reducing the anodic metal dissolution reaction through blocking of inhibitor molecules. But the similar change was not observed for cathodic current densities (b_c). There is no particular trend followed in the cathodic current densities in presence of ChPSB and a parallel cathodic Tafel curves indicates that the inhibitor does not modify the hydrogen evolution mechanism and the reduction of hydrogen ions on the mild steel surface takes place mainly through a charge transfer mechanism (**Issadai *et al*., 2011, Behpour *et al*., 2009**).

From the data in Table 19 & 20, it is evident that the ChPSB acted as an adsorptive inhibitor even at higher temperatures ie., it reduces anodic dissolution and also, retards the oxygen evolution reaction via blocking the active reaction sites on the MS surface and therefore protect it from the action of the corrosion medium (**Khaled, 2010a**). The values of E_{corr} do not change significantly in the presence of ChPSB in the temperature range of

313-343 K. An inhibitor can be classified as an anodic or cathodic type inhibitor if the change in value of E_{corr} is larger than 85 mV (**Assashi sorhabi *et al*., 2005**), but a minimal shift in the E_{corr} was seen in this present investigation, from which it can be concluded that ChPSB acts as mixed type inhibitor (**Zou *et al*., 2014**).

It is noticeable that the corrosion current density (I_{corr}) for mild steel in 1M HCl increased more rapidly by increasing the temperature. The increase in I_{corr} indicates the increase in hydrogen gas evolution (cathodic reaction) and also iron corrosion (anodic reaction) in the corrosive solution **(Amin *et al*., 2011**). The corrosion current density decreases in the presence of ChPSB compared to its blank across all the temperature range studied. The corrosion current density I_{corr} decreased significantly with increasing inhibitor concentration, it indicates that the addition of the inhibitor reduces the corrosion process in the aggressive medium (**Zou *et al*., 2014**).

The inhibition efficiency (IE%) increases with temperature upto 323 K indicating the stability of the inhibitor and the adsorbed film on the metal surface. This result ensures the ability of the polymeric adsorption layer formed on the MS at elevated temperature. The maximum inhibition efficiency was found to be 96% at 323 K for optimum concentration of 1500 ppm of ChPSB. There occurs a sudden fall at temperatures 333 K and 343 K, but still providing a better IE around 90%. This may be attributed to the degradation of the polymeric molecules into smaller segments thereby adhering to the active sites of the MS surface and hence larger IE obtained (**Fares *et al*., 2012a**). The decrease of inhibition efficiency with a rise in temperature was attributed to the alteration of the rate of adsorption/desorption ratios in favor of desorption process (**Zucchi *et al*.,1977).** Such behavior can be interpreted on the basis that the inhibitor acts by adsorbing onto the metal surface, and an increase in temperature results in desorption of some adsorbed inhibitor molecules, leading to a decrease in the inhibition efficiency.

The presence of ChPSB on the MS surface was indicated by the increase in Rp values. Increase in Rp at higher temperatures is an indication of higher protection of the interface against reactions associated with metal dissolution. With increase in the concentration of ChPSB, Rp values were found to increase leading to higher surface coverage at the investigated temperature range (Table 20). The inhibition efficiency increased with temperature upto 323 K. On further increase in temperature, the inhibition efficiency decreased and was ascribed to the increased desorption of the inhibitor from the surface.

4.2.5.4 Electrochemical behaviour of the other investigated Chitosan Schiff bases – Effect of concentration:

The current-potential characteristics of other Chitosan Schiff bases (ChSSB, ChVSB, ChTSB) under investigation were analyzed using potentiodynamic polarization measurements. Figure 33, 34 & 35 shows the polarization curves obtained for different concentrations of ChSSB, ChVSB, ChTSB at 303 K.

It is clear that both the anodic and cathodic reactions of MS in 1M HCl are highly inhibited in the presence of the inhibitors. Thus, addition of these inhibitors reduces the metal dissolution as well as retarding the hydrogen evolution reaction. The inhibitors produced a markedly decrease in the corrosion rate, i.e. shifts the anodic curves to more positive potentials and the cathodic curves to more negative potentials. This may be ascribed to adsorption of the inhibitors over the corroded surface. Values of the corrosion current densities (I_{corr}), corrosion potential (E_{corr}), cathodic Tafel slope (b_c), and anodic Tafel slope (b_a) were calculated from Figures 33-35 and are listed in Appendix A3.

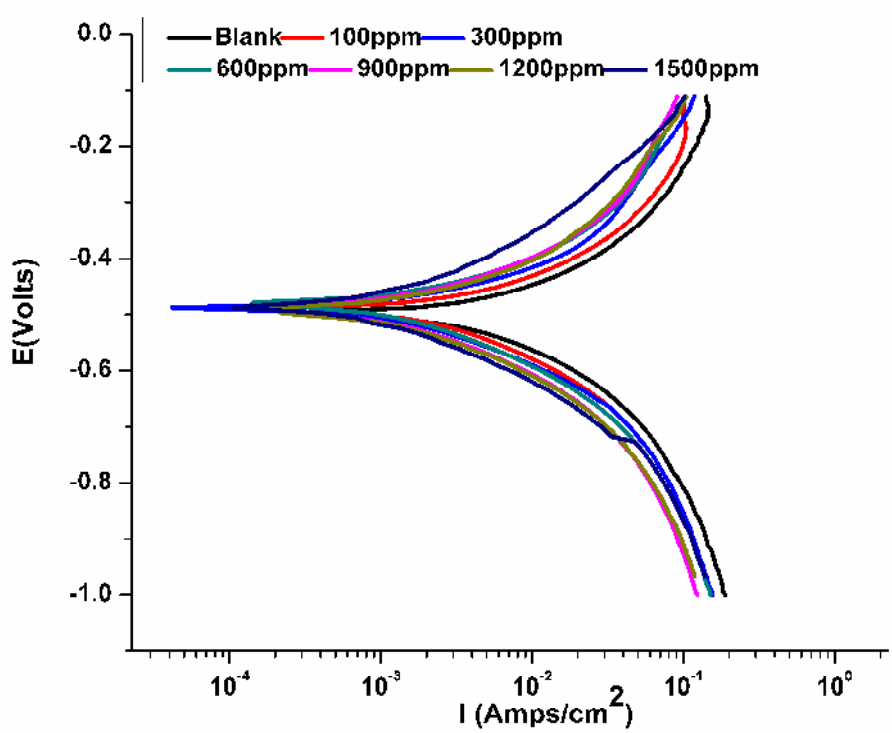

Figure 33 - Potentiodynamic polarization curves of MS in 1 M HCl in the absence and in the presence of ChSSB at various concentrations

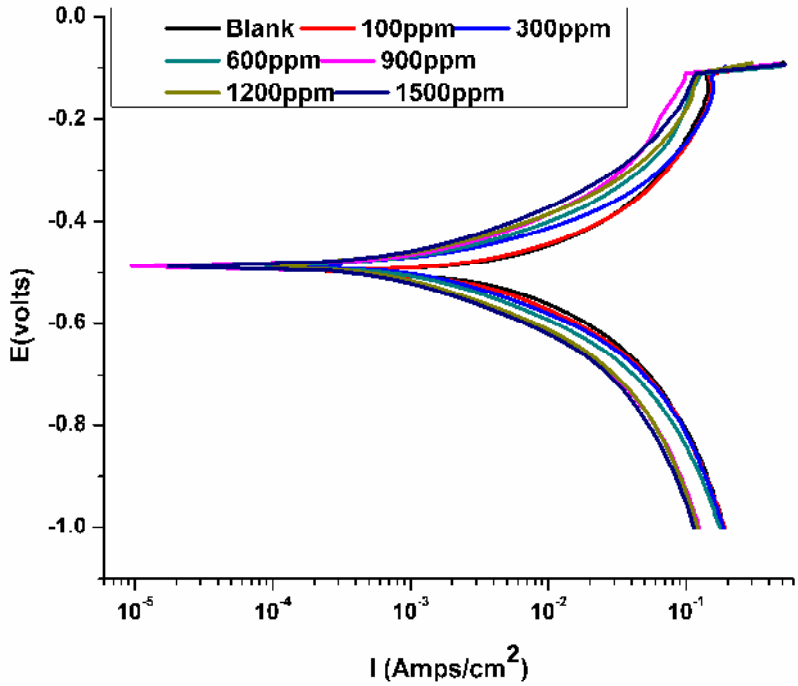

Figure 34 - Potentiodynamic polarization curves of MS in 1 M HCl in the absence and in the presence of ChTSB at various concentrations

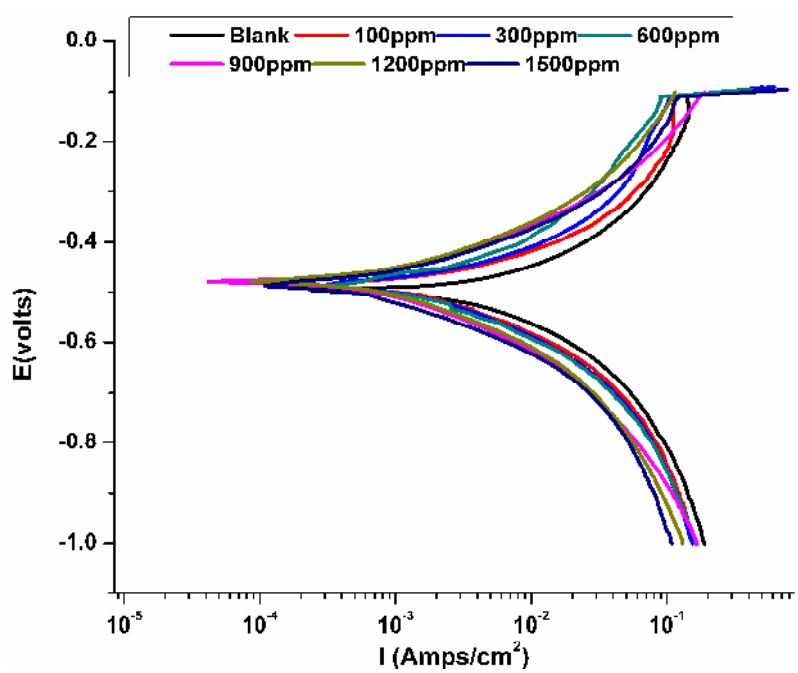

Figure 35 - Potentiodynamic polarization curves of MS in 1 M HCl in the absence and in the presence of ChVSB at various concentrations

The values of cathodic Tafel slope (b_c) and anodic Tafel slope (b_a) of Chitosan Schiff bases were found to change with inhibitor concentration, indicated that the inhibitors controlled both the reactions without affecting the mechanism. In other words, the inhibitors decrease the surface area for corrosion without affecting the mechanism of corrosion and only cause inactivation of a part of the surface with respect to the corrosive medium (**Al-sabagh *et al*., 2011**). From these data, it is clear that the corrosion current decreases with the increase of the inhibitor concentration. The presence of the synthesized Chitosan Schiff bases does not remarkably shift the corrosion potential, while the anodic and cathodic Tafel slopes change with the increase of the inhibitor concentration. Therefore, the investigated inhibitors can be categorized as mixed type of inhibitors. The value of inhibition efficiency was increased with increasing the inhibitor concentration indicating that the higher surface coverage of the adsorptive film was achieved at optimum concentration. This could be explained on the fact that the adsorption process enhances with increasing inhibitor concentration. Since the polymers being larger moieties impart a large surface coverage of the metal surface they can cover a number of active sites at optimum concentration.

Effect of Temperature:

Electrochemical behaviour of the Chitosan Schiff bases were investigated using Potentiodynamic polarization method at various temperatures (303-343 K). From the above discussion, it is clear that the concentration has a positive effect on the IE and a highest IE was obtained for 1500 ppm of inhibitor for all studied inhibitors. So the polarization data obtained from optimum concentration of the inhibitors at 303-343 K is listed in Table 21. The polarization parameters of all the Chitosan Schiff bases obtained for various concentrations at various temperatures are listed in the Appendix A4 - A6.

From the Table 21, it is seen that the corrosion potential values remain almost the same or slightly shifted in both the directions for all the polymers at all temperatures. The displacement in the E_{corr} values with respect to blank HCl solution is less than 85 mV which is indication of mixed inhibitory action of the inhibitors.

Table 21 - Polarization parameters for the other investigated inhibitors for concentration of 1500 ppm at 313 – 343 K

Inhibitor system at 1500ppm	Temp	b_a (V/dec)	b_c (V/dec)	I_{corr}(mA/cm^2)	IE I_{corr} (%)	Rp Ωcm^2	IE Rp Ωcm^2	E_{corr} (mV/SCE)
ChSSB	303	0.102	0.089	0.3965	90.50	26.407	75.35	-464.2
	313	0.152	0.126	0.724	90.86	35.929	87.99	-486.92
	323	0.120	0.127	0.635	94.75	26.816	88.35	-478.13
	333	0.102	0.163	1.409	88.62	15.36	86.38	-478.69
	343	0.156	0.116	4.612	78.13	5.4851	74.24	-485.27
ChVSB	303	0.102	0.078	0.371	91.11	30.791	78.86	-476.16
	313	0.109	0.090	0.104	98.68	29.7	85.47	-477.32
	323	0.197	0.151	1.502	91.34	25.236	87.62	-488.84
	333	0.111	0.129	1.662	86.57	14.127	85.19	-491.83
	343	0.159	0.162	3.738	82.28	4.5464	68.92	-483.29
ChTSB	303	0.136	0.152	1.102	73.60	30.213	78.45	-487.02
	313	0.124	0.098	1.227	84.50	16.805	74.33	-488.09
	323	0.078	0.086	0.28	97.69	25.14	87.57	-477.76
	333	0.130	0.144	1.038	91.62	15.534	86.53	-484.82
	343	0.129	0.126	1.751	91.70	3.9164	63.92	-470.59

Table 21 reveals that the IE (derived from I_{corr} and Rp) increases with temperature till 323 K for all the studied inhibitors. This confirms that the film forming property of the Chitosan favours in the formation of stable adsorptive film on the metal surface till 323 K. The slight fall in the IE is observed in the temperatures 333 K and 343 K, though the better IE is produced. The decrease in IE is due to the disturbed stability of the adsorbed film on the metal surface because of the induced polarization combined with high temperature. The inhibitive action of Chitosan Schiff bases mainly attributed to the presence of –HC=N groups in the polymer matrix along with π-electron clouds present in the anchoring groups of aldehydes. Moreover, the longer molecular size ensures the greater adsorption on the MS steel surface and decreases the effective area for corrosion reaction by blocking the reaction sites.

Comparative study of polarization behavior of native Chitosan with Chitosan Schiff bases:

For a better understanding, 1500 ppm concentration of Chitosan was evaluated for its inhibition performance using potentiodynamic polarization technique and compared with the optimum concentration of Chitosan Schiff bases (1500 ppm).

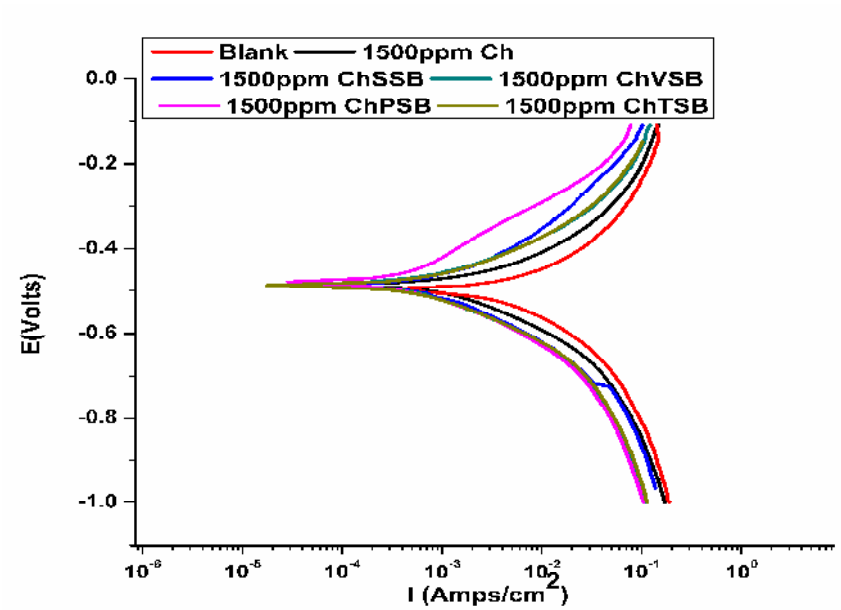

Figure 36 - Comparative Potentiodynamic polarization curves of MS in 1 M HCl in the absence and in the presence of Chitosan and Chitosan Schiff bases at 1500 ppm concentration

From the Figure 36, it is obvious that the Chitosan Schiff bases exhibit high inhibition performance than Chitosan. The Tafel behaviour of the Chitosan Schiff bases clearly suggests that they are better inhibitors on comparing to Chitosan.

4.2.6 Electrochemical impedance spectroscopy:

Electrochemical Impedance Spectroscopy (EIS) is a powerful, rapid and accurate non-destructive method. EIS has many advantages in comparison with other electrochemical techniques. In these experiments, a small amplitude AC signal that do not disturb the electrode properties to be measured is applied to the system for the evaluation of a wide range of materials, including coatings, anodized films and corrosion inhibitors. It can provide detailed information of the systems under examination such as corrosion rate, electrochemical mechanisms, reaction kinetics and detection of localized corrosion.

Chitosan Schiff bases as corrosion inhibitor – EIS method:

An EIS impedance measurement is a veritable tool, widely used in investigating corrosion inhibition processes. It provides information on both the resistive and capacitive behavior at interface and makes possible to assess the performance of the investigated compounds as possible inhibitors against metallic corrosion (**Bentiss *et al.*, 2010**). To get more information about the corrosion inhibition phenomenon i.e. the nature of the electrochemical process occurring at the solution/ metal interface and also to monitor the metal dissolution process in presence of inhibitors, impedance measurements have been carried out in 1 M HCl solution in the absence and presence of different concentrations of the Chitosan Schiff bases at the open circuit potential (OCP) at room temperature and at higher temperatures.

4.2.6.1 Impedance behaviour of Chitosan Thiophene 2- carboxaldehyde Schiff base (ChTSB) -Effect of concentration:

The representative Nyquist and Bode plots of mild steel in 1M HCl in the presence and absence of different concentrations (100-1500 ppm) of ChTSB at room temperature are given in Figure 37.

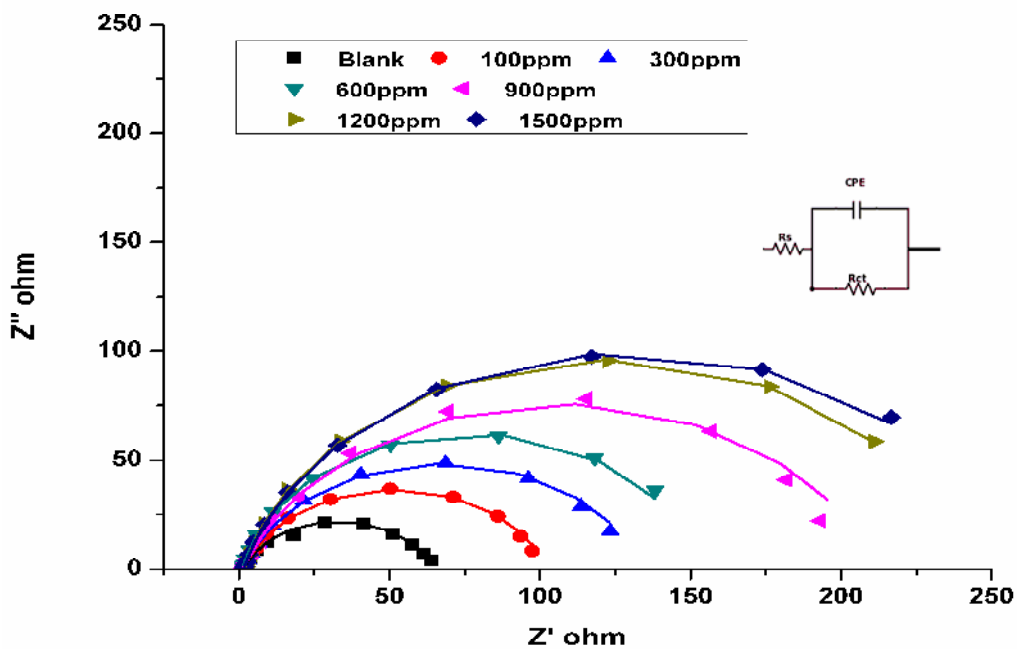

Figure 37 - Nyquist plots for mild steel in 1M HCl in the absence and presence of ChTSB.

The Nyquist plots are not perfect semicircles and this deviation from perfect circles often known as frequency dispersion which can be attributed to surface roughness and inhomogeneities of the solid surface (**Mansfeld, 1981, Growcock and Jasinki, 1989, Popova *et al*., 1996**, **Bentiss *et al*., 2000, Benabdellah *et al*., 2011, Deng *et al*., 2010, Bentiss *et al*., 2010**). According to the theory of EIS, real condenser that has charge distribution on both plates yield perfect semicircle. But, during corrosion, formation of a double layer at the metal/ solution interface occurs unevenly due to dispersing effect causing imperfect semicircles (**Senthilkumar *et al*., 2010).** The depressed semicircle shape of the Nyquist plots indicates that the corrosion of mild steel in acid solution is mainly controlled by charge transfer process (**Morad (2000), Ardelean *et al*., 2009**).

The impedance response i.e. the Nyquist plots of mild steel in 1M HCl was significantly changed after the addition of ChTSB. The Nyquist plots exhibit the single depressed capacitive loop over the frequency range studied and the diameter of the loop increased with increase in the concentration of ChTSB. This implies that the metal dissolution process is controlled by single transfer process that is unaffected by the addition of inhibitor molecules (**Sasikumar *et al*., 2015, Umoren *et al*., 2015**). The increase in the diameter of the loop suggests that the mild steel corrosion is inhibited with the increasing concentration of the ChTSB. It is worth noting that the change in concentration of ChTSB did not alter the profile of the impedance behaviour, suggesting ChTSB did not affect the corrosion mechanism. The similar shape of Nyquist plot also suggests the geometric blocking effect of the inhibitor (**Bentrah *et al*., 2014**).

In the evaluation of Nyquist plots, the difference in real impedance at lower and higher frequencies is considered as a charge transfer resistance. This charge transfer resistance corresponds to the resistance between the metal and outer Helmholtz plane (OHP). In this perspective, contribution of all the resistances corresponding to the metal/solution interface i.e., charge transfer resistance (R_{ct}), diffuse layer resistance (R_d), accumulation resistance (R_a), inhibitor resistance (R_f), etc must be taken into account. Thus, the difference in real impedance at lower and higher frequencies is considered as polarization resistance (R_p). The electrical double layer can be signified by the electrical equivalent circuit diagrams to model the metal/solution interface. The obtained EIS data were fitted according to the electrical equivalent circuit diagram and thereby calculating the impedance parameters.

Equivalent circuit for fitting the data:

The Nyquist plot can be represented and fitted using an equivalent circuit model called Randle's circuit. The equivalent circuit is generally comprised with a resistor, capacitor and inductor (Figure 38). For metal dissolution process, the equivalent circuit is designed with a resistor and capacitor in parallel with each other. The Nyquist Plot for Randle's cell consisting of the above elements is always semicircle. The solution resistance can be determined from the real axis value at the high frequency intercept. This is the intercept near the origin of the plot. The low frequency region gives us the sum of solution resistance and polarization resistance.

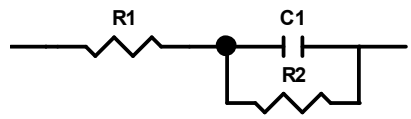

Figure 38 - Randle's Equivalent circuit

EIS spectra of the Schiff bases were analyzed using the equivalent circuit in Figure 39, which represents a single charge transfer reaction and fits well with our experimental results.

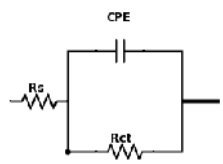

Figure 39 - Equivalent circuit used for fitting the data

In this circuit, R_s is the solution resistance and Rct is the charge transfer resistance. Rct is replaced by polarization resistance R_p, because of the aforementioned reason. Solution resistance (R_s) is the ionic resistance which depends on the concentration of the ions present in the solution, type of ions and geometry of the area through which the current is carried. The interface of metal in electrolyte is visualized as space that exists between assembly of ions on the electrode surface and assembly of solvated ions away from the surface. These two assemblages can store charge in them and acts as a capacitor element. Thus, the capacitance generated by them is represented as double layer capacitance, C_{dl}. The Nyquist plots obtained for the Chitosan Schiff bases are not perfect ideal plots as described in the EIS theory. This is because of the double layer which does not behave as an ideal capacitor. In the metal/solution interface, the charge transfer reaction is controlled by

both the charges from metal side as well as ions from the solution side. Obviously, the number of ions is more in the electrolytic solution than the charges present on the metal. Therefore the equivalent ions to the charges on the metal occupy a huge volume in the double layer from the solution side of the interface. This behaviour deviate the double layer from behaving as an ideal capacitor and thus the double layer capacitance are replaced by constant phase element CPE. By this suggestion, the capacitor in the equivalent circuit can be replaced by a so-called constant phase element (CPE). Generally, the use of CPE is required in the equivalent circuit because of the presence of inhomogeneties at the micro or nano level such as the surface roughness, adsorption or diffusion (**Atta *et al.*, 2015, Mobin and Rizvi, 2017**). A CPE element is used in place of C_{dl} in order to get better fitting results as the metal/solution interface does not behave as a real capacitor.

Double layer capacitance associated with the CPE element is calculated using the following formula:

$$CPE_{dl} = (Y_o.R_p1\text{-}n)^{1/n} \qquad (15)$$

Where Y_o is the magnitude of the CPE, and n is the phase shift which can serve as a measure of the surface heterogeneity. The n value usually lays around -1 to 1. Good surface condition of the metal was indicated by the values of n ranging from 0 to 1 (**Markhali *et al.*, 2013**). The impedance parameters derived from fitting the equivalent circuit are listed in Table 22. From the table, values of n found to be in the range of 0 to 1 and increases when compared with blank solution and with the concentration can be explained by some decrease of the surface heterogeneity due to the adsorption of the ChTSB on the most adsorption active sites (**Traisnel *et al.*, 2007, Lebrini *et al.*, 2009**).

Table 22 - Impedance parameters for mild steel in 1M HCl in presence and absence of Chitosan Schiff base (ChTSB)

Concentration (ppm)	Rs (Ωcm^2)	n	R_p (Ωcm^2)	$X^2 \times 10^{-3}$	IE%	$Y_o \times 10^{-6}$	CPE (F)	IE%
Blank	1.369	0.764	63.44	2.2891		416.6	9.63	
100	1.257	0.792	101.30	0.4538	37.37	321.5	4.88	49.31
300	1.368	0.803	131.00	1.4873	51.57	402.2	5.74	40.35
600	1.271	0.876	152.00	0.6518	58.26	407.7	1.94	79.84
900	1.500	0.830	204.00	6.3137	68.90	187.1	1.62	83.14
1200	1.717	0.850	241.00	0.3666	73.68	333.7	2.44	74.57
1500	1.554	0.839	256.00	0.3095	75.22	357.3	3.19	66.83

It is clear from Table 22, the CPE values decreased and polarization resistance increased after the addition of the inhibitor and increase in trend is more pronounced with increasing inhibitor concentration. R_p increased from 63.44 Ωcm^2 to 256 Ωcm^2 at 303 K for the concentration ranging from 100 to 1500 ppm. A large charge-transfer resistance is associated with a slower corroding system (**Traisnel *et al*., 2007, Bouanis *et al*., 2009, Bentiss *et al*., 2009a**). The change of R_p can be related to the gradual replacement of water molecules by ChTSB molecules on the surface and consequently leads to decrease in the number of active sites necessary for the corrosion reaction. R_p is inversely proportional to the corrosion rate, the increase in R_p value is attributed to the formation of protective film on the metal/solution interface. Moreover, the decrease in the CPE which can result from a decrease in local dielectric constant and/or an increase in the thickness of the adsorbed protective layer on the electrode surface and other ions originally adsorbed on the surface by adsorption of inhibitor molecules on the metal surface (**Ahamad *et al*., 2010**) therefore enhancing the corrosion resistance of the studied steel. The adsorptions of larger ChTSB molecules also reduce the capacitance through the increase in the double layer thickness.

It is generally assumed that acid corrosion inhibitors adsorb on the metal surface and the structure of double layer changes with reducing electrochemical partial reaction rate. The capacitance is considered as the electrical capacitor between charged metal surface and solution. Inhibition process takes place by a decrease in the electrical capacity of the mild steel surface in the presence of the inhibitor and this could be related with the decrease in the corrosive area on the mild steel surface owing to the increase of the inhibitor covered area. The decrease of capacitance values may be due to the adsorption of ChTSB on metal surface thus leading to a film formation on the mild steel surface that has led to an increase in percentage inhibition efficiency (IE). The capacitance values decrease due to an increase in the thickness of the electrical double layer and/or a decrease in local dielectric constant that are caused by the adsorption of ChTSB molecules on the mild steel surface.
The IE was determined from the Rp values by the following equation,

$$IE\% = \frac{Rp - Rp'}{Rp} \square 100 \qquad 16$$

The R_p values for the inhibited system is higher when compared to the uninhibited which is due to the reduction in metal dissolution and the increased R_p values with an increase in concentration attributed to the higher surface coverage of the inhibitors on the mild steel surface. The maximum inhibition efficiency (75%) was achieved at an inhibitor concentration of 1500 ppm. A strong adsorption of inhibitor on steel surface indicates a more surface

coverage by the inhibitor and accompanied by an increase in the polarization resistance (R_p) values (**Atta *et al*., 2015b**). It can be supposed that a protective layer covers the surface of the electrode. Its nature can be some solid film, inhibiting species or both (**Khaled, 2010b**).

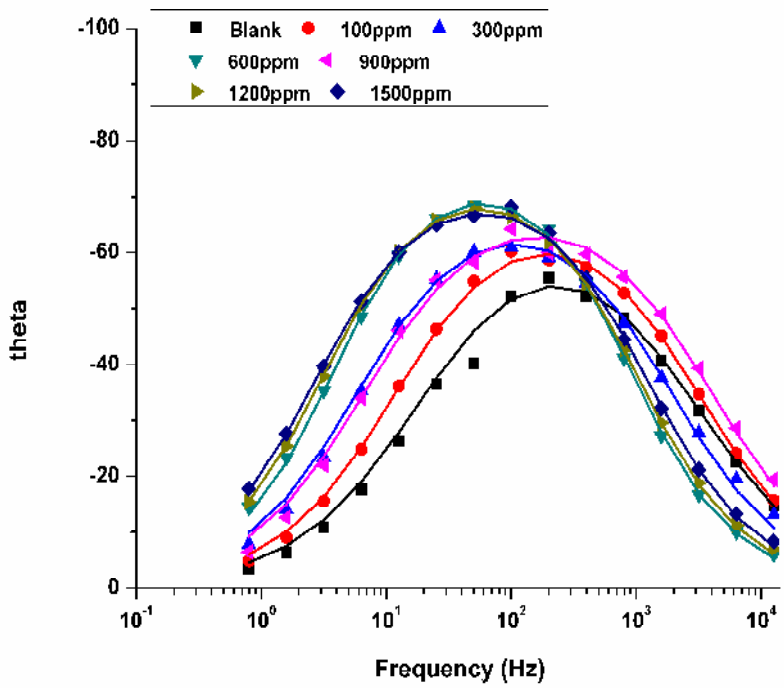

Figure 40 - Bode plot for ChTSB

The Bode plot is used to verify the results acquired from the Nyquist plots and the experimental EIS are presented as Bode plots in Figure 40. Bode and phase angle plots show a single relaxation process i.e. one time constant over the range of the studied frequencies**.** This refers to the existence of an equivalent circuit that contains a single constant phase element in the metal/ solution interface (**Odewunmi *et al*., 2015)**. The absolute impedance, IZI is one of the parameters which can be used to compare corrosion resistance of different samples. A larger IZI demonstrates a better protection performance. From the Bode plot, it could be observed that there is increase in the absolute impedance at low frequencies. The magnitude of IZI is found to increase with increasing the inhibitor concentration which suggests the formation of protective layer, which is due to the adsorption of the Chitosan Schiff base on the MS surface (**Yuce and Kardas, 2012**).

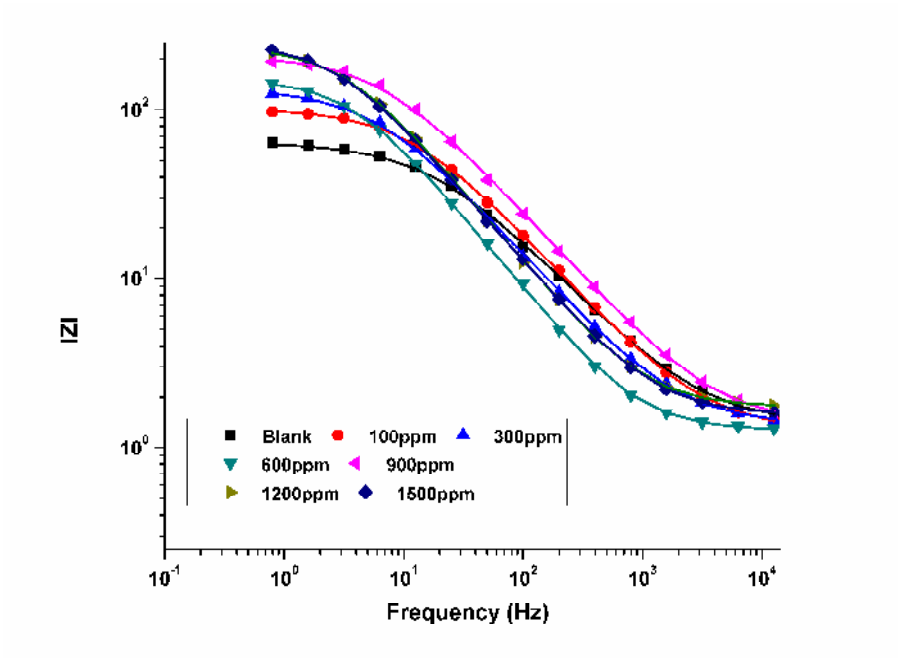

Figure 41 - Phase angle plot for ChTSB .

According to the phase angle plots for the MS in uninhibited 1M HCl solution and different concentration of ChTSB, it was found that the phase angles are shifted to more negative values with increasing concentration of ChTSB. This behaviour of shifting of phase angle to more negative values indicates the superior inhibitive behavior ChTSB molecules at higher concentrations (**Yuce and Kardas, 2012, Abd El-Lateef and Tantawy, 2016**). The increase in impedance IZI as well as the phase shift of MS with increase in concentration confirms the formation of protective layer on the metal surface due to the adsorption of more inhibitor molecules on the active sites of the metal surface (**Fekry *et al.*, 2010**)

4.2.6.2 Effect of immersion temperature on the impedance behaviour of ChTSB:

Temperature has a great effect on the rate of metal electrochemical corrosion. In case of corrosion in an acid medium (hydrogen depolarization), the corrosion rate increases exponentially with temperature increase because the hydrogen evolution over potential decreases (**Popova *et al.*, 2003**). Temperature dependence of the inhibitor efficiency (IE) and the comparison of the values of effective activation energy (E_a) of the corrosion process both in the absence and in the presence of inhibitors lead to some conclusions concerning the mechanism of the inhibiting action. Acid picking of steel is usually carried out at elevated temperatures up to 60 ^{o}C in hydrochloric and up to 90 ^{o}C in sulphuric acid. The inhibitors used are expected to be chemically stable to provide high protective efficiency under the conditions mentioned above. For practical application purposes effects of the inhibitor

concentration at various temperature range of 313 to 343 K on impedance behaviour of MS in HCl have been studied.

The impedance behaviour of MS in HCl in the presence of 1500 ppm of ChTSB at 313-343 K is shown in Figure 42. The Nyquist plot at various temperatures is a set of depressed capacitive loops which are due to the frequency dispersion effect **(Ghailane *et al*., 2013).** The shape of the semicircles are not affected with increasing temperature suggesting the geometric blocking effect of the inhibitor and unmodified mechanism of the corrosion process. The adsorption process is greatly affected by temperature effect and it was indicated by decrease in the diameter of the semicircles.

The impedance data were fitted into the equivalent circuit used earlier for room temperature and the obtained impedance parameters for MS in HCl in the presence of 100 ppm and 1500 ppm of ChTSB at different temperature range were listed in Table 23. The values of n found to increase with temperature which is an indication of the homogeneous metal surface due to adsorption of the inhibitor (**Morad and El-Dean, 2006).** The R_p values increase with increasing concentration at all temperatures studied but we could observe decreased R_p values at higher temperatures. The decrease in R_p values can be attributed to the probable partial desorption of the inhibitor under elevated temperatures. However the concentration of the inhibitor is high to sustain an inhibiting adsorption layer at a given temperature. It may be assumed that the density of the inhibitor adsorbed layer within outer Helmholtz layer (OHL) decreases, while the diffuse part of the double electrical layer increases with temperature. This effect is accompanied by a certain decrease in the depression of the adsorption capacitive semicircle (**Amin *et al.,* 2008**).

Table 23 - Impedance parameters of MS in 1 M HCl containing 100 ppm, 1500 ppm of ChTSB at various temperatures

Temperature (K)	Concentration (ppm)	R_s (Ω cm^2)	$Y_o \times 10^{-6}$	n	Rp (Ω cm^2)	IE (%)	CPE (F)
313K	Blank	1.362	418.15	0.81139	26.42		3.64
	100	1.202	379.74	0.78819	54.75	51.74	5.49
	1500	1.331	401.8	0.85417	114.6	76.95	2.51
323K	Blank	1.237	245.73	0.86152	24.02		0.99
	100	1.248	592.65	0.89433	45.4	47.09	1.98
	1500	1.353	733.81	0.84807	77.09	68.84	5.21
333K	Blank	1.075	436.74	0.84117	18.51		1.21
	100	1.061	533.54	0.86809	44.78	46.36	2.47
	1500	0.99783	482.65	0.8771	57.47	58.20	2.02
343K	Blank	0.9882	513.2	0.89739	13.99		1.42
	100	1.028	1003.7	0.84802	20.75	32.58	5.96
	1500	1.151	701.56	0.89419	30.25	53.75	2.28

From Bode and Phase angle plots (Figure 42b & 42c) for optimum inhibitor concentration at different temperatures 313-343 K, it is noted that IZI decreases and phase angles gets depressed with increase in temperature. This shows that the thickness of the outer porous layer of the inhibitor is decreased at high temperatures thereby furnishing decreased protection effect. This is an evidence for the desorbed or deprived adsorption of film at higher temperature. It is to be noted that the IE of ChTSB increased with concentration at all temperatures and increased till 323 K. After 323 K, the IE starts to decrease.

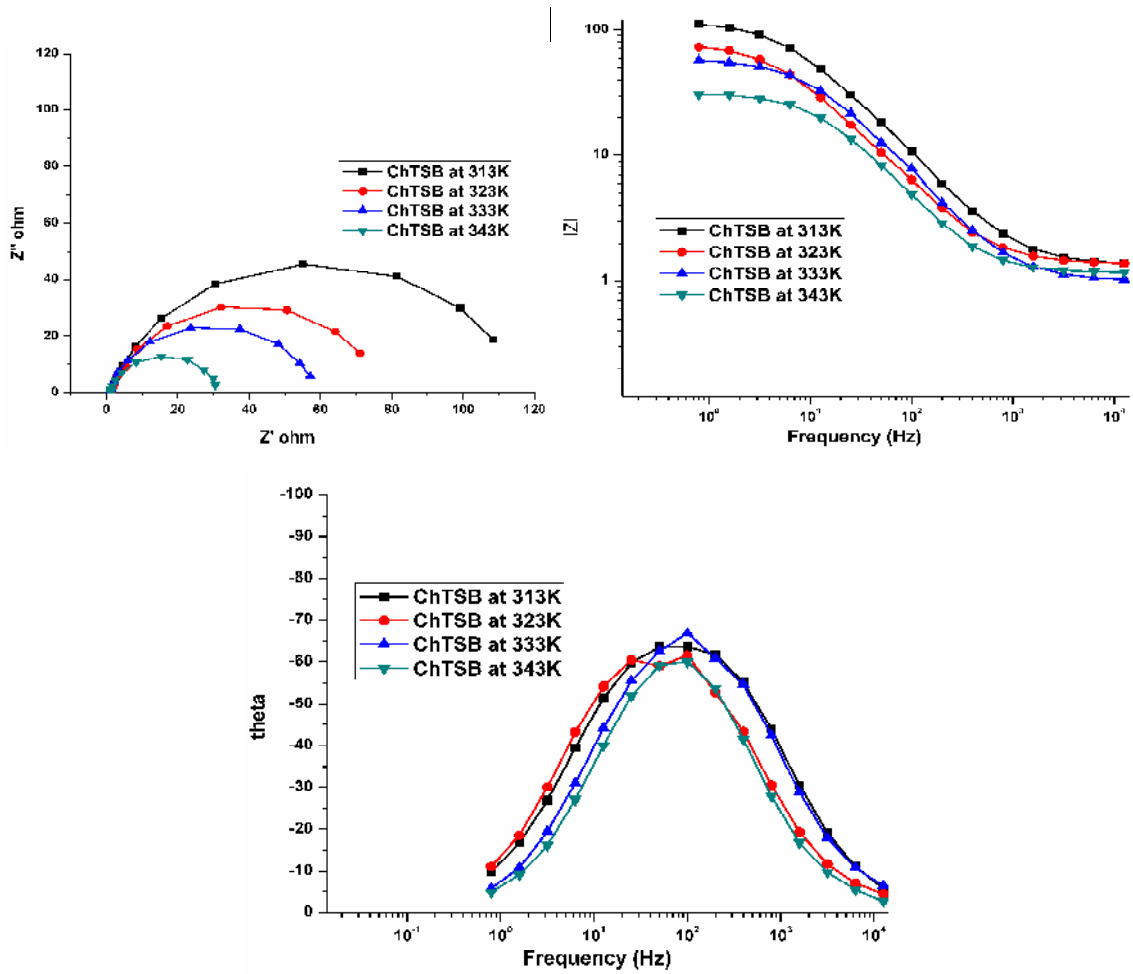

Figure 42 - a) Nyquist plots for mild steel in 1M HCl in the absence and presence of ChTS at higher temperatures (b) Bode plot for ChTSB (c) Phase angle plot for ChTSB.

4.2.6.3 Impedance Behavior of the other investigated Chitosan Schiff bases – Effect of Concentration:

The impedance behaviour of other Chitosan Schiff bases (ChSSB, ChVSB, ChPSB) under investigation were analyzed using Electrochemical impedance measurements.

Figure 43 shows the impedance curves obtained for different concentrations of ChSSB, ChVSB, ChPSB at 303 K.

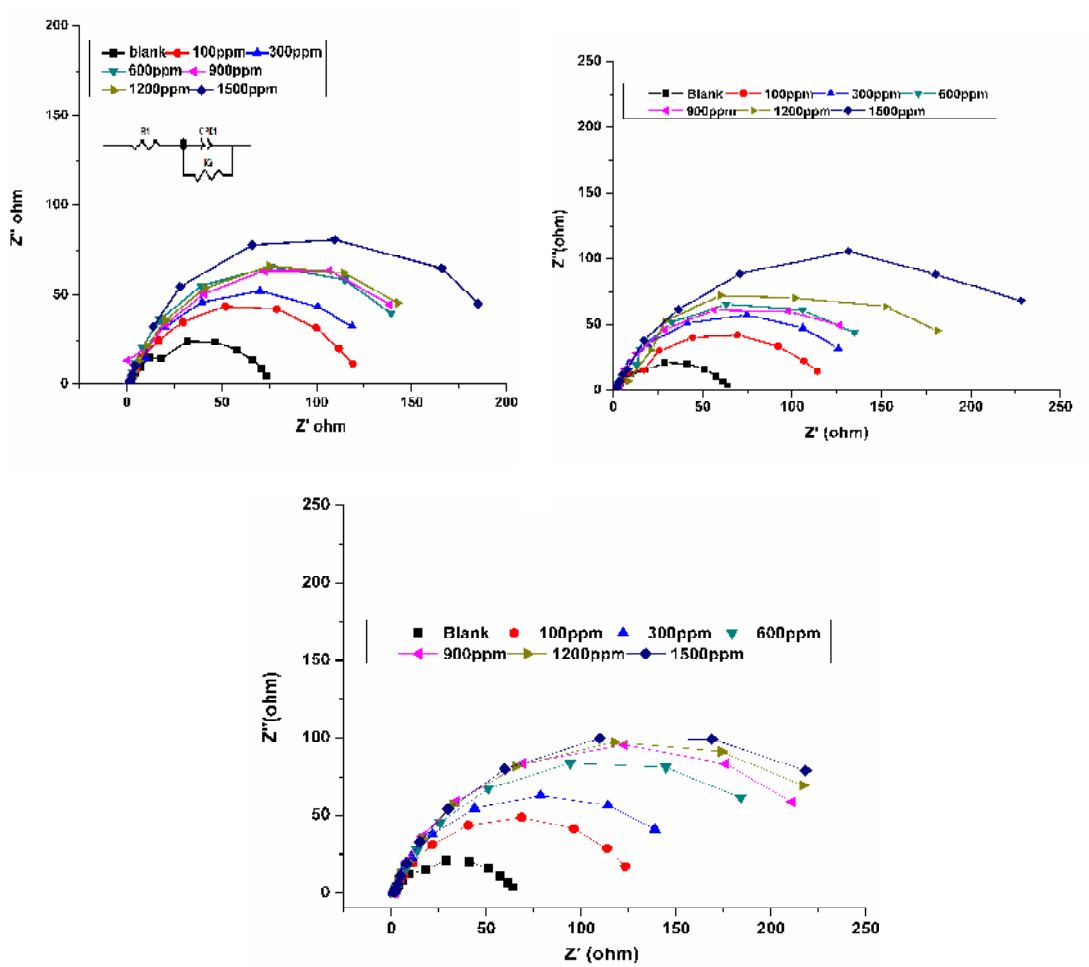

Figure 43 – Nyquist plots for different concentrations of a) ChSSB b) ChVSB c) ChPSB at room temperature 303 K

The impedance diagrams obtained for all the Chitosan Schiff bases are not perfect semicircles and this may be due to frequency dispersion. Single semicircle representation of the Nyquist plot corresponding one time constant in the Bode plot implies that the metal dissolution process controlled by single transfer process. The diameter of the semicircle in Nyquist plot and the magnitude of Bode modulus found to increase with increasing concentration of the inhibitor suggesting the formation of protective layer on the metal surface. The increase in impedance IZI as well as the phase shift (θ) of mild steel with increase in concentration may be due to the adsorption of more number of inhibitor molecules on the active sites of metal surface. Also, the rate of adsorption increases by

protecting the metal surface from the aggressive environment leading to decrease in hydrogen evolution or corrosion rate. Therefore the inhibitor is considered to be effective at lower concentration as it reduces the corrosion rate. The experimental data were fitted for the equivalent circuit (Figure 43) and the parameters are tabulated in Appendix A8. The R_p values increased with inhibitor concentration for all the studied Chitosan Schiff bases indicating the high surface coverage of the inhibitors in presence of aggressive solution.

Effect of Temperature:

The Nyquist plots for mild steel obtained in the absence and presence of all the inhibitors at optimum concentrations at various temperatures are given in Figure 44. The impedance parameters for all the investigated Chitosan Schiff bases at various temperatures were calculated and are presented in Appendix A9 - A12.

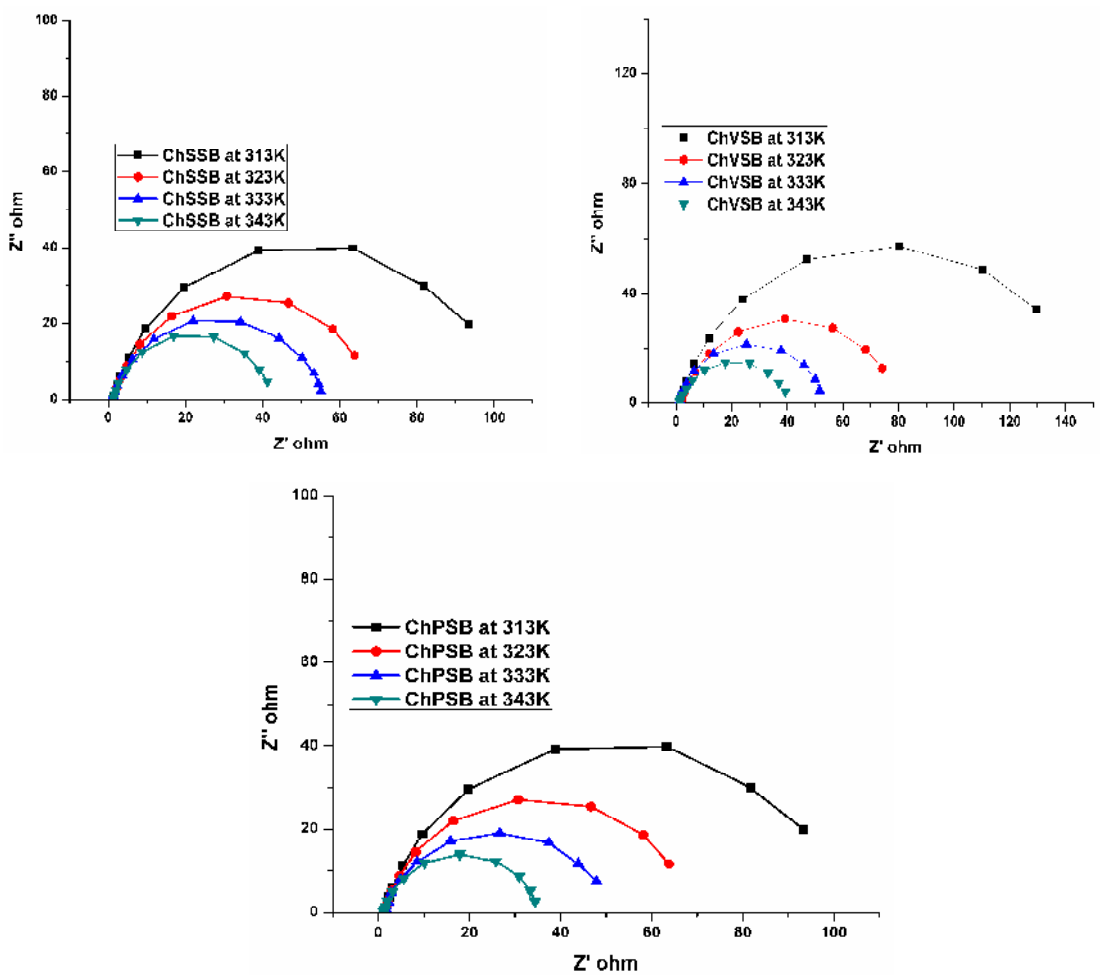

Figure 44 - Nyquist plots of optimum concentration of Chitosan Schiff bases at temperature range 313-343K

Impedance plots of all the inhibitors represent single capacitive loop and one time constant in the Bode-phase plot in the temperature range studied. The diameter of the semicircle increases till 323 K and then tends to decrease with rise in temperature. This can be attributed to the resistive nature of the inhibitor film formed on the metal surface towards higher temperature. The decrease in diameter of the semicircle can be acclaimed to the adsorption–desorption equilibrium towards desorption and roughening of the metal surface which results from enhanced corrosion.

From the impedance parameters of all the Chitosan Schiff base polymers, the increase in CPE was observed which may be due to the shifting of adsorption/desorption equilibrium towards desorption. The increase in n values with temperature reflects that the electrode surface is more homogeneous after the adsorption of Schiff base polymers. The IE calculated from R_p is listed in Apendices (A9 – A12). All the investigated polymers found to follow the same trend in the IE. The IE of the Schiff base polymers are highly effective till 323 K and then decrease gradually with increase in temperature. But on the whole, the Schiff polymers exhibited a consistent inhibition performance.

Phase - III

4.3 Adsorption Phenomenon:

Adsorption, in general is the mechanism underlying the inhibitory action of inhibitor molecules. The adsorption of inhibitor compounds can affect the corrosion rate in two ways:

(i) by decreasing the available reaction area or the so-called geometric blocking effect;

(ii) by modifying the activation energy of the cathodic and/or anodic reactions occurring in the inhibitor-free metal in the course of the inhibited corrosion process.

The adsorption of inhibitor molecules can be described by two main types of interaction: physisorption and chemisorption. These are influenced by the nature and charge of the metal, the chemical structure of the inhibitor and the type of electrolyte.

Physisorption or physical adsorption involves electrostatic forces between ionic charges or dipoles on the adsorbed species and the electric charge at the metal/solution interface. The interaction between the adsorbate and metal surface is achieved through Vanderwaal's intermolecular interactions. The heat of adsorption is low and therefore this type of adsorption is stable only at relatively low temperatures.

Chemisorption, involves charge sharing or charge transfer from the inhibitor molecules to the metal surface to form a coordinate type bond. Chemisorption is typically much stronger adsorption energy than physical adsorption. Such a bond is therefore more stable at higher temperatures.

Generally, the first step in inhibition of metallic corrosion is the adsorption of inhibitor molecules at the metal/solution interface. The adsorption depends on the molecule's chemical composition, temperature and the electrochemical potential at the metal/solution interface. The adsorption of an inhibitor molecules on a metal surface is regarded as a substitutional adsorption process between the organic molecule in the aqueous solution ($Org_{(sol)}$), and water molecules adsorbed on the metallic surface ($H_2O_{(ads)}$),

$$Org_{(sol)} + xH_2O_{(ads)} \longleftrightarrow Org_{(ads)} + xH_2O_{(sol)}$$

where x is the size ratio representing the number of water molecules replaced by one molecule of inhibitor.

4.3.1 Adsorption isotherms:

Basic information about the interaction between inhibitor molecules and the metal surface can be provided by adsorption isotherm. The relationship of surface coverage with the concentration of the inhibitor is expressed by different isotherms based on the experimental conditions. The type of adsorption isotherm also affords additional information like monolayer/ multilayer, repulsive/ attractive between adsorbed molecules. The degree of surface coverage (θ) calculated from the weight loss measurements are fitted with several isotherms including Frumkin, Langmuir, Temkin, Freundlich and Flory–Huggins isotherms.

Langmuir adsorption isotherm:

Langmuir adsorption isotherm can be expressed according to equation **(Eddy *et al.,* 2010)**

$$\frac{C}{\theta} = \frac{1}{k} + C \qquad (17)$$

where K is the equilibrium constant, C is the concentration of inhibitor and θ is the degree of surface coverage of the inhibitors. The plots of Langmuir adsorption isotherm is (C/ θ) Vs C.

Temkin adsorption isotherm can be represented according to equation **(Umoren *et al.,* 2007)**

$$\theta = \frac{1}{f}\ln K + \frac{1}{f}\ln C \qquad (18)$$

$$\exp(-2a\theta) = KC \qquad (19)$$

where 'a' is molecular interaction parameters, θ is the degree of surface coverage, K is the equilibrium constant of adsorption process and C is the concentration of the inhibitors. The plots of Temkin adsorption isotherm is θ Vs ln C.

Frumkin adsorption isotherm can be deduced according to equation **(Oguzie *et al*., 2004)**

$$log \frac{\theta}{1-\theta} = \log B + \log C + 2a\,\theta \quad (20)$$

where 'a' is the lateral interaction term describing the molecular interaction in the adsorbed layer, θ is the degree of surface coverage, and C is the concentration of inhibitors. The plots of Frumkin adsorption isotherm is θ Vs ln [θ/C (1- θ)].

Freundlich adsorption isotherm can be written according to equation **(Umoren *et al.,* 2007)**

$$\ln \theta = \ln K + \frac{1}{n} \ln C \quad (21)$$

where n is the adsorption intensity, C is the inhibitors concentration and K is the equilibrium constant of adsorption reaction. The plots of Freundlich adsorption isotherm is ln θ Vs ln C. **Flory-Huggins adsorption isotherm** can be explained according to equation **(Umoren *et al.,* 2007)**

$$log \frac{\theta}{C} = \log xK + x \log(1 - \theta) \quad (22)$$

where θ is the degree of surface coverage, C is the concentration of the system studied, x is the number of water molecule replaced by one inhibitor molecule and K is the equilibrium constant for the adsorption process. The plot of Flory- Huggins adsorption isotherm is log (θ /C) Vs log (1- θ).

The degree of surface coverage (θ) can be calculated from the inhibitor efficiency using the relationship, %IE = 100 × θ for different concentration of the inhibitors. In the present study, the degree of surface coverage (θ) for the various inhibitor concentrations in 1 M HCl at 303-343 K for 1/2 h immersion time has been evaluated from weight loss studies. The data are tested graphically by fitting to various adsorption isotherms. The best fit was determined using the regression values (R^2). A particular model which has highest value of R^2 can be considered as the best model to explain the changes in performance of polymeric type of inhibitors.

4.3.2 Investigation of adsorption properties of Chitosan Schiff bases in acid medium:

In the range of temperature studied, best correlation between the calculated surface coverage and the concentration of the inhibitors found to be given by Temkin adsorption

isotherm (Equation) with R^2 close to unity. Temkin adsorption isotherm is given by the equation,

$$\exp(-2a\,\theta) = K_{ads}C \quad (23)$$

where θ is the surface coverage, K_{ads} is the adsorption equilibrium constant and C is the concentration of the inhibitor, 'a' is the molecular interaction parameter which can be negative or positive. Positive 'a' values indicate the attractive force between the adsorbed inhibitor molecules while negative values represent the repulsive force between them.

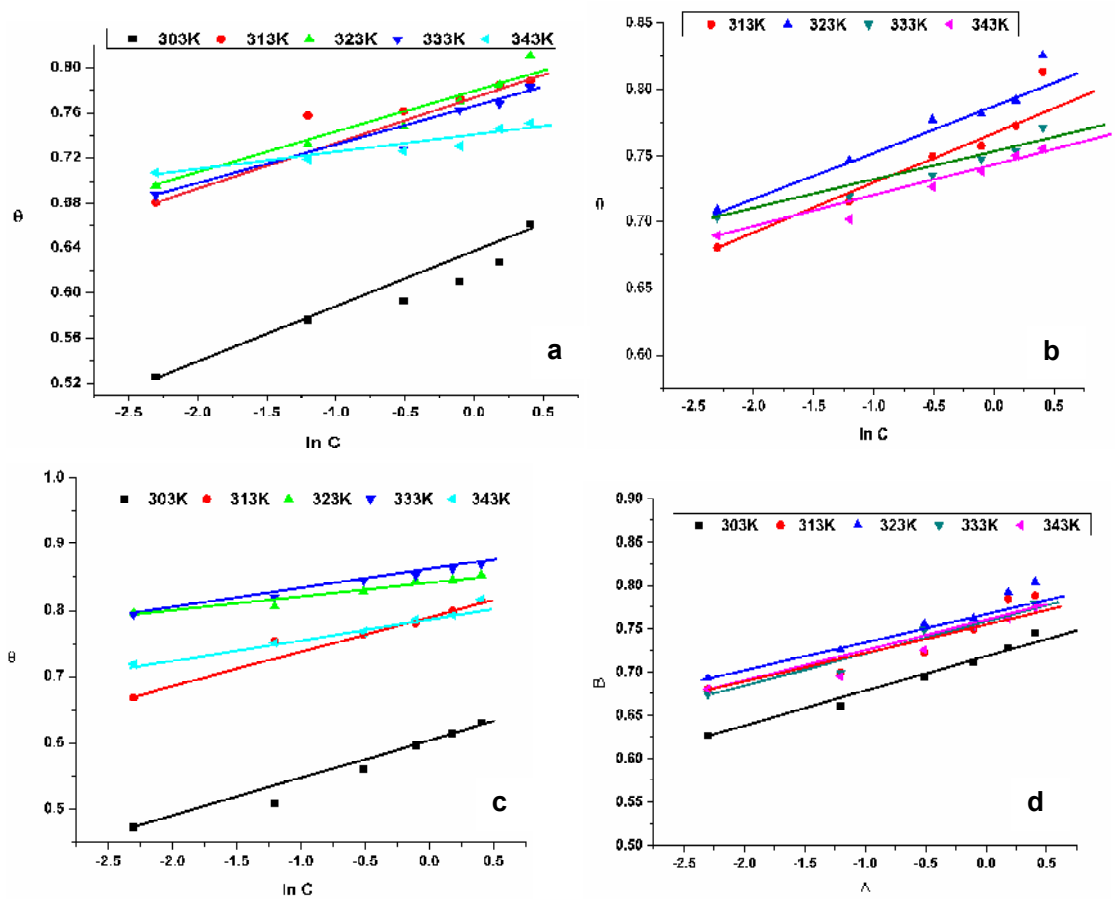

Figure 45 – Temkin adsorption isotherm of a) ChSSB b)ChVSB C) ChTSB d) ChPSB

When -2a is represented as 'f' which describes the heterogeneity that prevail between the molecular interactions in the adsorption layer and the heterogeneity of the metal surface. The value of 'f' depends on the intermolecular interaction in the adsorbed layer and on the heterogeneity of the surface. Temkin equation can be represented in the transformed form as shown here,

$$\theta = \frac{1}{f}\ln K + \frac{1}{f}\ln C \quad (18)$$

The sign of 'f' is always opposite of 'a' thus, if a< 0, then f>0; if a>0, then f<0. If f is positive, mutual attraction of molecules occurs, and if f is negative repulsion takes place (**Li *et al*., 2009**).

The linear regression between θ vs. ln C for the investigated Chitosan Schiff base polymers at various temperatures is depicted in Figure. The regression coefficients ((R^2) of the isotherms are around unity implies that the inhibiting tendency of the inhibitors is due to the adsorption of polymer molecules on the metal surface (**Badawy *et al*., 2006, Negm *et al*., 2010**).

Basically, Temkin isotherm is a preliminary evidence for the chemisorptive nature of the adsorption (**Geethanjali and Subhashini, 2015**). The position of the lower temperature isotherm below the higher temperature isotherm in the Figure 45 supports the chemisorption of the Schiff bases on the metal surface (**Ebenso (2003)**). The calculated isotherm parameters for all the investigated Schiff base polymers were given in Table 24. From the table, the calculated 'f' values for all the inhibitor system are found to be positive and greater than zero which indicates the existence of a strong attractive interaction between adsorbed Chitosan Schiff bases in the adsorbed layer (**Morad, (2008)**).

The adsorption equilibrium (K_{ads}) value signifies the strength of the adsorption forces between the inhibitor molecule and metal surface, the larger values of K_{ads} suggests greater adsorption efficiency, stronger and more stable adsorbed layer with better inhibition performance (**Ahamad *et al*., 2010**). The increase in the K_{ads} values with increase in temperature (Table 24) for all the studied inhibitor system except ChTSB system signifies the strong adsorption of inhibitor molecules onto the metal surface. The increase in K_{ads} values with temperature is directly proportional to the adsorption efficiency of the inhibitor with temperature **(Shukla and Ebenso, 2011)**.

In the inhibitor system ChTSB, a drop in the K_{ads} values at higher temperatures was observed. This smaller values of K_{ads} reveal that the interaction between the adsorbing inhibitor molecules and the metal surface becomes weaker (**Obi-Egbedi and Obot, 2011**) and the protective layer formed gets perturbed at higher temperatures, however offering better inhibition performance.

Table 24 - Thermodynamic parameters of adsorption of Chitosan Schiff bases on MS electrode surface in 1 M HCl solution from weight loss results

Inhibitor system	Temperature (K)	R^2	f	K_{ads} dm^3mol^{-1}	a
ChSSB	303	0.95	22.50	$7.20*10^8$	-11.25
	313	0.90	26.91	$3.92*10^9$	-13.45
	323	0.95	25.62	$2.41*10^9$	-12.81
	333	0.95	29.25	$7.18*10^9$	-14.62
	343	0.90	64.82	$1.52*10^{13}$	-32.41
ChVSB	303	0.91	13.18	$1.08*10^6$	-6.59
	313	0.99	22.87	$3.08*10^9$	-11.44
	323	0.95	26.01	$3.39*10^9$	-13.00
	333	0.98	42.49	$1.34*10^9$	-21.25
	343	0.94	33.07	$1.75*10^9$	-16.54
ChPSB	303	0.98	23.17	$4.0*10^8$	-11.59
	313	0.89	24.21	$1.09*10^9$	-12.10
	323	0.96	25.08	$1.93*10^9$	-12.54
	333	0.93	25.37	$1.24*10^9$	-12.69
	343	0.93	27.77	$3.65*10^9$	-13.89
ChTSB	303	0.97	16.57	$2.24*10^6$	-8.29
	313	0.96	20.06	$2.47*10^8$	-10.03
	323	0.95	45.22	$1.52*10^{12}$	-22.61
	333	0.99	35.74	$1.73*10^{11}$	-17.87
	343	0.97	29.84	$1.3*10^{10}$	-14.92

The high values of K_{ads} for studied Chitosan Schiff bases indicate stronger adsorption on the mild steel surface in 1M HCl solution. This may be due to the presence of hetero-atoms like nitrogen, oxygen and sulphur atoms, an electron cloud on the aromatic ring in the carbonyl compounds and presence of azomethine (–HC=N-) group in the inhibitor molecules.

4.3.3 Thermodynamic Parameters of adsorption:

Thermodynamic parameters of adsorption are useful to explain the adsorption behavior of inhibitor molecules. These quantities can be calculated depending upon the estimated values of K_{ads} from adsorption isotherms at different temperatures. The thermodynamic free energy of adsorption ΔG_{ads} is related to K_{ads} with the following equation,

$$\log Kads = -logCH2O - \frac{\Delta Gads}{2.303\ RT} \quad (24)$$

where C_{H2O} is the molar concentration of water (mol/dm^3), R is the molar gas constant (g/mol/K) and T is the temperature (K). ln K_{ads} vs 1/T was plotted to determine the adsorption of enthalpy ΔH_{ads} and the adsorption of entropy ΔS_{ads} using Vant Hoff's equation,

$$\ln Kads = -\frac{\Delta Hads}{RT} + \frac{\Delta Sads}{R} + \ln\frac{1}{55.5} \quad (25)$$

In the plot of ln K versus 1/T gives a straight line. The slope of the straight line is ($-\Delta H_{ads}/R$) and intercept is ($\Delta S_{ads}/R+\ln 1/55.5$) from which the values of ΔS_{ads} and ΔH_{ads} can be calculated respectively. The calculated thermodynamic parameters of adsorption are listed in Table.

Free energy of adsorption:

The negative values of ΔG_{ads} ensure the spontaneity of the adsorption process of Chitosan Schiff bases onto the metal surface (**Tang *et al.*, 2006**) and strong interaction between the inhibitor molecules and the metal surface (**Sibel *et al.*, 2005**). Generally, the energy values of ΔG_{ads} with -20 kJ mol^{-1} or less negative are associated with an electrostatic interaction between charged molecules and charged metal surface, i.e. physisorption. The free energy values of -40 kJ mol^{-1} or more negative involve charge sharing or transfer of electrons from the inhibitor molecules to the metal surface to form a coordinate covalent bond, chemisorption (**Abdallah *et al.*, 2015**). The calculated ΔG_{ads} values for the Chitosan Schiff bases on mild steel in 1M HCl solution are greater than -40 KJ mol^{-1} (Table 25) indicating that the adsorption mechanism of Schiff base polymers in the studied acid medium was typical of chemisorption. The ΔG_{ads} values for all the four studied Chitosan Schiff bases increases with temperature. This increase in ΔG_{ads} values suggests a strong interaction between inhibitor molecules and surface iron atoms at higher temperatures. Thus, the adsorption of all Chitosan based inhibitors on the mild steel in 1M hydrochloric acid is complex in nature and predominantly chemisorption.

Enthalpy of adsorption and Entropy of adsorption:

The sign of the ΔH_{ads} differentiate exothermic or endothermic adsorption process. The positive ΔH_{ads} reflects the endothermic process and negative ΔH_{ads} reflects the exothermic process. Endothermic process is generally attributed to chemisorption. But exothermic process can be associated with physisorption or chemisorption, depending on absolute values. A physisorption process reflects an enthalpy around 40 kJ mol^{-1} while chemisorption process reflects an enthalpy around 100 kJ mol^{-1}.

The ΔH_{ads} obtained for the investigated Chitosan Schiff base polymers were positive that reflects the adsorption is endothermic. It also implies that the dissolution of metal in presence of Chitosan Schiff bases was non-spontaneous (**Hegazy *et al.,* 2012**). The ΔH_{ads} values for the Chitosan Schiff base polymers were found to be around and greater than 100 kJ mol^{-1} (Table 25). This is also evidence for the chemisorptive nature of the inhibitors to absorb on the metal surface. The orderliness/disorderliness of an adsorption process can be determined using entropy of adsorption. The decrease in entropy or negative entropy is a due to the adsorption of inhibitor molecules in an orderly fashion onto the mild (**Li *et al*., 2012** and **Singh (2010)**). Similarly, the positive entropy is attributed to the solvent entropy that is associated with the disorderliness of the solution during the adsorption process.

The values of entropy of adsorption are positive in all the cases. In fact, it is well known that adsorption is an exothermic phenomenon accompanied by a decrease in entropy. In contradiction to literature results, the positive enthalpy is associated with the positive entropy. This may be explained in aqueous solution, the adsorption of inhibitor molecule is generally accompanied with desorption of water molecules. The adsorption of an inhibitor adsorbate at the metal/solution interface is considered a ‘‘substitutional adsorption’’ phenomena. The Chitosan Schiff bases are long chain polymeric compounds with hetero atoms and more adsorption sites; before adsorbing onto the metal surface, Schiff base polymers should orient themselves in the solution phase to extend the bonding with the metal surface. For this orientation of the polymer some energy is required, that exceeds the exothermic energy of the polymers which adsorbs on the metal surface. The total enthalpy of the system is an algebraic sum of adsorption enthalpy and desorption enthalpy. Thus desorption of the water molecules becomes implicitly an endothermic process resulting in a positive enthalpy for the whole system.

Adsorption of the inhibitors from the aqueous solution is regarded as quasi-substitution process between the inhibitor in the solution phase and water molecules at the metal surface. The adsorption of inhibitors on metal surface takes place by replacing the water molecules. The total entropy is calculated as an algebraic sum of adsorption of inhibitor molecules and desorption of water molecules. The gain in entropy is related with the solvent entropy. the disorderliness increases from the solvent side resulting in increased entropy. Therefore, the positive values of ΔH_{ads} and ΔS_{ads} related to ‘‘substitutional adsorption’’ that can be attributed to the increase in the solvent entropy and to a more positive water desorption enthalpy. (**Singh and Quraishi, 2010b**). According to the absolute values for ΔG_{ads}, ΔH_{ads} and ΔS_{ads} at each temperature, the inhibitive action of the investigated inhibitors or the spontaneity of the adsorption process.

Table 25 – Free Energy of adsorption, Enthalphy and Entropy values for Chitosan Schiff bases on MS electrode surface in 1 M HCl solution from weight loss results

Inhibitor system	Temperature (K)	ΔG_{ads} ($kJmol^{-1}$)	ΔH_{ads} ($kJmol^{-1}$)	ΔS_{ads} ($Jmol^{-1}\ K^{-1}$)
ChSSB	303	-45.54	585.09	2056.47
	313	-62.96		
	323	-60.43		
	333	-66.24		
	343	-130.80		
ChVSB	303	-34.86	167.98	701.59
	313	-56.54		
	323	-66.30		
	333	-99.63		
	343	-82.46		
ChTSB	303	-35.16	378.34	1403.46
	313	-50.19		
	323	-106.00		
	333	-87.28		
	343	-69.66		
ChPSB	303	-52.16	73.84	419.07
	313	-56.60		
	323	-59.34		
	333	-58.71		
	343	-62.80		

The values of thermodynamic parameters for the adsorption of inhibitors can provide valuable information of corrosion inhibition. In the present case, the calculated ΔG_{ads} values of Chitosan Schiff bases are negative and greater than 40 kJ mol^{-1}, the calculated ΔH_{ads} values are positive and greater than 100 kJ mol^{-1} indicating that these inhibitors can be considered chemically adsorbed on the metal surface. The high values of ΔH_{ads} the strong adsorption on the mild steel surface. The chemisorption can be explained as due to the donation of lone pair of electrons by the hetero atoms N, O and S on the polymer chain to the empty d-orbitals of iron atom forming coordinate bond.

4.3.4 Adsorption monitoring technique - Cyclic Voltammetric studies:

Cyclic Voltammetry (CV) has become one of the important electrochemical techniques used in many areas of research. It is widely used to study the variety of redox processes, to determine the stability of the reaction products, to identity the intermediates in redox reactions, to determine the reduction potential of an analyte and so on. This technique has been also used to investigate corrosion behavior of metals in the electrolytic solution and to analyze the inhibiting activity of the inhibitor solution. Many authors have reported CV studies to explain the nature of the inhibitor solution on the corrosion activity of the metal in acid solution (**Shahabi *et al*., 2015, El-Etre (2007), Pathak *et al*., 2007, Shahabi *et al*., 2014**)

Cyclic Voltammetric (CV) analysis was carried out for all the synthesized Chitosan Schiff bases in order to examine their adsorption effect on the metal surface. Bio-Logic SP-150 electrochemical system served with three electrode configuration was used for the purpose of analysis here. In a typical set up, mild steel (with an exposure area of 1 cm^2), saturated calomel and platinum electrodes were chosen as working electrode, reference electrode and counter electrode respectively. The electrochemical set up used here was similar to the experimental set up of polarization and EIS studies. The medium to connect all the three electrodes in the electrochemical system is aqueous based solution, i.e. Schiff bases dissolved in acid (1500 ppm). This solution was treated as the electrolytic solution for the analysis.

The CV analyses of all the Chitosan Schiff bases were recorded in the potential region of -1 to -0.2 V with a scan rate of 50 mV/sec. since aqueous based electrolyte solution possess limited stability for longer duration of time and cycles, the higher scan rate in the range of 50 mV/sec is chosen.

4.3.4.1 Adsorption behavior of Chitosan Schiff bases on the metal surface – CV technique:

The adsorption of Chitosan Schiff bases (ChSSB, ChVSB, ChTSB, ChPSB) on the mild steel sample studied are discussed based on cyclic voltammetry analysis and the corresponding graphs. For all the CV graphs given, the initial CV curve was excluded for the reason that information obtained from first cycle CV is not the accurate results belonging to the sample under investigation (**Shahabi *et al*., 2015**). The rate of change of charge accumulation on the mild steel sample for different solutions containing Chitosan Schiff bases was analyzed to have insight onto the adsorption behaviour of the Chitosan Schiff

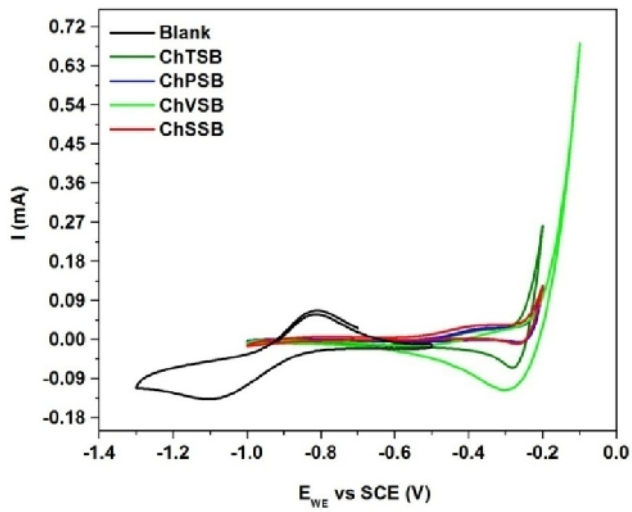

bases. Continuously 90 cycles were recorded for all the Schiff bases reported here in order to observe the changes occurred on the metal surface during the immersion time. Figure 46a shows CV graphs recorded at 5th cycle for mild steel sample in 1M HCl and for investigated Chitosan Schiff bases.

Figure 46a – Cyclic voltammograms of mild steel surface in presence and absence of Chitosan Schiff bases

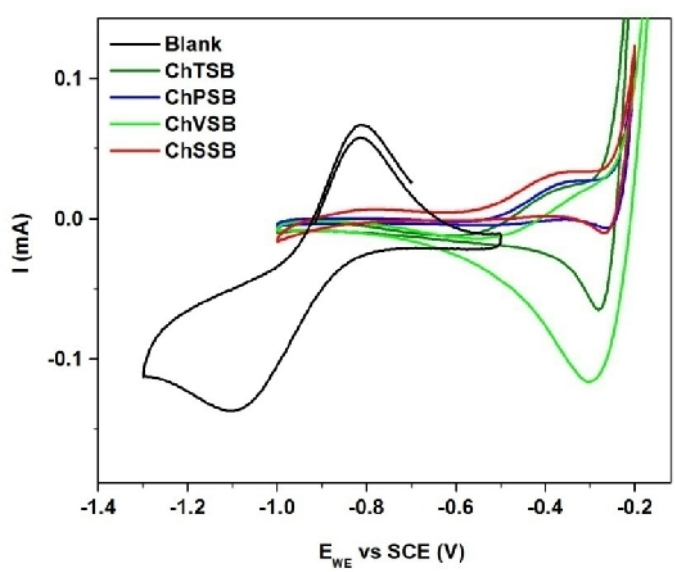

Figure 46b – Enlarged view of Cyclic voltammograms without O_2 evolution

Compared to the blank, electrochemical reactions of all the Schiff bases are found to be stable for extended potential window without any detectable redox peaks. This proves that

inhibitor prevents the metal from redox activity inside the electrochemical system which leads to higher stability of electrolyte solution without H_2 evolution. Still, for comparison all the CVs reported here were recorded in similar potential windows; which includes the O_2 evolution reaction. This is clear from the sharp & high current peaks observed at the higher potential (-0.2 V) region. Excluding the O_2 evolution region, the CV graphs showing redox activity of all the Chitosan Schiff bases are shown in Figure 46b. The reduction peak current values of Schiff bases added solutions were almost negligible compared to the blank electrolyte solution. Whereas, higher O_2 evolution exhibits protective layer formation, as seen from the strong droop observed for Chitosan Schiff bases added solutions. With increasing the number of cycles, high current values were observed at this protective layer region. This ensures the effective adsorption process occurred on the metal surface with Schiff bases added electrolyte solution. This also clarifies the stability of steel component against corrosion in the chosen medium.

The thickness of protective layer can be found by estimating the weight of the mild steel used for CV analysis. The effective thickness of the layer can be calculated from the formula,

$$t = \frac{m}{a \times d}(cm) \tag{26}$$

where,

t is thickness of the film (cm)
m is mass of the protective layer adsorbed on the metal surface (g)
a is exposed area of the metal (cm^2)
d is density of the solution (g/cm^3)

The change in the depth of the droop shows the variation of protective layer formation with different Schiff bases as seen in Figure 46b. The protective layer thicknesses are calculated and displayed in the Table 26. Figure 46b clearly depicts that ChVSB shows strongest droop, ensuring the thickest film among all other Schiff bases. Whereas, next to ChVSB component, ChTSB, ChSSB and ChPSB Schiff bases show protective layer thickness in the order of 10^{-3} cm. However, the observed protective layers are quite elevated in the aspect of thickness. This may be due to the high scan rate preferred for recording 90 numbers of cycles in the CV studies. In general, higher the scan rates, higher the peak current value because of fast drifting of the charge carrier. In this view point, protective layers width appears to be high.

Table 26 – Calculated Protective layer thickness values for Chitosan Schiff bases

S.No	Inhibitor	Protective layer thickness $*10^{-3}$ (cm)
1	ChSSB	0.17
2	ChVSB	0.29
3	ChTSB	0.21
4	ChPSB	0.14

The quantity of charge (Q) that is passed through the electrode during electrochemical process can be effectively found by analyzing the Q with respect to the time period. The net quantity of charge produced can be calculated from the formula,

$$Q = \frac{1}{v}\int_{E2}^{E1} i(E)dE \qquad (27)$$

where,

Q is the quantity of charge in the potential window E_1-E_2 in V

v is scan rate in V/sec

i(E) is amount of current produced in the potential window E_1-E_2 in mA

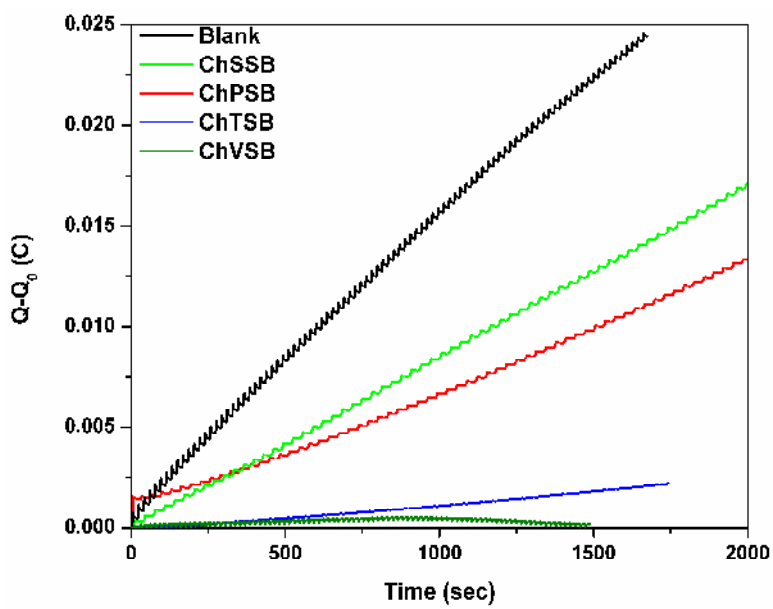

Figure 47 – Plot of Total charge acquired by MS sample (ΔQ) vs time in blank and in Chitosan Schiff base solutions

The reduction of Q is direct indication of corrosion inhibiting nature and effective adsorption of Schiff base polymers on the mild steel surface. Figure 47 shows the response of Q with time duration taken for complete-90 cycles. In the present case of investigation, since O_2 evolution is prominent in the Schiff base added solutions, the net charge produced in these solution was dominating compared to the corrosion of mild steel in the blank solution. Thus net quantity of charge was calculated excluding the O_2 evolution region in the CV graphs. In result, the quantity of charge found to decrease with the inhibiting efficiency of the solutions with inhibitors. As it is seen in other techniques, ChVSB Schiff base shows the lower number of charge which is an indication of high corrosion inhibiting activity of the material among the four inhibitors (**Pathak *et al*., 2007, Shahabi *et al*., 2014, Shahabi *et al*., 2015).** After which ChTSB, ChSSB and ChPSB polymers show the better inhibiting efficiency. Among all, mild steel electrode in blank solution shows the highest quantity of charge, indicating the maximum redox activity leading to rapid corrosion rate of the sample.

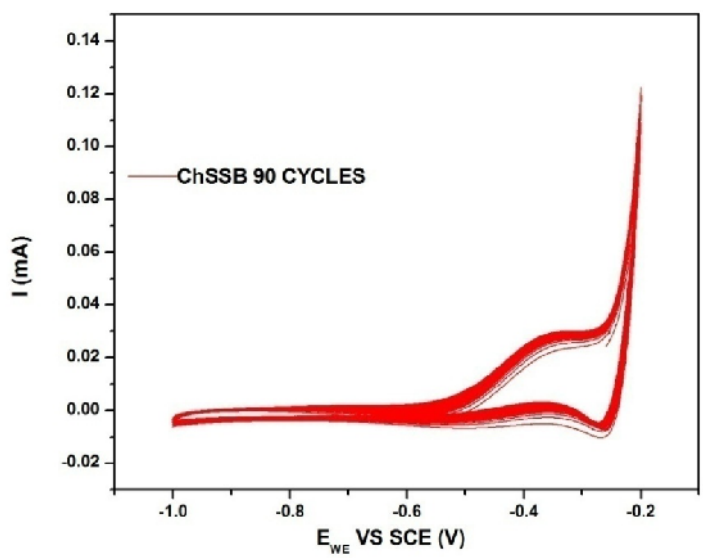

Figure 48 – CV graphs recorded for 90 cycles for MS electrode in ChSSB inhibitor

The representative CV graphs of all the four inhibitor solutions obtained for complete 90 cycles are shown in Figures 48-51. It is clear from these CV graphs, mild steel component in presence of Schiff bases did not exhibit any redox activity throughout the analysis. This ensures the complete shielding of metal against corrosive acid environment by Chitosan Schiff bases. Hence, redox process in the metal surface is suppressed by the inhibitor solution which was reversible up to 90 numbers of cycles. The poor redox activities exhibited by the Chitosan Schiff bases are in the following order; ChVSB, ChTSB, ChSSB and ChPSB. In line with this, the thickness of protective layers observed is in the same order. Hence

Schiff base with highest protective layer thickness- ChVSB shows very poor redox process, ensuring the best inhibiting activity compared to other Schiff bases.

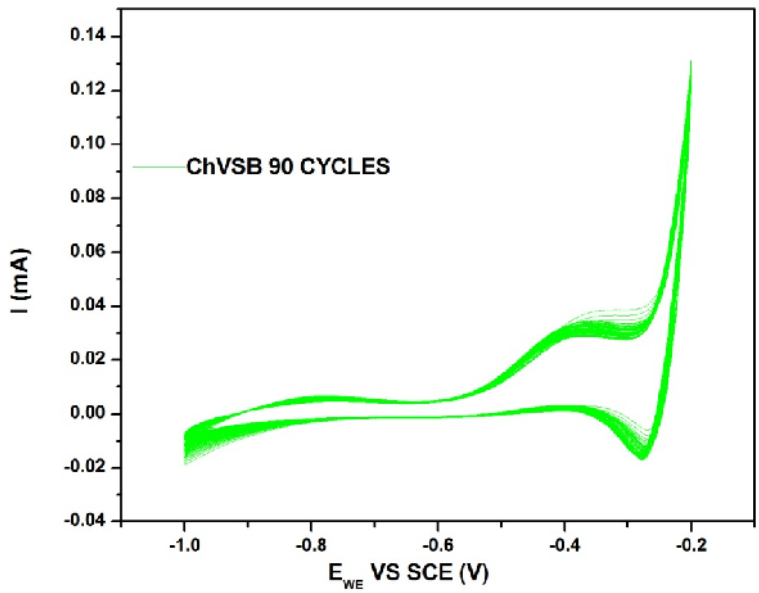

Figure 49 – CV graphs recorded for 90 cycles for MS electrode in ChVSB inhibitor

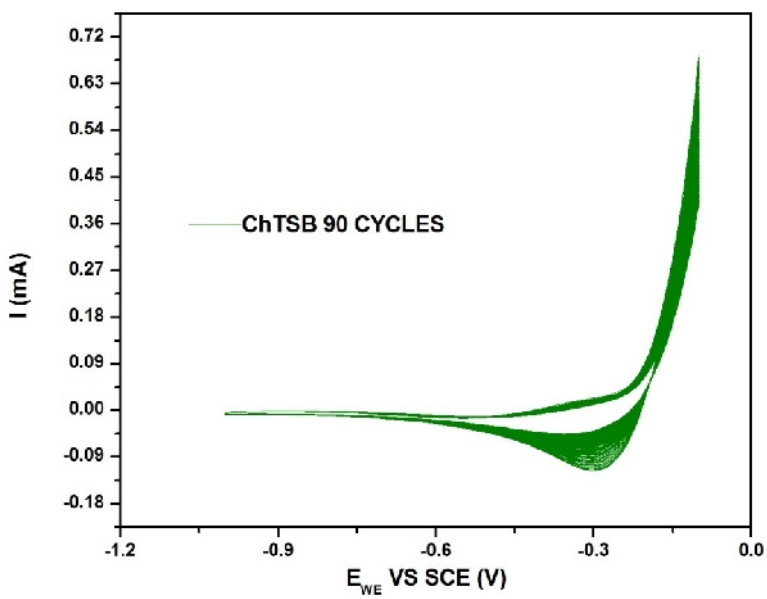

Figure 50 – CV graphs recorded for 90 cycles for MS electrode in ChTSB inhibitor

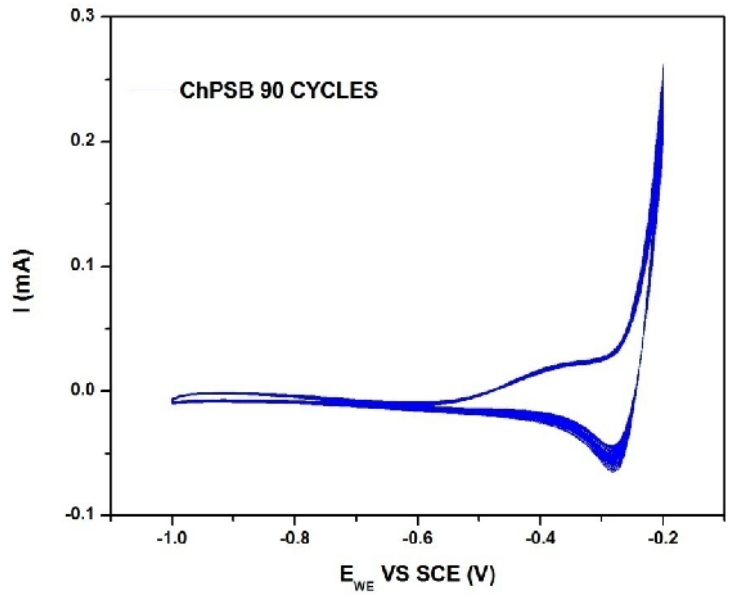

Figure 51 – CV graphs recorded for 90 cycles for MS electrode in ChPSB inhibitor

4.3.5 Surface Characterization Techniques:

The weight loss measurements confirmed the chemisorption of the Chitosan Schiff base polymers. Chemical adsorption of inhibitors was further supplemented by the surface imaging and analytical techniques. Surface imaging techniques are used to study the morphological changes observed on the surface and surface analytical techniques are used to analyze the chemical composition of the modified mild steel surface. The surface characterization techniques carried out in the present work are:

i) Scanning Electron Microscope (SEM)

ii) Energy dispersive X-ray analysis (EDAX)

iii) Atomic Force microscope (AFM)

iv) Contact angle Measurements

v) Fourier transform infra red spectroscopy (FTIR)

vi) X-ray photon spectroscopy (XPS)

All the surface analytical techniques were performed as *Ex-situ* type of analysis by immersing the samples in the absence and presence of the inhibitor solution for about 6 hours at room temperature.

4.3.5.1 SEM analysis

SEM analysis of polished and corroded metal surface:

Figures 52 shows the SEM images recorded for polished metal surface and metal surface immersed in 1M HCl. The smooth surface (Figure 52a) with parallel features on the polished MS surface was observed before exposure to the corrosive solution, which are associated with polishing scratches. The morphology of MS surface in Figure 52b reveals that, in the absence of inhibitors the surface was highly damaged with areas of typical uniform corrosion on the surface. The metal surface was covered with huge amount of irregular cracks and pits throughout the surface. The cracks are clearly visible in the enlarged portion the micrograph. The depth of the cracks was measured (547 nm, 473.5 nm, 255 nm, 628 nm) which imply the severity of corrosion by acid.

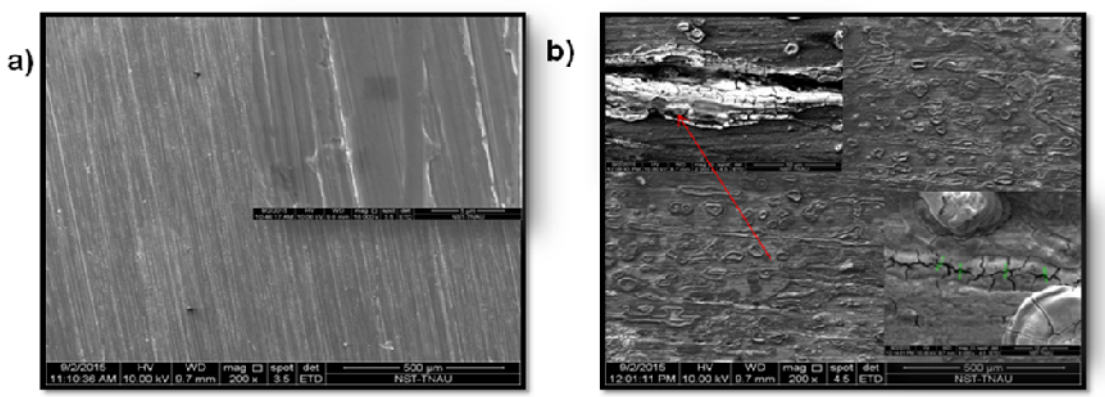

Figure 52 – SEM images of mild steel (a) Polished surface and (b) immersed in 1M hydrochloric acid solution

SEM analysis of metal surface in presence of Chitosan Schiff bases:

General inspection of the SEM micrographs in presence of inhibitors clearly suggested that the damaging effect is greatly reduced and the polymers are adsorbed on the metal surface. The formation of the film of Chitosan Schiff bases hindered the dissolution of the metal in acid.

The SEM micrograph of the mild steel specimen in presence of ChSSB (Figure 53a) appears with smooth surface due to the formation of an adsorbed film of the inhibitor along with granular morphology.

The SEM result of the metal specimen immersed in ChVSB (Figure 53b) shows an extensive coverage of polymeric clusters along with thin film formation.

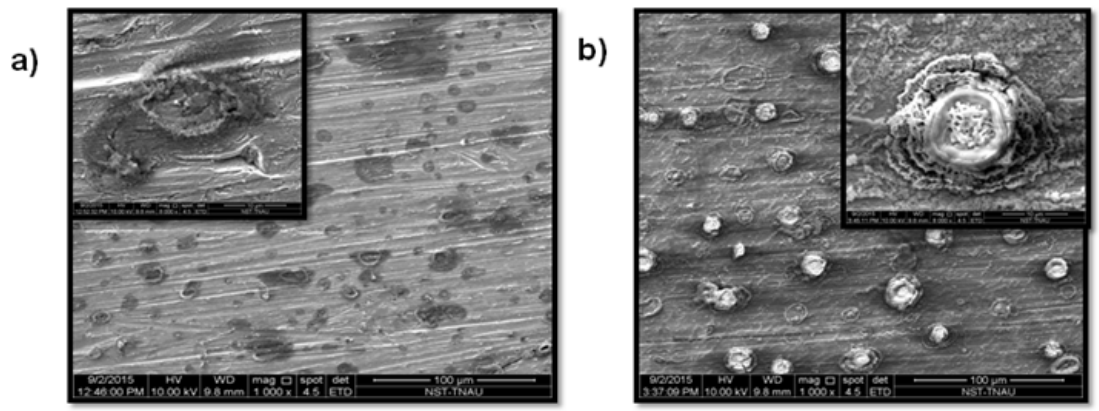

Figure 53 – SEM images of mild steel immersed in the presence of (a) ChSSB (b) ChVSB

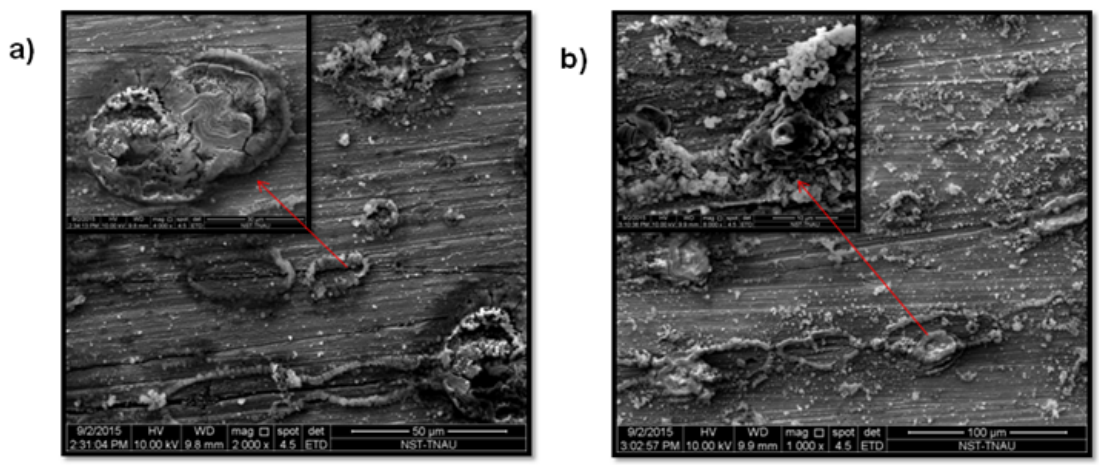

Figure 54 – SEM images of mild steel immersed in the presence of (a) ChTSB(b) ChPSB

In presence of ChTSB, the SEM micrographs of MS specimen (Figure 54a & 54b) have film formation of globular morphology with polymeric globules.

A dense and compact structure was seen in the ChPSB SEM micrograph. Upon magnification of ChPSB surface, the compact structure is associated with some cracks. The micrographs also depict the uniform film formation on the metal surface.

Thus the morphology of the MS surface was greatly influenced in the presence of the Chitosan Schiff bases. In all the images, the surface was totally free from pits and cracks. This improvement in surface morphology is due to the formation of a good protective film of polymeric Schiff bases on the metal surface which is responsible for the inhibition of

corrosion. The cracks observed in the ChPSB morphology may be the reason for its comparatively less inhibitive action than the other Schiff bases.

4.3.5.2 Electron Dispersive X-ray Analysis (EDAX):

Energy dispersive X-ray analysis (EDX) technique was used to analyze the composition of the protective film formed on the metal surface. The EDX mapping was carried out for the selected areas of SEM images of MS in presence of ChSSB, ChVSB, ChTSB and ChPSB.

The results of EDX spectrum of polished metal surface presented in Figure 55a shows the characteristics peaks of the elements constituting the mild steel specimen. The spectrum shows the presence of elements such as C, Si, Mn, Mo and Fe.

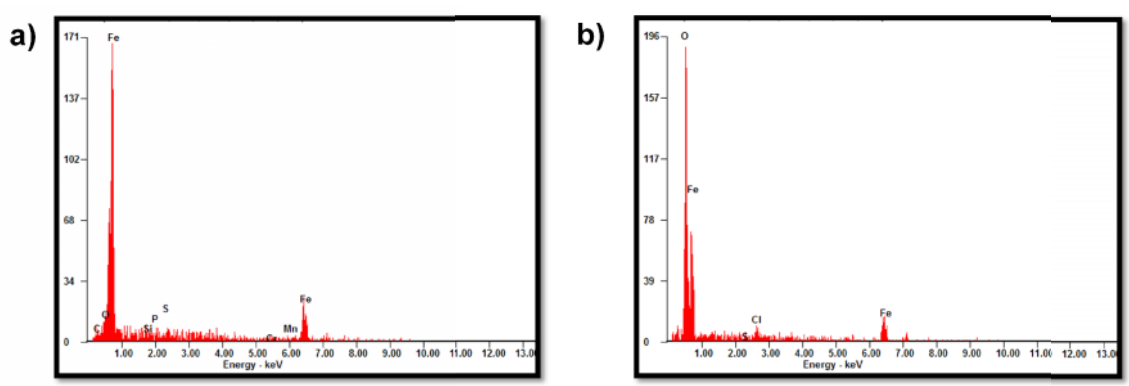

Figure 55 – EDX spectrum of mild steel for (a) Polished surface and (b) immersed in 1M hydrochloric acid solution

For the metal surface without inhibitor treatment Fe, O and Cl are detected (Figure 55b). The oxygen signal is significantly enhanced due to iron oxide formation. The presence of chlorine signal implies the metal dissolution due to chloride ions.

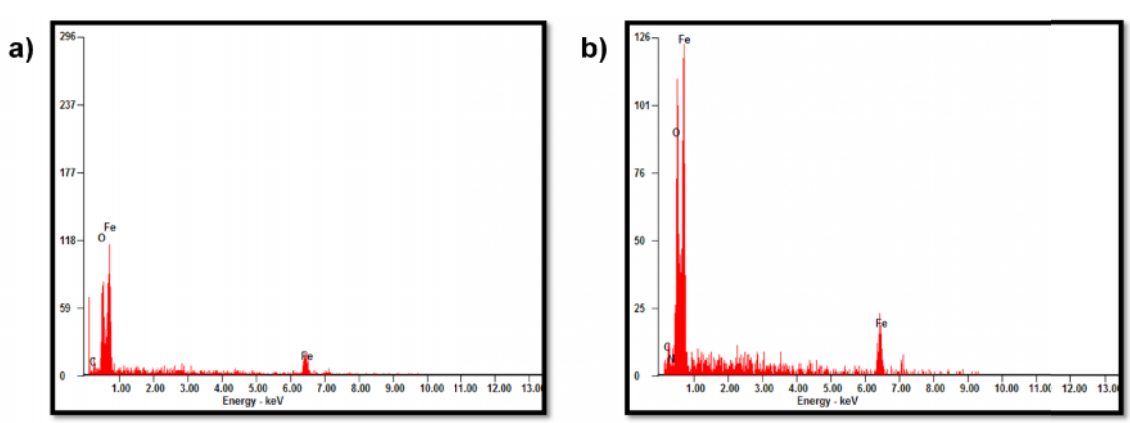

Figure 56 – EDX spectrum of mild steel for immersed in 1M hydrochloric acid solution along with (a) ChSSB and (b) ChVSB

However, in inhibited solutions the EDX spectra showed additional lines characteristic for the existence of carbon and nitrogen (due to the carbon and nitrogen atoms of the chitosan Schiff base polymers). In addition, the sulphur signal was observed on the metal surface exposed to ChTSB. It is obvious from the Table 27 that iron peaks are dramatically suppressed relative to the polished sample. The suppression of Fe lines undoubtedly occurs because of overlying inhibitor film. Moreover, the absence of chloride ions responsible for the metal dissolution confirms the reduction in the metallic corrosion. The reduction in oxygen percentage indicates the suppression of iron oxide formation on the metal surface. These results confirm that the inhibitor forms a surface film on the metal surface.

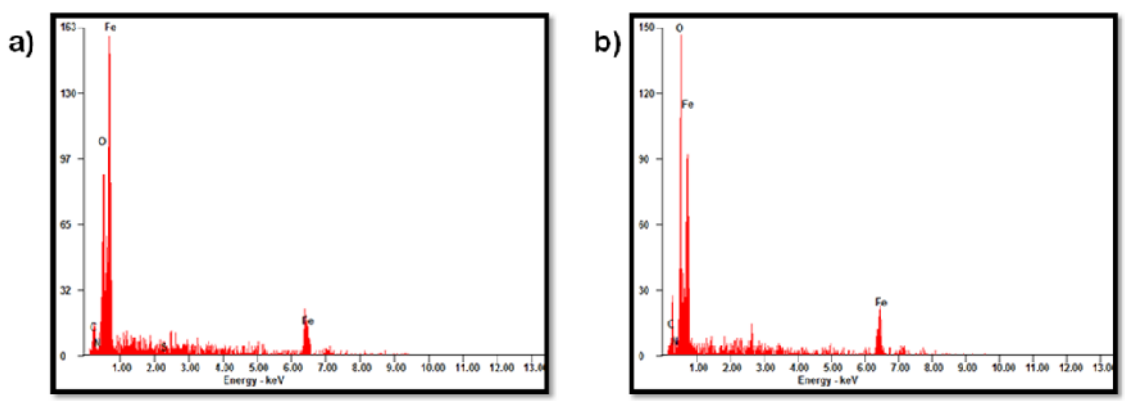

Figure 57 – EDX spectrum of mild steel for immersed in 1M hydrochloric acid solution along with (a) ChTSB and (b) ChPSB

Table 27 – Atomic wt.% of the elements observed in *EDX* analysis

Surface analyzed	Atomic weight %					
	Fe	O	Cl	C	**N**	S
Polished	78.40	06.32		-		
Blank	33.66	63.56	02.78	-	**-**	
ChSSB	54.54	30.38	-	12.08	**03.01**	-
ChVSB	53.35	33.21	-	09.02	**04.43**	-
ChTSB	51.77	27.01	-	15.70	**05.01**	0.51
ChPSB	43.80	38.00	-	14.69	**03.51**	-

4.3.5.3 Atomic Force Microscopy (AFM):

Atomic force microscopy (AFM) is receiving considerable attention in the field of corrosion, since it has been proved to be an excellent tool to study the surface morphology of the adsorbed film at the metal/solution interface. Atomic force microscopy is a powerful technique to examine the adsorbed film formed on the metal surface from nano to micro scale.

The exposed mild steel surfaces were subjected to AFM analysis using Gwyddion software to obtain the average roughness, Ra - the average deviation of all points' roughness profile from a mean line over the evaluation length, and root mean square roughness Rms - the average of the measured height deviations taken within the evaluation length and measured from the mean line.

The microstructures has been achieved using the three dimensional and two dimensional surface topography of mild steel specimens immersed in HCl and in presence and absence of inhibitors. The three dimensional AFM surface images of mild steel specimen immersed for 6 hours in 1M HCl with and without Chitosan Schiff base polymers were shown in Figure 58a. The corresponding two dimensional images also illustrated in Figure 58b.

AFM analysis of corroded metal surface:

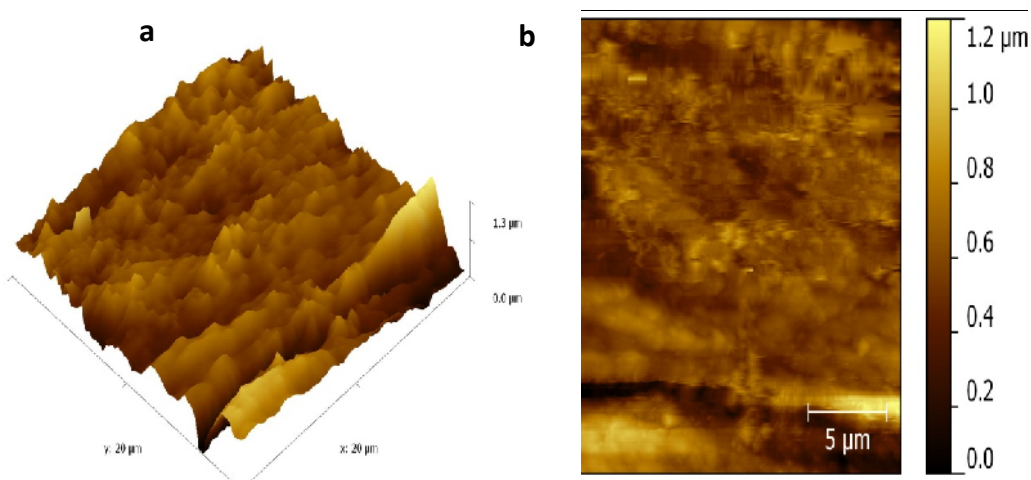

Figure 58 - AFM image of MS specimen in 1M HCl a) three dimensional image b) two dimensional image

The presence of some defected sites, number of protrusions and mountain like structures could be seen in the AFM images of metal surface due to the rapid attack of acid (Figure 58a). The rough surface of the metal with some cracks and pores could be observed in the two dimensional image (Figure 58b) which also augment the dissolution of metal in the acid solution (**Okafor and Zheng, 2009 & Umoren *et al*, 2010**).

AFM analysis of Chitosan Schiff bases inhibited metal surface:

In the presence of Schiff bases, the surface roughness is visibly reduced which could be attributed to the inhibition efficiency of the Schiff base polymers. The three dimensional and two dimensional surfaces of the specimens in presence of inhibitors are shown in Figure 59a & b. Generally, the micrographs in presence of all the inhibitors appear to be smooth, homogenous and uniform compared to the surface in absence of inhibitors. The smoothening of the surface could have caused by the deposition of inhibitor molecules on the mild steel surface.

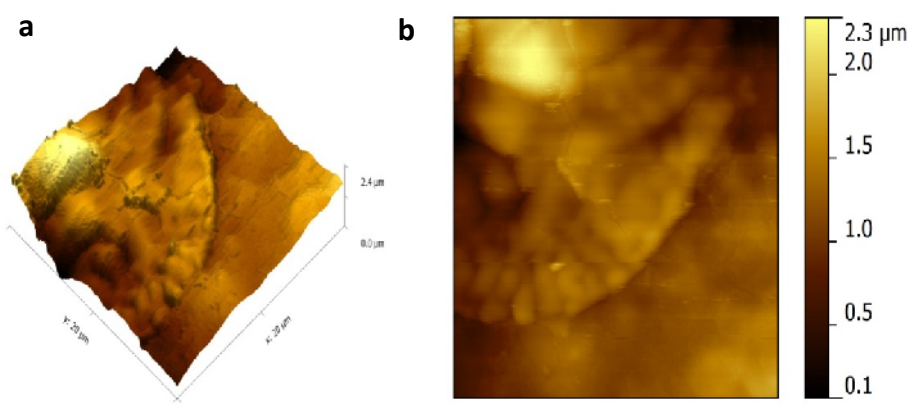

Figure 59 - AFM image of MS specimen in 1M HCl + ChSSB a) three dimensional image b) two dimensional image

The bumpy structure appearance with considerable reduction of protusions and low mountain structure could be observed in the AFM image of ChSSB treated MS specimen along with some agglomerates (Figure 59a) which is clearly visualized in two dimensional image. This may be attributed to the adsorption of inhibitor film on the metal surface.

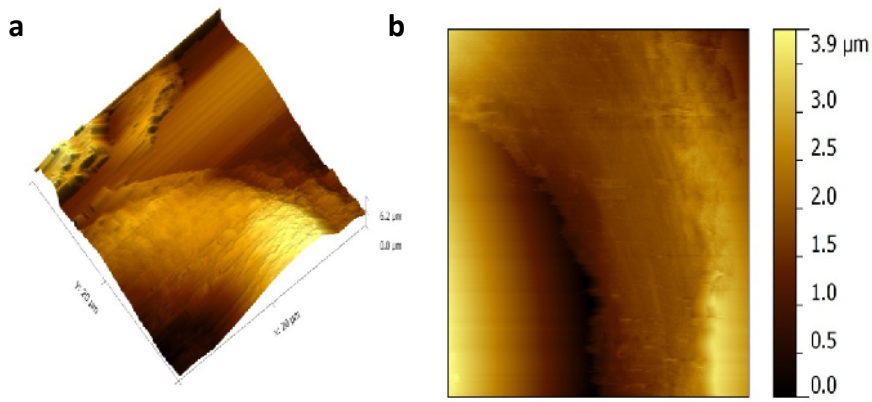

Figure 60 - AFM image of MS specimen in 1M HCl + ChVSB a) three dimensional image b) two dimensional image

The three dimensional and two dimensional AFM images of metal surface exposed to ChVSB and ChTSB were smooth which could be attributed to the more compact and homogeneous film formation by the inhibitors on the metal surface.

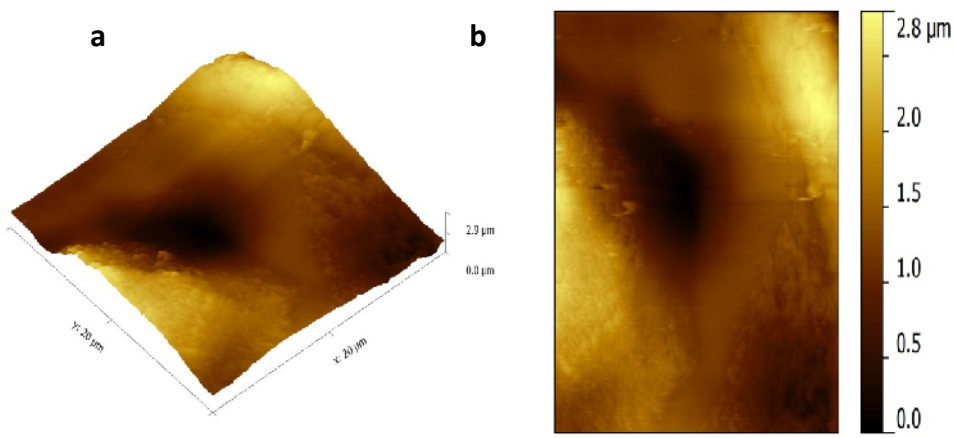

Figure 61 - AFM image of MS specimen in 1M HCl + ChTSB a) three dimensional image b) two dimensional image

The height profile of the metal surface in presence of ChPSB (Figure 61a) is decreased, owing to the protective formation of the inhibitor layer. However the coverage was not uniform leading to the low performance of the inhibitor than others. The average roughness of mild steel in acid with and without inhibitor is presented in Table 28. The mild steel surface in free acid was cracked and surface roughness was 0.559 nm, however in

presence of 1500 ppm of Chitosan Schiff bases the average roughness was reduced to around 0.240 nm.

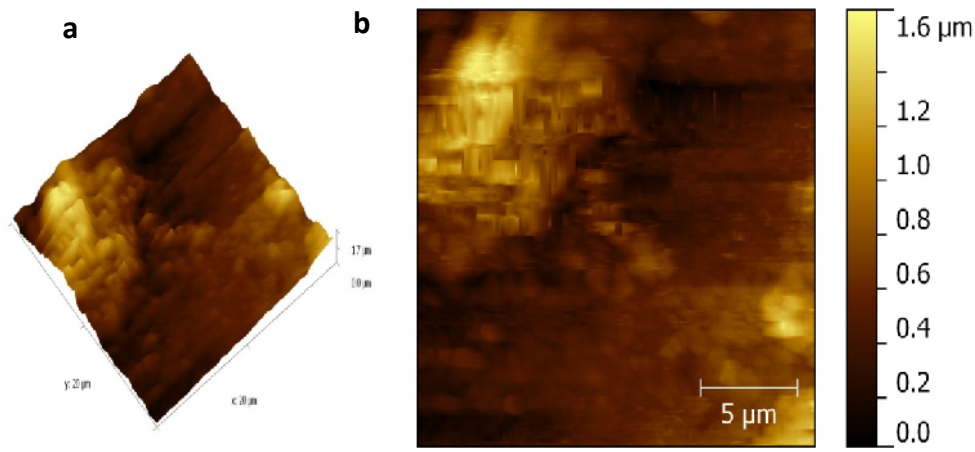

Figure 62 - AFM image of MS specimen in 1M HCl + ChPSB a) three dimensional image b) two dimensional image

Table 28 – Surface roughness parameters obtained for Chitosan Schiff bases

System	Ra (µm)	RMS (µm)
Polished (MS)	0.162	0.155
Blank	0.806	0.559
ChSSB	0.220	0.235
ChVSB	0.206	0.334
ChTSB	0.260	0.271
ChPSB	0.235	0.240

4.3.5.4 Contact angle Measurements:

The measurement of contact angle of the metal surface can determine the nature of the surface. The contact angle is the quantitative measure of the wetting of a solid by a particular liquid. The contact angle is defined as the angle formed by the intersection of the liquid-solid interface. Wettability studies usually involve the measurement of contact angles as the primary data, which indicates the degree of wetting when a solid and liquid interact. The contact angle is an inverse measure of the ability of a particular liquid to wet the surface.

Small contact angles (<<90°) correspond to high wettability, while large contact angles (>>90°) correspond to low wettability. The surface wetting property depends on chemical composition and surface morphology. The mild steel surface is highly wettable, the adsorption or any change on the metal surface decreases the wettability and thereby reduces the metallic corrosion.

The wettability of mild steel surfaces after 6 hours of immersion in solution with and without Chitosan Schiff bases are analyzed using Goniometer. Figure 63 shows the contact angle between the metal surface and water droplet. The contact angles measured with the investigated Schiff bases are given in Table 29.

Table 29 – Contact angle measurements for the metal with Chitosan Schiff bases

Sample	Contact angle (^{o})
Blank	21.5
ChSSB	45.7
ChVSB	60.5
ChTSB	42.4
ChPSB	44.1

The contact angle for a water droplet on the mild steel surface after immersion in 1M HCl for 6 h was found to be 21.5^o (Figure 63a) which indicates the increase in wettability. The increase in wettability allows the attack of corrosive ions with metal surface. The low contact angle is possibly due to presence of hydrophilic corrosion products on the metal surface in the acidic environment, which modify the composition and properties of the surface. This also implies the roughness of the surface brought about by the attack of the corrosive ions present in the aggressive environment (**Umoren *et al*., 2015**).

From the Table 29, it can be noticed that in presence of (ChSSB), (ChTSB), (ChPSB), the water droplet contact angle was found to be 45.7 ^{o} (Figure 63b), 42.4 ^{o} (Figure 63c) and 44.1^o (Figure 63d) respectively. The increase in the contact angle is the indication of formation of hydrophobic film due to the adsorption of Schiff base molecules onto the metal surface (**Khan *et al*., 2015, Ashhari and Sarabi, 2015).** The contact angles on the metal specimens exposed to solutions containing Chitosan Schiff bases are found to increase compared to that on the specimen exposed to the uninhibited solution. This infers that the coarseness of the surface was reduced by virtue of adsorption of the polymer molecules onto the mild steel surface. It also indicates that the surface roughness decreases with the adsorption of Chitosan Schiff bases on the metal surface which also proved by SEM images.

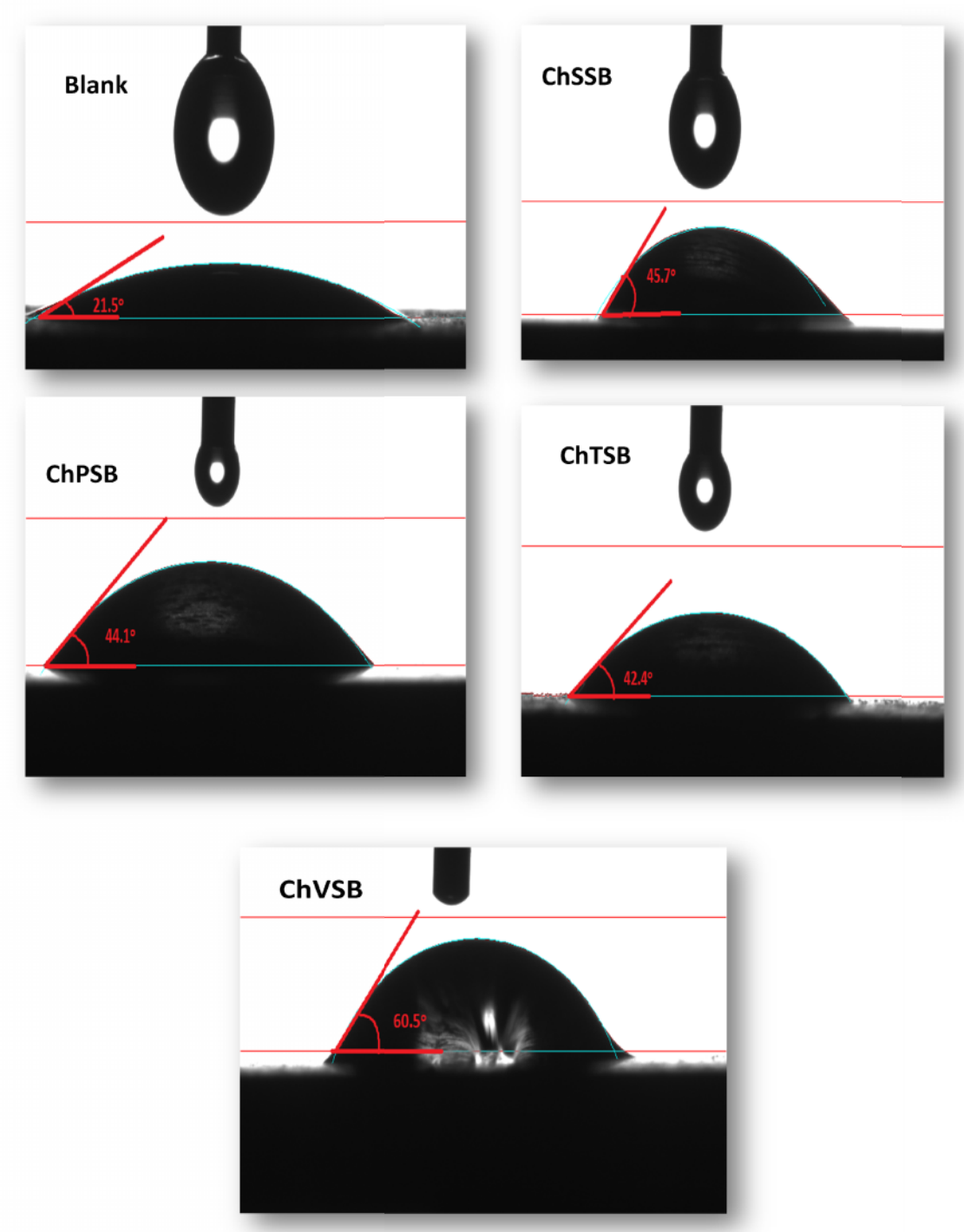

Figure 63 - Water droplet contact angles on mild steel surfaces immersed in a) Blank b) ChSSB c) ChPSB d) ChTSB e) ChVSB

The high contact angle observed for the coupons treated with ChVSB (Figure 63e) indicates that the electrolyte attack is more difficult and therefore better corrosion inhibition performance is obtained for ChVSB. Whatever the protection mechanism, the results presented in Table 29 indicates a stronger hydrophobic nature of the Chitosan Schiff bases adsorption layer, which must delay the corrosion processes.

From the literature survey, the results suggest that the inhibition behaviour of the Chitosan Schiff bases is due to

(i) improved barrier properties of the formed Chitosan Schiff base layer which would block preferential pathways for electrolyte penetration,

(ii) Increased thickness of the adsorbed layers. (**Palomino *et al.,* 2008**).

Therefore, it is clear that the protective layer is formed by Chitosan Schiff bases in the corrosive media. This change in the surface morphology could inhibit the corrosion of the Mild steel specimen by suppressing the aggressive ions permeation and incorporation.

4.3.5.5 FTIR –Analysis:

FTIR analysis is a powerful technique that can be used to analyze the protective film formed on metal surface and also to determine the new bonding involved during adsorption of the inhibitor. The FTIR spectra of the adsorbed protective layers formed on the mild steel surface after immersion in 1M HCl containing 1500 ppm of Chitosan Schiff bases for about 6 hours were shown in Figures 64 - 67.

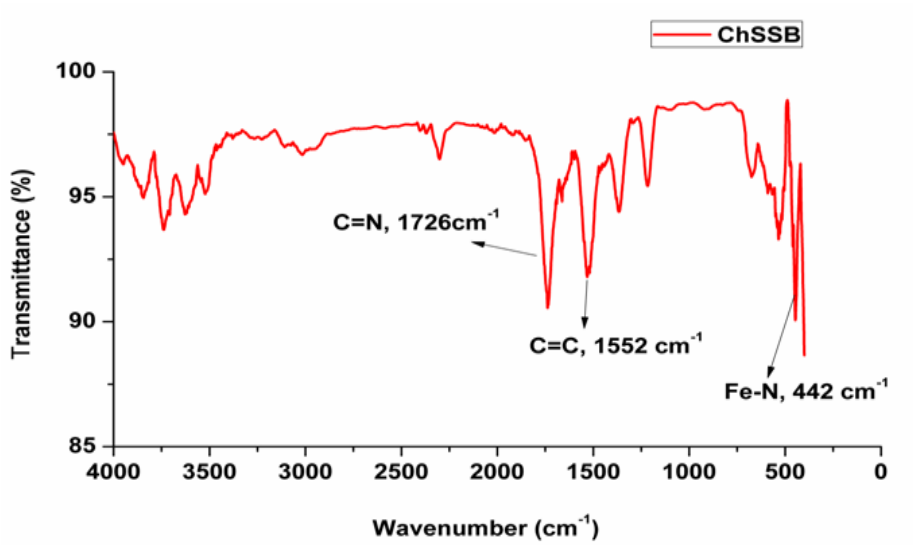

Figure 64 – FTIR spectrum of ChSSB adsorbed mild steel surface

A detailed study on the FT-IR spectra of native Chitosan Schiff bases and those adsorbed on the mild steel surface has revealed some key information regarding the mode of adsorption of the inhibitors on the metal surface.

On comparing the FTIR spectra of native Chitosan Schiff bases (Figure 10 - 13) and adsorbed metal surface, the distinctive peaks responsible for the confirmation of modified Schiff bases has been shifted to higher frequency region in the adsorbed metal surface. Also, certain additional peaks appeared indicate that some interaction/adsorption occurs over metal surfaces.

The strong absorption peaks in the region 3400-3800 cm^{-1} are seen to be more intense in the Chitosan Schiff bases adsorbed metal surface than the native. The high intensity peaks clearly indicates the extent of hydrogen bonding in adsorbed metal surface is more compared to native Schiff bases. This in turn, reveals that some of the hydroxyl groups of Chitosan backbone involved in adsorption of metal surface (**Roy *et al.*, 2014**). Moreover, the presence of superficial adsorbed water in the metal surface also supports the increase in the intensity of absorption region (**Chauhan and Gunasekaran, 2007**). These peaks are absent in native Schiff bases could also be attributed to the Fe-O bending, (**Li *et al.*, 2010, Qu *et al.*, 2007**) which reveal the fact that inhibitors can adsorb on the metal surface between lone-pair electrons of oxygen and the vacant d-orbital of Fe substrate.

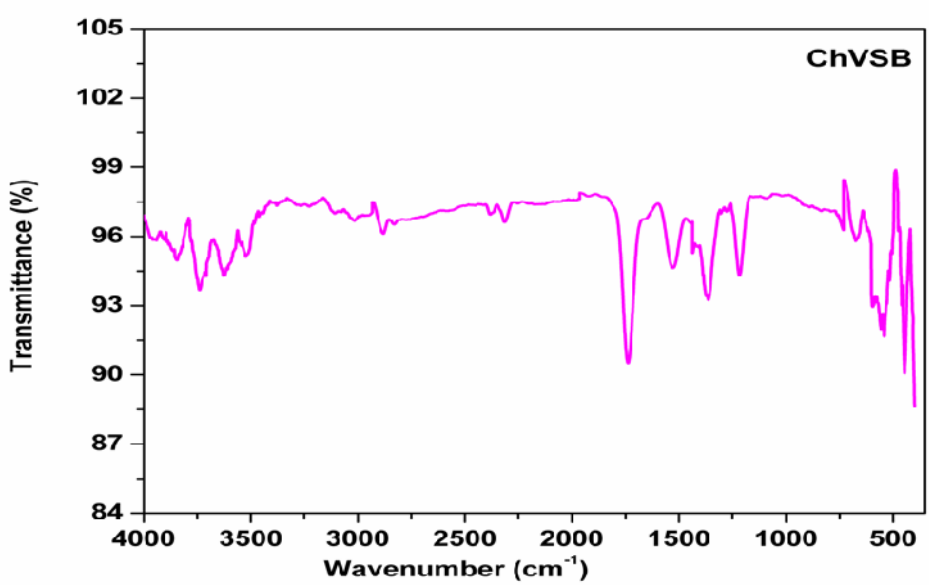

Figure 65 – FTIR spectrum of ChVSB adsorbed mild steel surface

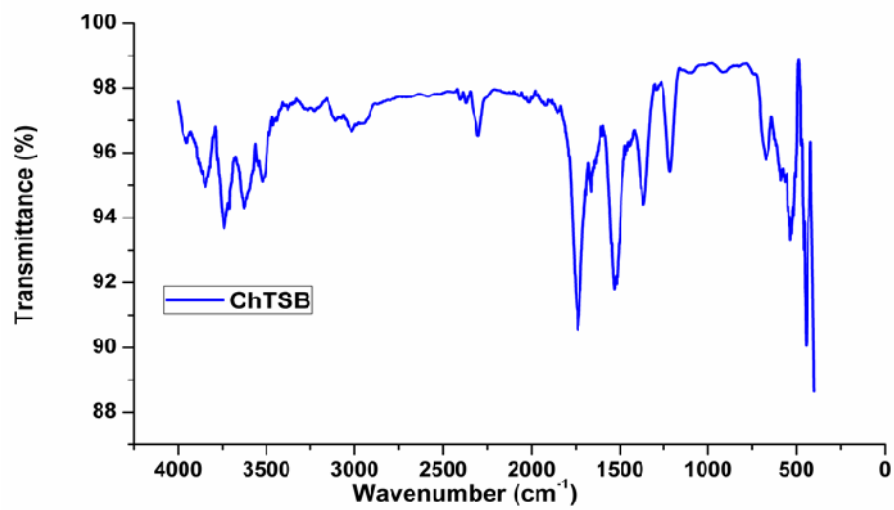

Figure 66 – FTIR spectrum of ChTSB adsorbed mild steel surface

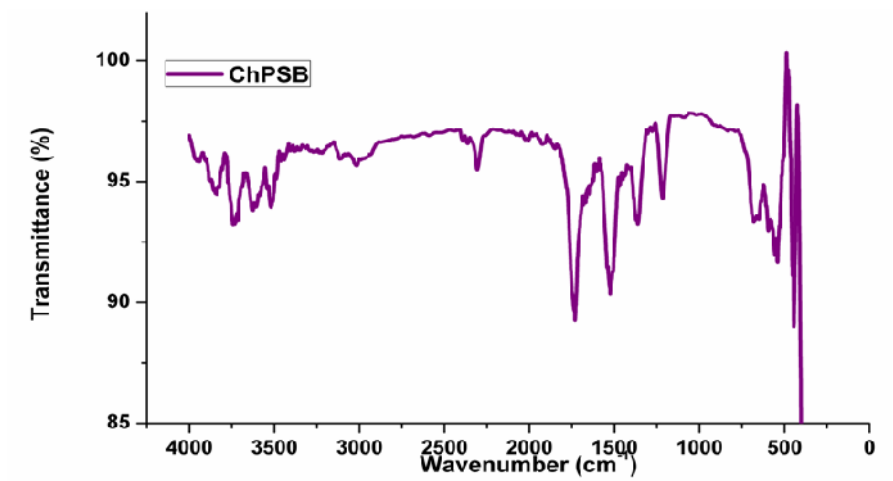

Figure 67 – FTIR spectrum of ChPSB adsorbed mild steel surface

The peaks corresponding to stretching vibration of -HC=N imine group shifted from the range of 1631-1649 cm^{-1} to 1726 cm^{-1}, which confirmed that the Chitosan Schiff bases coordinates through nitrogen atom with Fe^{2+} . The characteristic strong peak at 442 cm^{-1} due to Fe-N stretching also confirmed the formation of coordinate bond between the nitrogen atom present in the inhibitor and the Fe^{2+} ions present on the metal surface.

The peak at 1537 cm^{-1} is due to the C=C stretching vibrations of aromatic system and its shift from 1552 cm^{-1} reveals the existence of interaction between the aromatic pi electrons and the Fe substrate.

The peaks at 1156.70, 1023.16, 841.19 cm^{-1} which are assigned to different vibrational modes of C-O-C stretching vibrations of Chitosan backbone are seen to be distinctly shifted to 1098, 907, 746 cm^{-1} respectively with lower intensities. Therefore, it is presumed that the horizontal orientation of Chitosan backbone structure with respect to metal surface could be occurred and subsequent adsorption of Chitosan molecules on metal leading to a decrease in the rate of metal corrosion. Involvement of Chitosan molecules in the adsorption process is further confirmed by the shift of the peaks 1357 and 1210 cm^{-1} which is due to the CH_3 deformation and C-N amino groups present in the Chitosan structure.

From the above observations, it can be concluded that the mode of adsorption of Chitosan Schiff base polymers on the mild steel surface is due to simultaneous adsorption of Chitosan backbone and anchoring units of Chitosan Schiff base polymers. These groups are responsible for high degree of corrosion inhibition of mild steel in acid medium.

4.3.5.6 Surface analysis by X-ray photoelectron Spectroscopy:

XPS is arguably one of the most effective surface analysis techniques because of its relative simplicity in use and data interpretation. The sample is irradiated with monoenergetic X-rays causing photoelectrons to be emitted from the sample surface. An electron energy analyzer determines the binding energy of the photo electrons. From the binding energy and intensity of a photoelectron peak, the elemental identity, chemical state and quantity of an element can be determined (**Ideo *et al*., 1991**).

XPS analysis has been of key importance in the field of corrosion science, since it helps to

- Confirm the formation of inhibitor film on the metal surface.
- Obtain more detailed information about the assumption of adsorption (i.e, chemisorption)
- Investigate the composition of inhibitor layer adsorbed on the mild steel surface.

Since all the four Chitosan Schiff bases were found to be producing similar results in almost all surface analytical techniques and to confirm the formation of chemisorption bond on the metal surface, XPS technique for one Chitosan Schiff base was carried out.

Analysis of Survey spectrum:

XPS measurement was carried out with mild steel surface immersed for 6 h in 1M HCl with 1500 ppm of Chitosan salicylaldehyde Schiff base (ChSSB). Survey scan of the

sample was first recorded and is presented in Figure 68. The obtained XPS survey spectrum provides information about the presence of elements such as Fe, C, N, O. The spectrum also provides the detail about the presence of characteristic peak of elements with their respective binding energy values. The elements and their binding energy values along with the atomic weight percent values are presented in Table 30.

Table 30 – Binding energy values and Atomic % of the elements using XPS technique

Name	Peak BE	Atomic %
C 1s	285.31	37.39
N 1s	400.49	0.90
O 1s	530.55	45.55
Fe 2p	711.66	16.17

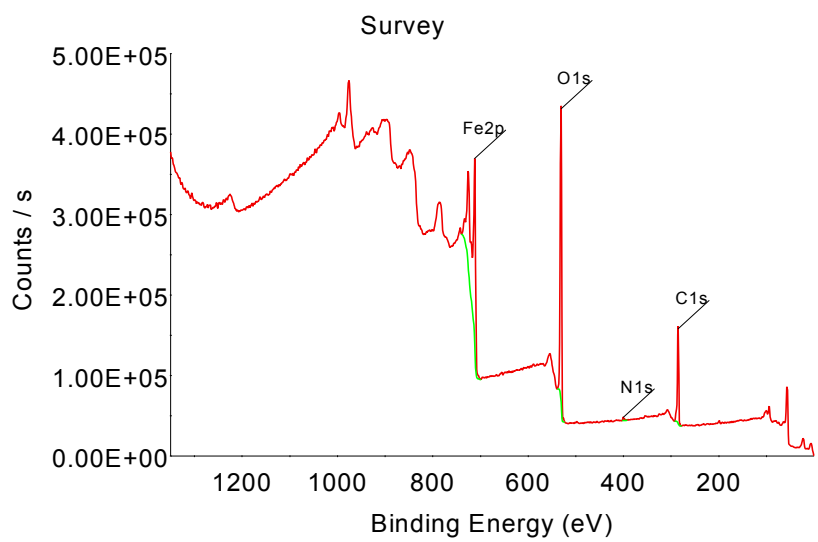

Figure 68 - Survey spectrum of mild steel surface treated with ChSSB

The main feature in the survey spectrum is the presence of nitrogen peak which can be attributed to the fingerprint region of the inhibitor layer formed on the mild steel surface. The high resolution spectra for C 1s, O 1s, N 1s and Fe 2p studies were carried to get a better understanding and more information about the adsorbed ChSSB molecules on the metal surface and the corrosion inhibition mechanism.

Analysis of C 1s spectrum:

The deconvoluted C 1s core level spectrum for MS immersed in inhibitor ChSSB is presented in Figure 69. The spectrum represents three main peaks which indicate that three

chemical forms of carbon atom present on the surface of the mild steel. The first peak at binding energy 285.38 eV has largest contribution and is attributed to the C-C, C=C and C-H aromatic bonds (**Tourabi *et al.*, 2013**). The same peak 285.38 eV which is approximately 286 eV can also be attributed to C-O-C linkage of Chitosan matrix (**Abu-Dalo *et al.*, 2012**). The second peak at 287.08 eV can be ascribed to the carbon atom of the C-O bond in the hydroxyl group (C-OH). The third peak at higher binding energy 288.78 eV (approx 289) may be ascribed to the carbon atom of the $–HC=N^+$ resulting probably from the coordination of nitrogen in the Chitosan Schiff base with metal surface (**Bentiss *et al.*, 2009b**).

Table 31 – Binding energy and their assignment for the major core lines observed for C 1s of MS treated ChSSB

Sample	BE (eV)	Assignment
MS + ChSSB	285.38	C-C, C=C and C-H aromatic bonds, C-O-C linkage
	287.08	C-O of hydroxyl group
	288.78	$C=N^+$ of imine group

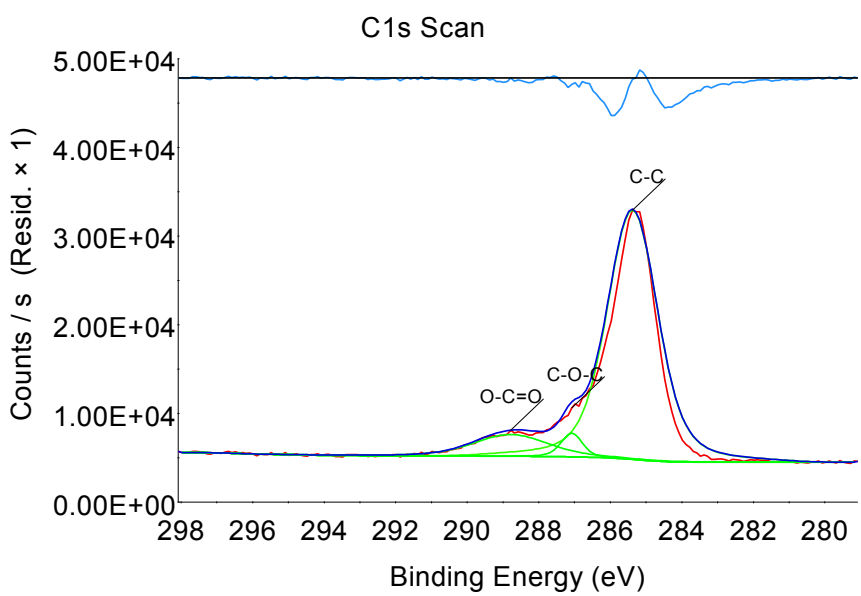

Figure 69 – XPS convoluted spectrum of C 1s for MS treated with ChSSB

Analysis of O 1s spectra:

The deconvoluted O 1S spectrum for mild steel surface after immersion in 1M HCl solution containing ChSSB may be fitted into four main peaks as shown in Figure 70. The peaks were fitted as follows:

- The first peak at 530.18 eV is attributed to O^{2-}, which represents the lattice oxygen (**Shubina *et al.*, 2015**). This could also relate to oxygen atom bonded to Fe^{3+} in Fe_2O_3 and Fe_3O_4.
- The second peak observed at 531.38 eV is related to OH and can be associated with the presence of hydroxide layer on the mild steel surface, such as FeOOH and/or $Fe(OH)_3$.
- The third peak at 532.38 eV relates to oxygen from the chemically or physically adsorbed water (**Gunasekaran and Chauhan, 2004**)
- Finally, the fourth peak at 533.38 eV can be related to the oxygen of the hydroxyl group in the Chitosan Schiff base.

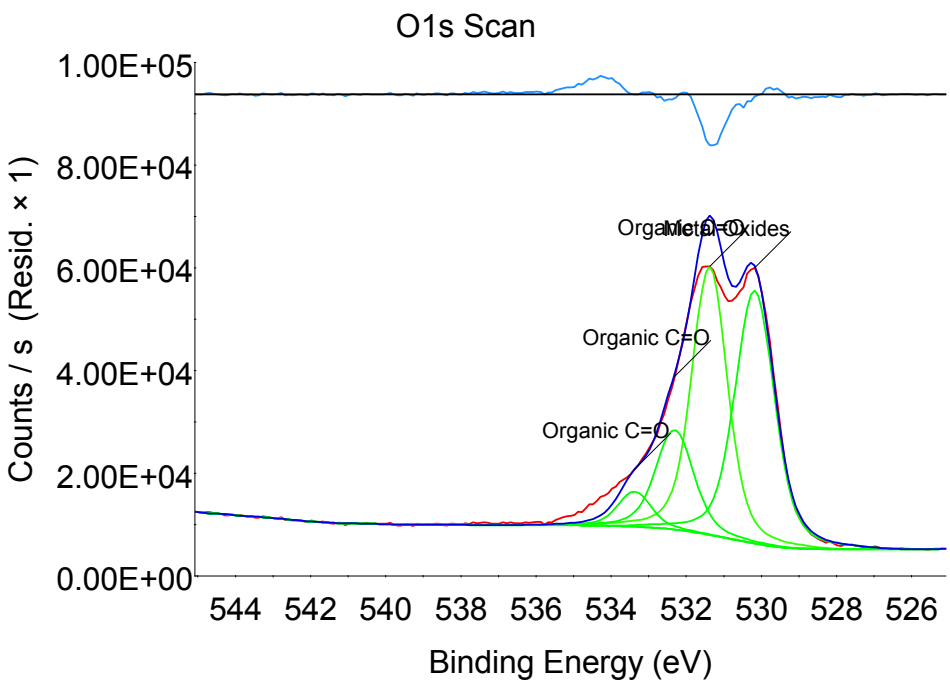

Figure 70 – XPS convoluted spectrum of O 1s for MS treated with ChSSB

Table 32 – Binding energy and their assignment for the major core lines observed for O 1s of MS treated ChSSB

Sample	BE (eV)	Assignment
MS + ChSSB	530.18	Fe_2O_3/ Fe_3O_4
	531.38	FeOOH/$Fe(OH_3)$
	532.38	Adsorbed water molecules
	533.38	Oxygen of hydroxyl group

Analysis of N 1s spectrum:

The N 1s spectrum envelopes for the ChSSB treated MS sample were fitted into two peaks as shown in Figure 71. The first peak at 400.18 eV has the highest contribution and is mainly attributed to nitrogen atoms characteristic of non-protonated nitrogen, N=CH. **Meneguzzi *et al.*, 2001** has reported that the peak at 399.9 eV could be attributed to the neutral imine (-N=) and amine (-N-H) nitrogen atoms. This component is typical for amines, imines, amides and also ascribed to the nitrogen atom coordinated to the steel surface (N-Fe). The second peak at 401.08 eV indicates a new bond involving nitrogen groups attributed to positively charged nitrogen (**Bentiss *et al*., 2012**). From these observations, the presence of coordinated nitrogen on the metal surface confirmed the chemisorption of the inhibitor molecule on the metal surface.

Table 33 – Binding energy and their assignment for the major core lines observed for N 1s of MS treated ChSSB

Sample	BE (eV)	Assignment
MS + ChSSB	400.18	Imine, amine
	401.08	N-Fe

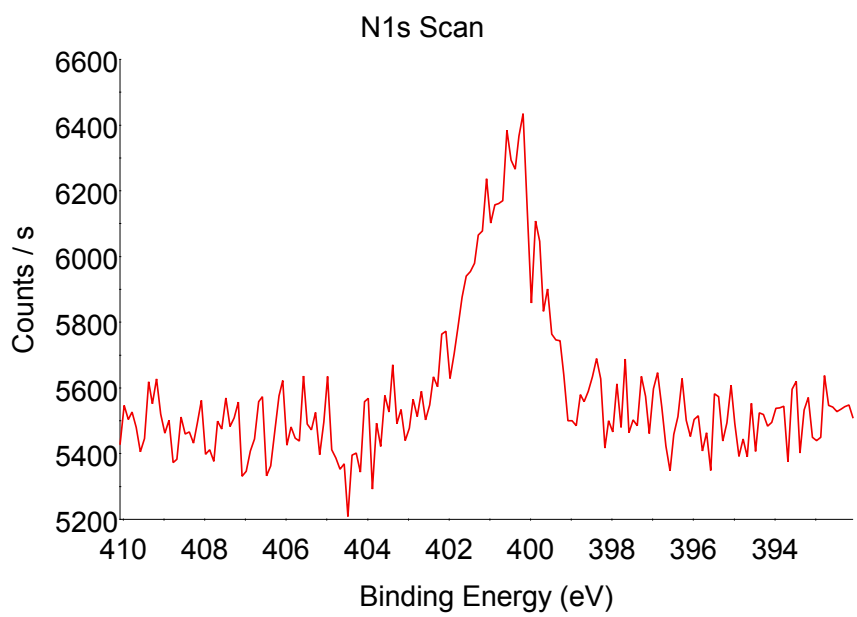

Figure 71 - XPS Deconvoluted spectrum of N 1s for MS treated with ChSSB

Analysis of Fe 2p spectrum:

Iron spectra composed of a doublet structure due to spin orbit splitting (Fe 2p3/2 and Fe 2p1/2) as seen in Figure 72. Two peaks are observed for Fe 2p one at 711.78 corresponding to Fe 2p3/2 and other peak at 725.28 eV corresponding to Fe 2p1/2 electron. The peak due to Fe 2p3/2 is interpreted for the determination of chemical state of iron in the surface film. Thus the peak suggests that the iron is present in Fe^{3+} state in the surface film. In the literature, the peak at 711.0 eV was ascribed to the presence of FeOOH and $Fe(OH)_3$. The binding energy of Fe 2p3/2 due to Fe_2O_3 was reported to be 711.0± 0.15 eV. Thus the peak could be attributed to the Fe of Fe_2O_3 which means that a certain degree of oxidation of Fe happened. It was inevitable for Fe to be oxidized during the process of preparing specimen due to its activity (**Wang *et al*., 2011**).

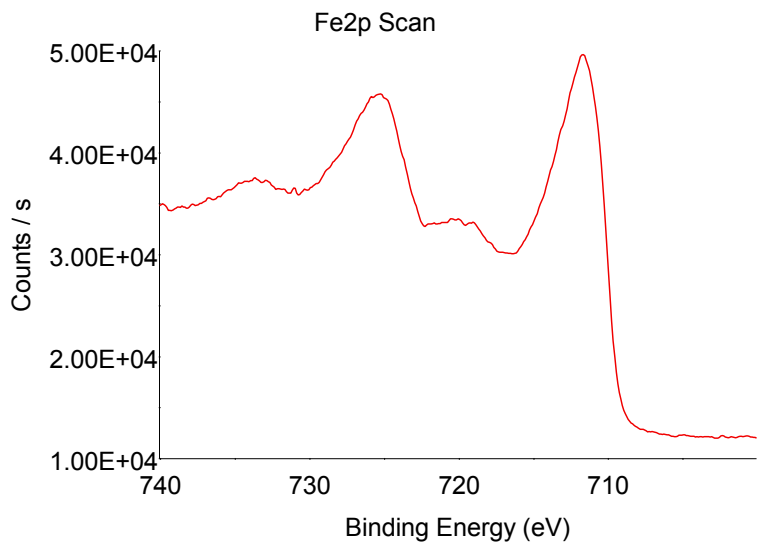

Figure 72 – XPS Deconvoluted spectrum of Fe 2p for MS treated with ChSSB

Table 34 – Binding energy and their assignment for the major core lines observed for Fe 2p of MS treated ChSSB

Sample	BE (eV)	Assignment
MS + ChSSB	711.78 725.28	Fe^{3+}, Fe_2O_3

Conclusions drawn from XPS results:

From the XPS studies, the obtained results support the adsorption of inhibitors on the metal surface and gives evidence for chemical interactions between the Chitosan salicylaldehyde Schiff base (ChSSB) and mild steel surface. The presence of nitrogen

species on the steel surface such as –HC=N and C-O-C linkage of Chitosan chain corroborates for the formation of Chitosan Schiff base film on the metal surface. The peak N-Fe confirms that the investigated ChSSB was chemisorbed on the steel surface and agrees well with the other surface analytical techniques.

Phase - IV

4.4 Quantum chemical calculations:

Quantum chemical methods are particularly important in the study of electrochemistry to provide a relatively quick way of predicting the structure and behaviour of corrosion inhibitors. The concept of assessing the efficiency of a corrosion inhibitor with the help of computational methodology paves the way to screen the inhibitor compounds by correlating their structure and inhibiting activity or property. As reported by many researchers inhibiting effect of the corrosion inhibitors mainly depend on some of their physicochemical and electronic properties which relates to its functional groups, steric effects, electronic density of donor atoms and orbital character of donating electrons (**Gece, 2008**). Since quantum chemical methods will provide more information about the reactivity, active sites and mechanism of interaction of inhibitors with the metal surface, theoretical interpretation of corrosion inhibitors has become more essential in parallel to the experimental results. Therefore, an attempt was made to use theoretical data in the present study to support the experimental results.

Semi empirical methods

Semi empirical methods serve as an efficient computational tool which can yield fast quantitative estimates for a number of properties. The MNDO, AM1 and PM3 methods were designed to reproduce heats of formation and structures of a large number of organic molecules.

AM1 (Austin model 1) method- is a semi empirical method developed by Michael Dewar and co-workers in 1985 (**Dewar *et al*., 1985**). AM1 method was used in the calculations since it has proved to be highly reliable for calculating the physical properties of molecules (**El Ashry *et al*., 2006**)

PM3 (parameterized model number 3) method- is another semi empirical method developed by Stewart and first reported in 1989 (**Stewart, 1989**). The PM3 method uses the same formalism and equations as the AM1 method while the difference lies in the philosophy and the methodology during the parameterization.

Density functional theory

Density functional theory (DFT) is used to investigate the electronic structure, principally the ground state of many-body systems, in particular atoms, molecules and the condensed phases. The main objective of DFT is to replace the many-body electronic wave function with the electronic density as the basic quantity. Any exchange functional can be combined with any correlation functional in DFT calculations. For example, the notation BLYP/ 6-311G* denotes a density functional calculation done with the Becke 1988 exchange functional and the Lee-Yang-Parr correlation functional, with the orbitals expanded in a 6-311G* basis set (**Gece, 2008**).

Quantum chemical parameters

Molecular orbital energies

The most significant quantum chemical parameters are the highest occupied molecular orbital energy (E_{HOMO}) and the lowest unoccupied molecular orbital energy (E_{LUMO}) collectively called as frontier orbitals. These frontier orbitals are used to predict the adsorption centres of the inhibitor molecule. The HOMO is the orbital that could act as an electron donor, since it is the outermost (highest energy) orbital containing electrons. The LUMO is the orbital that could act as the electron acceptor, since it is the innermost (lowest energy) orbital that has space to accept electrons. According to the frontier molecular orbital theory, the formation of a transition state is due to an interaction between the frontier orbitals (HOMO and LUMO) of reactants (**Yadav, 2016**). The energy of the HOMO is directly related to the ionization potential (IP) and the energy of the LUMO is directly related to the electron affinity (EA) and are calculated using the relationship,

$$EA = -E_{LUMO} \quad (28)$$

$$IP = -E_{HOMO} \quad (29)$$

The difference in energy between the HOMO and LUMO i.e the energy gap of HOMO-LUMO is an important stability index (**Al-sabagh *et al*., 2011**). A large HOMO–LUMO gap implies high stability for the molecule in chemical reactions (**Zhang *et al*., 2011**). The concept of ‘‘activation hardness” has been also defined on the basis of the HOMO–LUMO energy gap. The qualitative definition of hardness is closely related to the polarizability, since a decrease of the energy gap usually leads to easier polarization of the molecule.

Electronegativity (χ) is related to electron affinity and ionization potential according to the equation as follows:

$$\chi = (IP+EA)/2 \quad (30)$$

Chemical hardness is the measurement of resistance of an atom to a charge transfer and it is calculated by by the equation

$$\lambda = (IP-EA)/2 \quad (31)$$

Chemical softness (σ) describes the capacity of an atom or group of atoms to receive electrons and is calculated

$$\sigma = 1/\lambda = -2/(E_{HOMO} - E_{LUMO}) \quad (32)$$

When metal (Fe) and inhibitor molecule are in contact, the higher electronegative species (Fe) will attract electrons to itself until there is a balance in chemical potential. Therefore a fraction of electrons (ΔN) are transferred from the inhibitor molecule to the metallic atom and was calculated using quantum chemical method.

$$(\Delta N) = \chi_{Fe} - \chi_{inh} / 2(\lambda_{Fe} + \lambda_{inh}) \quad (33)$$

where χ_{Fe} and χ_{inh} denotes the absolute electronegativity of Fe and the inhibitor molecule respectively; λ_{Fe} and λ_{inh} denote the absolute hardness of Fe and the inhibitor molecule respectively. Theoretical value of χ_{Fe} as 7 eV mol^{-1} and λ_{Fe} as 0 eV mol^{-1} were used to calculate the number of electrons transferred (ΔN) from the inhibitor molecule to the Fe atom (**Deyab, and Abd El-Rehim, 2013).**

Dipole moment

Dipole moment, a widely used quantity describes the measure of polarity of a polar covalent bond. It is defined as the product of charge on the atoms and the distance between the two bonded atoms. The total dipole moment, however, reflects only the global polarity of a molecule. For a complete molecule the total molecular dipole moment may be approximated as the vector sum of individual bond dipole moments.

Total energy

The total energy calculated by quantum chemical methods is also a beneficial parameter. The total energy of a system is composed of the internal, potential, and kinetic energy. **Hohenberg and Kohn,1964** proved that the total energy of a system including that of the many body effects of electrons (exchange and correlation) in the presence of static external potential (for example, the atomic nuclei) is a unique functional of the charge density. The minimum value of the total energy functional is the ground state energy of the system. The electronic charge density which yields this minimum is then the exact single particle ground state energy.

4.4.1 Theoretical investigation of Chitosan Schiff bases using quantum chemical methods

Quantum chemical calculations were conducted with three different quantum chemical methods (AM1, PM3 and DFT) by geometry optimization of the investigated compounds in order to support experimental data and to investigate the relationship between molecular structure of the Chitosan Schiff bases and their inhibition effects. Semi empirical methods (AM1 and PM3) were carried out using Hyperchem 7 software and optimized using built in Polak-Ribiere algorithm with root mean square gradient of 0.05kcal/mol in-vacuo method. The molecular structures of the Chitosan Schiff bases were also optimized with DFT method using 6-311G (d,p) basis set. The molecules were built with the Gauss View 5.0 implemented in Gaussian 09 package.The B3LYP function is a hybrid method (HF wave function + DFT energy calculation) that adds the exchange and electronic correlation in DFT terms including the Lee, Yang and Parr (LYP) functional. The structures of biopolymeric Schiff bases viz., ChSSB, ChVSB, ChPSB, ChTSB were drawn using Chem. Draw ultra 2.0 software. Since Chitosan is a long polymer chain, an oligomer model with three repeating units consisting of two glucosamine unit and a Schiff base unit was constructed for the quantum studies. The structures were saved as Mol file and taken as input for the quantum chemical studies.

4.4.1.1 Quantum chemical calculations for Chitosan Schiff bases – Semi-empirical methods

The relationship between the inhibitor ability and their quantum chemical parameters were established by theoretical calculations using Austin model 1 (AM1) and parametric method 3 (PM3) in Hyperchem software. The oligomer model developed with two glucosamine unit and a Schiff base unit with imine linkage between the Chitosan and carbonyl group were used for quantum chemical studies by AM1 and PM3 semi empirical methods. The schematic representation of the biopolymeric Schiff bases, ChSSB, ChVSB, ChTSB, ChPSB are shown in Table 6 (Phase-I). The optimized structures of the biopolymeric inhibitors are shown in Figure 73.

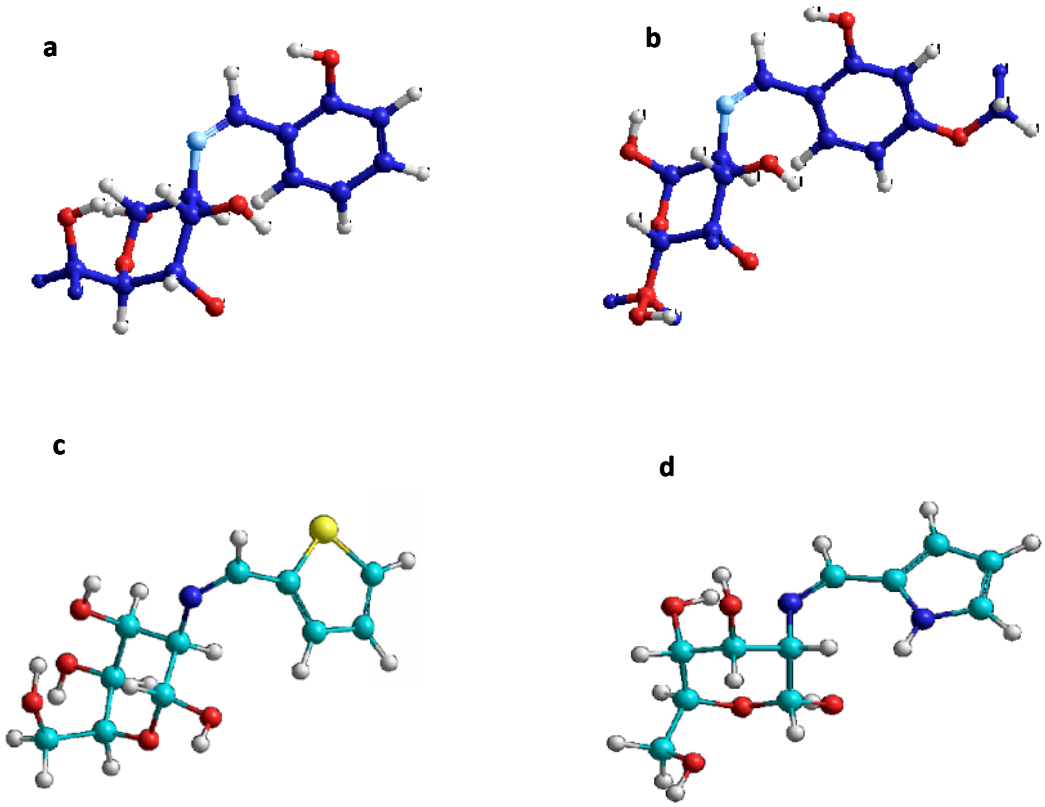

Figure 73 – Optimized structures of Chitosan Schiff bases a) ChSSB b) ChVSB c) ChTSB d) ChPSB

Generally, the molecular reactivity will be discussed on the basis of frontier orbital energies (E_{HOMO} and E_{LUMO}) since they are responsible for the interaction of inhibitor with the metal surface. Figure 74 shows the HOMO density and LUMO density distribution of the Chitosan Schiff bases from AM1 method. Figure 75 shows the HOMO density and LUMO density distribution of the Chitosan Schiff bases from PM3 method. HOMO orbitals of the molecules are the sites at which electrophiles attack and represent the active centers with the ability to interact with the atoms on the metal surface. LUMO orbitals of the molecules predict the sites at which the molecules can accept electrons from metal thereby forming bonds (**Obot *et al*., 2014**). From the Figures 74 & 75, it can be seen that the HOMO orbital is mainly located on the –HC=N group, aromatic rings of the substituents and reactive hydroxyl groups of the Chitosan Schiff bases whereas its LUMO spreads over the anchored aldehyde molecules. Thus these active sites are responsible for the strong interaction of the biopolymeric Schiff base molecules with the metal surface.

Inhibitor	Frontier molecular distribution - HOMO	Frontier molecular distribution – LUMO
ChSSB	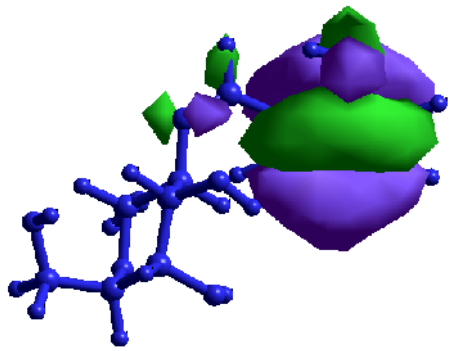	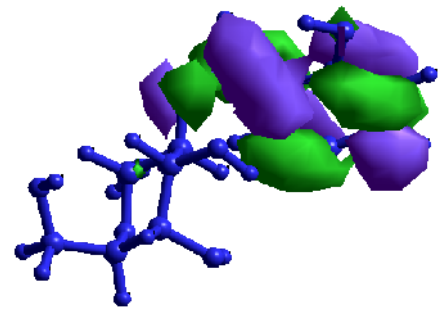
ChVSB	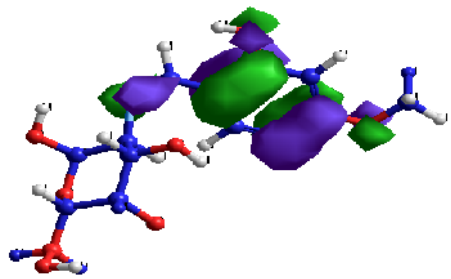	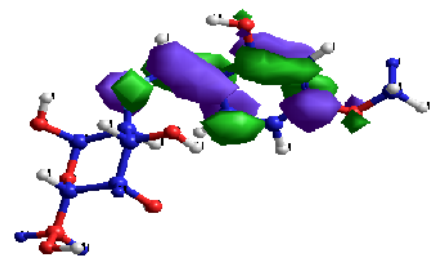
ChTSB	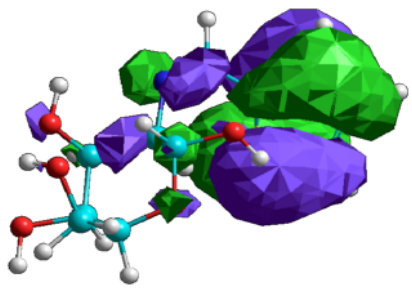	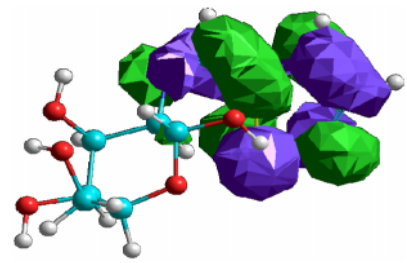
ChPSB	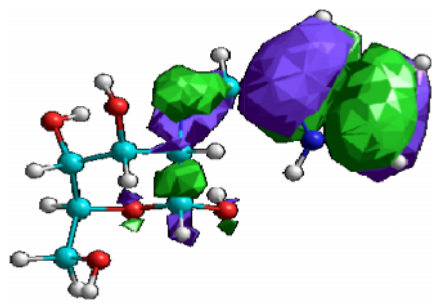	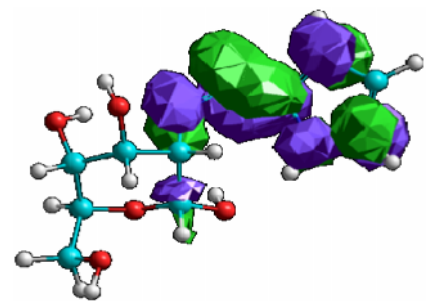

Figure 74 – Frontier Molecular orbitals of Chitosan Schiff bases by AM1 Method

Inhibitor	Frontier molecular distribution - HOMO	Frontier molecular distribution – LUMO
ChSSB	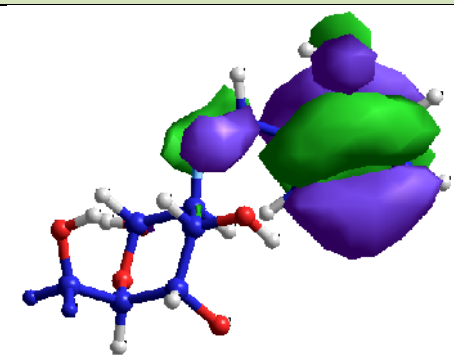	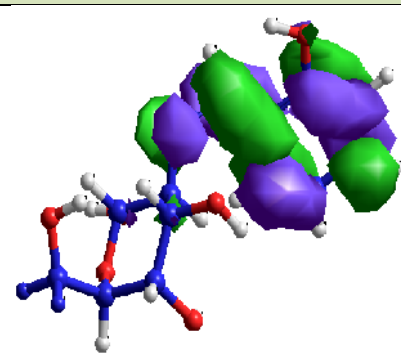
ChVSB	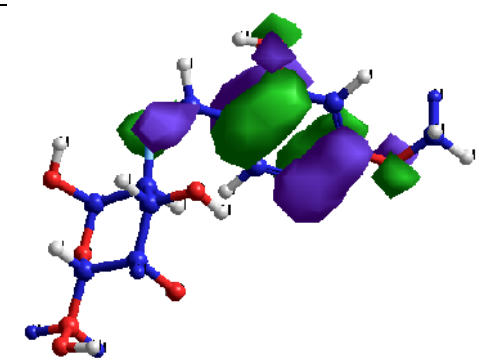	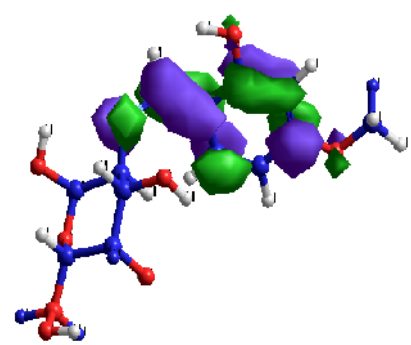
ChTSB	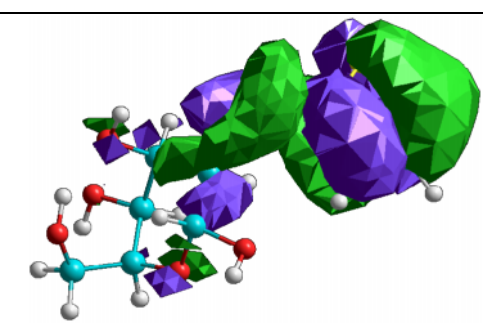	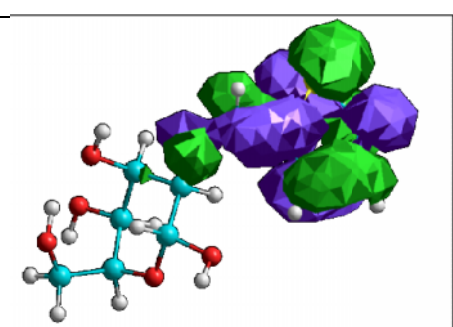
ChPSB	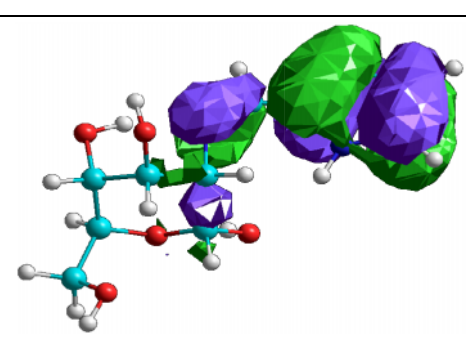	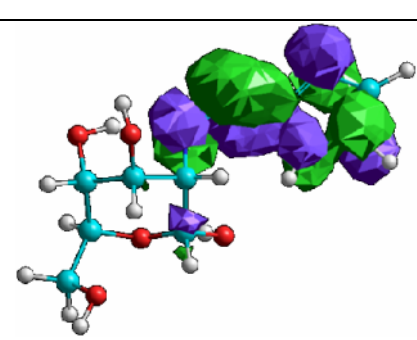

Figure 75 – Frontier Molecular orbitals of Chitosan Schiff bases by PM3 Method

Quantum chemical parameters such as the $E_{HOMO,}$ E_{LUMO}, energy band gap ($\Delta E=E_{LUMO}-E_{HOMO}$), dipole moment (μ), absolute electronegativity (χ), global hardness (γ), softness (σ) and fraction of electrons transferred from the inhibitor molecule to the metal surface (ΔN) were calculated for both the semi empirical methods and are presented in Table 35.

E_{HOMO} is often associated with the capacity of the molecule to donate electrons and the high values of E_{HOMO} represent the greater ability of that molecule to donate electrons. On the other hand, E_{LUMO} indicates the ability of the molecule to accept the electrons and the lower values of E_{LUMO} represents the greater ability of that molecule to accept electrons (**Kabanda *et al*., 2012)**.The highest E_{HOMO} values (refer Table 35) calculated for the biopolymeric inhibitors showed their high nucleophilicity. These values assure the spontaneous adsorption of the inhibitors on the metal surface.

The energy gap (ΔE) has been used in the literature to interpret the binding ability of the inhibitor molecules onto the metal surface. If the absolute values of the energy gap between the frontier orbitals gets smaller for a molecule, reactivity of the molecule increases and can easily get adsorbed on the metal surface thus resulting in better inhibition efficiency. The inhibitor molecule with low energy gap is more polarizable and is generally associated with high chemical reactivity and low kinetic stability (**Obi-Egbedi and Obot, 2011**). The low energy gap values of the Chitosan Schiff bases explain the better efficacy of the compounds.

The distribution of electrons in a molecule and its strong adsorption of the inhibitors on the mild steel are governed by the dipole moment values. Inhibitors with high dipole moment tend to have strong dipole - dipole interactions with the metal, resulting in strong adsorption on the mild steel surface (**Singh *et al*., 2015, Dauod *et al*., 2014**). All the Chitosan Schiff bases have finite dipole moment values proving maximum interaction with the metal surface.

Chemical hardness (λ) and softness (σ) are the properties which help in the analysis of the molecular reactivity and selectivity. In the evaluation of corrosion inhibitors and their inhibiting ability to bind onto the metal surface, the relationship was explained on the basis of hard and soft acid–base (HSAB) theory (**Pearson, 1963**). A hard molecule has a large λ (small σ) while a soft molecule has a small λ (large σ). By the relation, soft molecules therefore could easily offer electrons to an acceptor system which makes them more reactive than the hard molecules (**Amin *et al*., 2010**). In this regard, adsorption could occur most probably at the region of the molecule where σ has the highest value. The order of increasing the softness of the inhibitors means increasing their adsorbing ability on the metal surface

and also increasing their inhibition efficiency. As the chemical hardness decreases, the inhibition efficiency increases. The values of chemical hardness and softness of the biopolymeric inhibitors are given in Table 35 which suggests the inhibition action of the inhibitor compounds.

The electrons transferred from the inhibitor molecule to the Fe atom, i.e ∆N was calculated. The fraction of electrons transferred (ΔN) informs the ability of the molecule to donate electrons and bind to the surface of metals. Greater the ΔN values, greater the inhibition efficiency since more electrons will be donated to the surface of the metal. According to **Lukovits *et al*., 2001**, if the values of ΔN are less than 3.6 indicates the increase in high inhibition efficiency with increasing in electron donating ability of the inhibitor at the metal surface (**Khaled, 2010a, Biswas *et al*., 2015**).

From the above results obtained from theoretical studies, it is well confirmed that all the Chitosan Schiff bases possess active adsorption sites that could adsorb on the metal surface rendering effective inhibition efficiencies. On comparing the E_{HOMO} values of the Chitosan Schiff bases, ChPSB was found to have higher E_{HOMO} values (less negative values) followed by ChSSB, ChVSB and ChTSB. This in turn reflects the trend in their respective inhibition efficiencies. The obtained quantum chemical results are consistent with the experimental results discussed earlier. The frontier orbital structures of the Chitosan Schiff bases clearly showed that the HOMO orbitals are located on the imine groups of the Schiff bases and reactive hydroxyl groups of the Chitosan backbone matrix whereas the LUMO orbitals are located on the substituted aldehyde moity of the Chitosan Schiff bases. These groups can be directly adsorbed onto the metal surface on the basis of donor – acceptor interactions between the unshared electron pairs in nitrogen, π electrons of the imine groups, aromatic rings of the Chitosan Schiff base compounds and several oxygen atoms with excessive negative charges with the d-orbitals of Fe atoms. Thus the Chitosan Schiff bases may inhibit the mild steel surface by forming coordinate bond between the active sites and vacant d-orbitals of mild steel surface.

From the quantum chemical parameters, higher E_{HOMO}, a lower E_{LUMO}, a lower energy gap, and a higher dipole moment obtained from both semi-empirical methods (AM1 and PM3) suggested that higher ability of Chitosan Schiff bases to form a strong adsorption bond with the mild steel surface. Therefore, interaction of Chitosan Schiff bases with metal surface resulting in the blocking of the active corrosion sites leading to the better inhibition action.

Table 35 – Quantum chemical parameters calculated for Chitosan Schiff bases using semi-empirical methods

Properties	ChSSB		ChVSB		ChTSB		ChPSB	
	PM3	AM1	PM3	AM1	PM3	AM1	PM3	AM1
$-E_{HOMO}$ (eV)	9.3280	9.1742	9.27	9.02	9.9126	9.6726	9.01	8.70
$-E_{LUMO}$ (eV)	0.4640	0.0208	0.61	0.48	0.8126	0.6256	0.24	0.22
ΔE (eV)	8.864	9.153	8.660	9.08	9.1	9.047	8.771	8.48
μ (D)	1.162	3.07	4.459	4.23	5.032	4.056	2.55	3.55
Electronegativity(χ (eV)	4.896	4.598	4.949	4.75	5.3626	5.1491	4.62	4.46
Hardness (λ) (eV)	4.432	4.577	4.33	4.27	4.55	4.5235	4.38	4.24
Softness (σ) (eV^{-1})	0.2256	0.2185	0.2309	0.234	0.2197	0.2210	0.2280	0.2358
ΔN	0.2301	0.2624	0.4757	0.263	0.179	0.204	0.23	0.26

4.4.1.2 Quantum chemical calculations for Chitosan Schiff bases – DFT approach

The density functional theory (DFT) is one of the most important theoretical models used in explaining the science of solids and chemistry. A number of chemical concepts have been correlated within the framework of DFT. Since the theory is simpler than quantum mechanics, the interest has grown in understanding the structure, properties, reactivity, and dynamics of atoms, molecules and clusters using DFT. Recently, the density functional theory (DFT) has been used to analyze the characteristics of the inhibitor/surface mechanism and to describe the structural nature of the inhibitor on the corrosion process (**Obot *et al*., 2012, Bentiss *et al*., 2010**). Furthermore, DFT is considered as a very useful technique to probe the inhibitor/surface interaction as well as to analyze the experimental data. Thus in the present investigation, quantum chemical calculation using DFT was employed to explain the experimental results obtained in this study and to further give insight into the inhibition action of Chitosan Schiff bases on the mild steel surface.

Two Chitosan Schiff bases namely ChVSB, ChPSB were considered for the quantum chemical calculations using DFT. The geometry optimization and quantum chemical calculations were performed using Becke's three parameter and the Lee–Yang–Parr correlation functional theory (B3LYP). The 6-311G(d,p) basis set was selected for the study. The optimized structures of the Chitosan Schiff bases are shown in Figure 76 & 77.

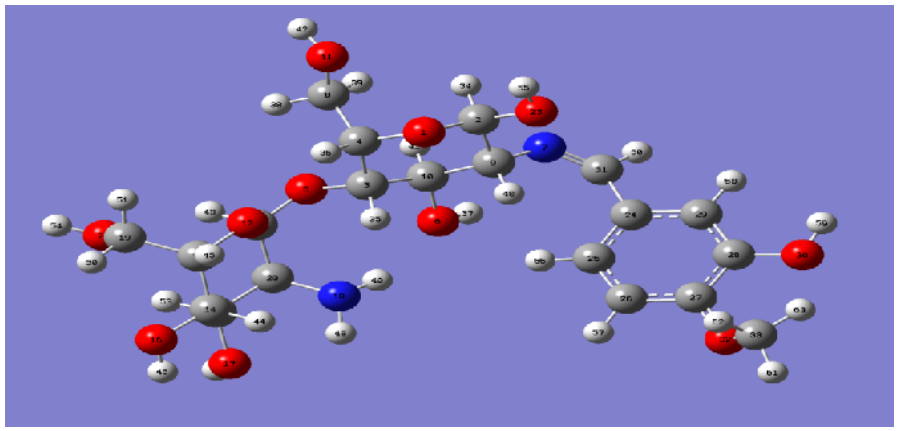

Figure 76 - Optimized structure of Chitosan Vanillin Schiff base

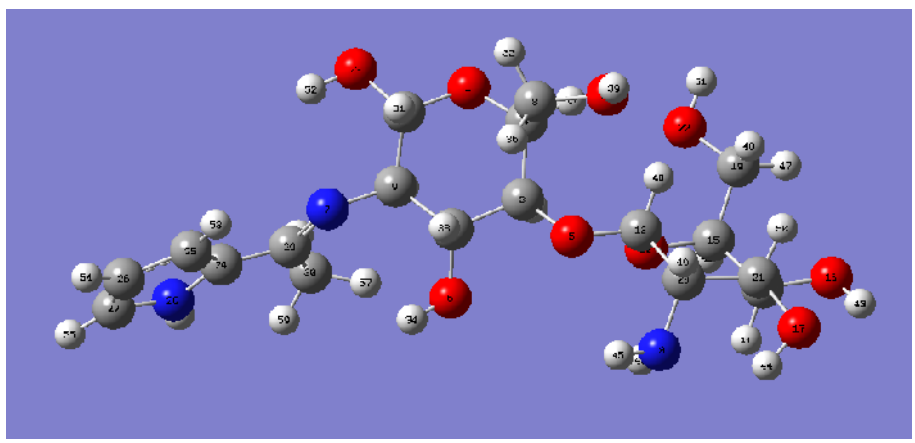

Figure 77 - Optimized structure of Chitosan Pyrrole Schiff base

As discussed in semi empirical methods, quantum chemical parameters such as the energy of the highest occupied energy orbital (E_{HOMO}), the energy of lowest molecular orbital (E_{LUMO}), energy gap between LUMO and HOMO orbitals (ΔE) are very useful in determining the reactivity of the inhibitor molecule. In DFT, the same quantum chemical parameters were determined in addition Mulliken charges on the atoms present in inhibitor molecules were determined by optimization and they can be related to the metal- inhibitor interactions (**Hamani *et al.*, 2014**). For the purpose of determining the active sites of the inhibitor molecule, the distribution of frontier orbital and nature of atomic charges on the molecules are considered to be more important. According to the classical chemical theory, all chemical interactions are formed by either electrostatic or orbital interactions. In such case, obviously electrical charges present in the molecule must be the driving force of electrostatic interactions and also the charges and the electron densities in the molecules are proven to be more significant for the chemical reactions and physico- chemical properties of the particular compound (**Gece, 2008**)

The chemical reactivity of the inhibitors is closely related to their frontier molecular orbitals (HOMO, LUMO). The electron density distribution of HOMO and LUMO orbitals for ChVSB and ChPSB are depicted in Figures 78 & 79. The HOMO electron density surface of the Chitosan Schiff bases reveal that the electron rich sites present in them from which the electrons could be donated to suitable vacant d- orbitals of the metal surface. The LUMO electron density surface point outs the electron deficient sites of the Chitosan Schiff bases and these regions have greater chances of accepting electrons from the occupied orbitals of the metal surface.

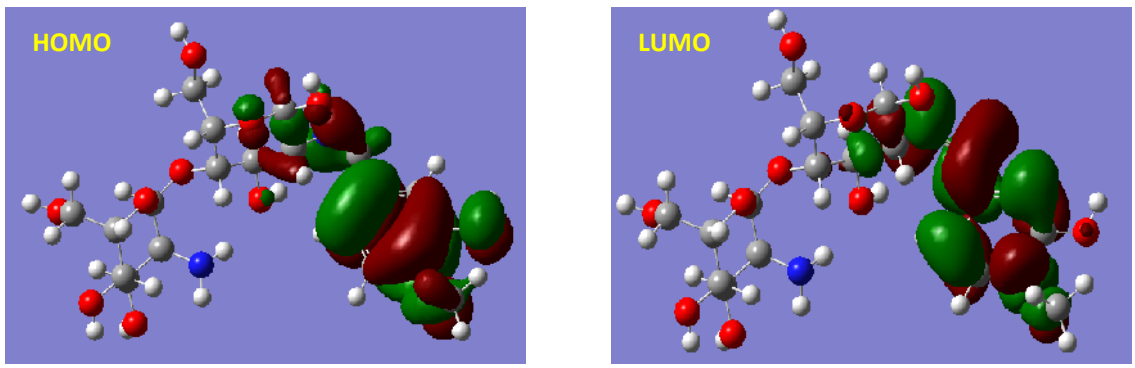

Figure 78 - Frontier molecular orbital distribution – ChVSB

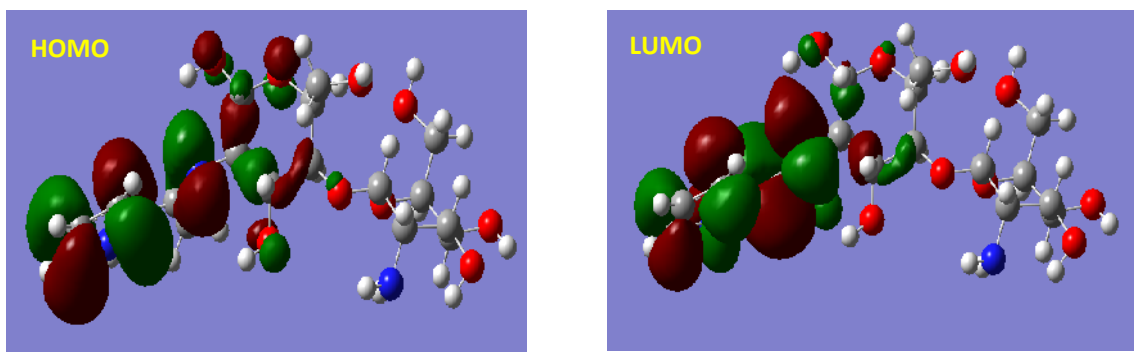

Figure 79 - Frontier molecular orbital distribution – ChPSB

It could be seen that the HOMO and LUMO orbitals of the Chitosan Schiff bases (ChVSB, ChPSB) are found on the imine (-C=N-) substituted glucopyranose ring and the anchoring aldehydeic groups. The HOMO orbitals of Chitosan Schiff bases are mainly located on the pi- orbitals and the electron densities are distributed over the phenyl ring of the substituted aldehyde compounds. The HOMO orbitals of these Schiff base compounds found extend to the C=C π - electron centres of glucopyranose rings and also to the electron donating $–CH_3$ and –OH substituents on the phenyl ring in case of the ChVSB. This may give an idea of flat or parallel adsorption of the inhibitor molecules onto the metal surface.

This should be the reason for the strong interaction with the metal surface and thereby giving high inhibition efficiency.

The list of selected quantum chemical parameters of Chitosan Schiff bases are given in Table 36. The calculated quantum chemical data show the highest occupied molecular orbital values (E_{HOMO}= -6.0883 eV for ChVSB, -5.9876 eV for ChPSB). The high value of E_{HOMO} indicates the tendency of the Chitosan Schiff bases to donate electrons to the appropriate acceptor molecule with low energy and empty molecular orbital. The E_{HOMO} of ChPSB is found to be higher than ChVSB indicating that former facilitates the adsorption easily than the and therefore the inhibition efficiency. The lower values of E_{LUMO} indicate the ability of the Chitosan Schiff bases to accept electrons from an electron rich species. From the E_{LUMO} values (-1.1507 eV for ChVSB, -1.2754 eV for ChPSB), ChPSB found to have lower E_{LUMO} values than ChVSB revealing that pyrrole substituted Chitosan Schiff base have the higher capability of accepting electrons. The energy gap between the frontier molecular orbitals is an important factor which describes the molecular reactivity of the inhibitor molecule. As stated by many authors (**Zhang *et al*., 2011, Obot and Obi-egbedi, 2010, El-haddad, 2013, Umoren *et al*., 2015, Boussalah *et al*., 2012**), if the energy gap between the molecular orbital's decreased, there will be an improvement in inhibition efficiency. In the present quantum chemical investigation of Chitosan Schiff bases, ChPSB found to have lesser energy gap. The low energy gap compounds will render good inhibition efficiencies, because the energy to remove an electron from the last occupied orbital will be low. The dipole moment is the measure of the polarity of the covalent bond, which is related to the distribution of electrons in a molecule (**El Sayed *et al*., 2006, Daoud *et al*., 2014**). Though literature have some inconsistency with the use of μ as a predictor to decide corrosion inhibition reaction, it is generally assumed and agreed that the large values of μ favours for the adsorption of inhibitor molecules. The higher values of μ for both the inhibitor compounds suggest that the both inhibitors are polar compounds and they can easily donate electrons to the metal surface hence forming strong adsorptive bond.

Table 36 - Properties of Chitosan Schiff base inhibitors calculated using DFT at the B3LYP/6-311G (d,p) basis set.

Inhibitor	$-E_{HOMO}$ (eV)	$-E_{LUMO}$ (eV)	ΔE (eV)	μ (D)	Total energy
ChVSB	-6.0883	-1.1507	4.9375	3.1306	-1717.5157
ChPSB	-5.9876	-1.2754	4.7122	4.4517	-1544.9827

Mulliken atomic charges:

The partial charges present on the individual atoms in an inhibitor molecule also indicate the reactive centres responsible for the corrosion inhibition reaction. The use of Mulliken population analysis for the estimation of the adsorption centers of inhibitors has been widely reported. Mulliken charge analysis normally used for the calculation of the charge distribution present over the whole skeleton of the inhibitor molecule. Atoms possessing the highest negative charge are considered to have an electron donating capacity role when interacting with metal surfaces. It is generally reported by several authors that if the hetero atoms present in the inhibitor molecule has more negative charge, the ability to adsorb on the metal surface will be more for the particular hetero atom. The calculated Mulliken charges for the heteroatoms present in Chitosan Schiff bases are listed in the Table 37 and the Mulliken charge population analysis obtained for Chitosan Schiff bases are shown in Figure 80.

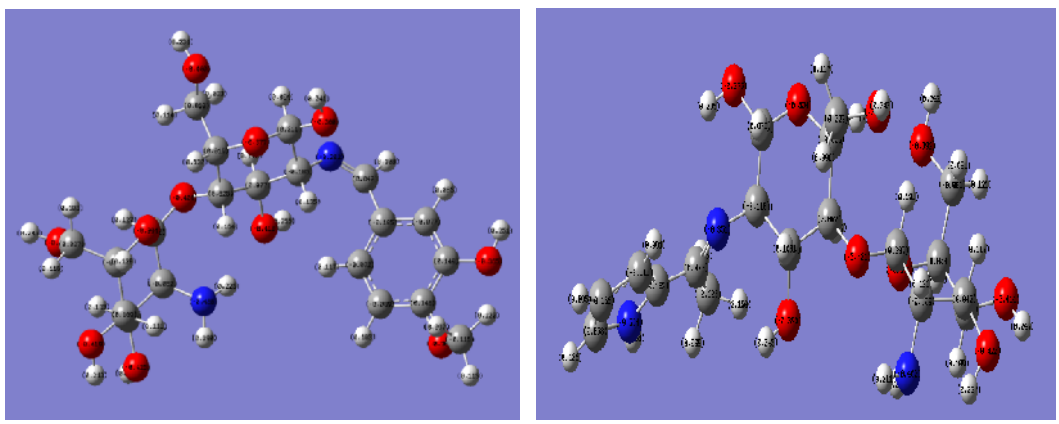

Figure 80 - Mulliken population analysis calculated for ChVSB and ChPSB

Table 37 - Calculated Mulliken charges for Chitosan Schiff bases

ChVSB		ChPSB	
Atoms	**Charges**	**Atoms**	**Charges**
1 O	-0.4043	1 O	-0.3541
5 O	-0.4291	5 O	-0.4010
6 O	-0.4386	6 O	-0.3962
7 N	-0.2922	7 N	-0.3505
11 O	-0.4189	16 O	-0.4139
12 O	-0.4189	17 O	-0.4197
16 O	-0.4382	18 N	-0.4624
17 O	-0.4440	22 O	-0.3921
18 N	-0.5002	23 O	-0.3752
23 O	-0.4074	28 N	-0.3944
30 O	-0.3928		
32 O	-0.3901		

By careful observation of the values of Mulliken charges, the larger negative N atoms are present on the imine group (-HC=N) of the Chitosan Schiff bases in ChVSB and in case of ChPSB, the negative N atoms are present on both the imine nitrogen and also substituted pyrrole ring nitrogen. These atoms could donate its lone pair of electron to unoccupied orbital of the metal atom thereby the inhibitor can be adsorbed onto metal surface through donor-acceptor reaction. Thus, these centres present in the Chitosan Schiff base compounds are considered to be the coordinating sites through which the Schiff bases compounds can be adsorbed onto the positively charged metal surface.

4.4.2 Mechanism of inhibitive action of Chitosan Schiff bases

The mechanism of corrosion **i**nhibition can be explained by means of adsorption phenomenon. Adsorption of the inhibitor molecules is influenced by the chemical structure and donor atom of the molecule (heteroatoms like N,O,S,etc). It also depends on the nature or charge on the surface of the metal and vacant d orbitals of the metal. Generally in acidic medium mainly in HCl solution, metal surface acquires a negative charge because of specific adsorption of chloride ions and the metal surface attract positively charged species in the medium. The inhibitor molecules stay in strong acid medium, either as neutral molecules or

in protonated form. The neutral inhibitor molecules are absorbed on the mild steel surface by the replacement of surface adsorbed water molecules through chemisorption mechanism. Inhibitor molecules can also be adsorbed on the metal surface through the donor acceptor interaction with vacant d-orbitals of iron.

Adsorption of inhibitor molecules on metal surface may take place in four possible ways:

(a) Electrostatic interaction between the charged inhibitor molecules and the charged metal surface.
(b) The metal and inhibitor molecules interact through an unshared electron pair of molecules.
(c) π-electron interaction with metal.
(d) A combination of (a) and (c).

The protonated molecules of the inhibitors are adsorbed on mild steel surface with the help of chloride ions as interconnecting bridges between metal and inhibitor molecules. As a result a triple layer close packed structure is formed on the surface, which reduces the surface charge density.

Electrostatic interaction of inhibitor molecules may occur in case of physisorption but the interaction of lone pair of electrons and π-electron interaction with the metal surface will lead to chemisorption. In the present case of inhibiting action of Chitosan Schiff bases, the inhibitor molecules are expected to get adsorbed on the metal surface by means of all three possible ways (a,b,&c). To propose the mechanism of the inhibiting action of the Chitosan Schiff bases certain factors have to be considered namely,

- Charge on the metal surface
- Behaviour of the Chitosan Schiff bases during the temperature studies of the corrosion monitoring techniques.
- Nature and modifications occurred on the metal surface after the adsorption of inhibitor molecules
- Reactive sites, reaction parameters, and the charges present on the hetero atoms of the inhibitor molecule.

4.4.2.1 Determination of charge on the metal surface – Potential zero charge

The absorbability of the inhibitors will depend first on the charge of the metal or more particularly on the potential of the metal. E_{corr} value for the MS working electrode in 1M HCl is -491mV. To determine the potential of zero charge (PZC), the impedance measurements were carried out at a potential range of -725 mV to -375 mV. The polarization resistances obtained from impedance measurements are plotted against the applied potentials and is presented in Figure 81. The Figure shows the maximum at the potential -500mV. This corresponds to the potential zero charge. The difference between of E_{corr} and PZC values is denoted by E_r which is the Antropov 'rational' corrosion potential and its sign represent the net charge of the metal surface. Negative E_r indicated the presence of net negative charge on the working electrode surface. On contrary, the positive E_r values showed net positively charged metal surface (**Ali Fathima sabirneeza *et al*., 2015**). In the present case, the difference between E_{corr} and PZC was found to be +9mV. This rational potential indicates the charge of the Mild steel surface at its open circuit potential.

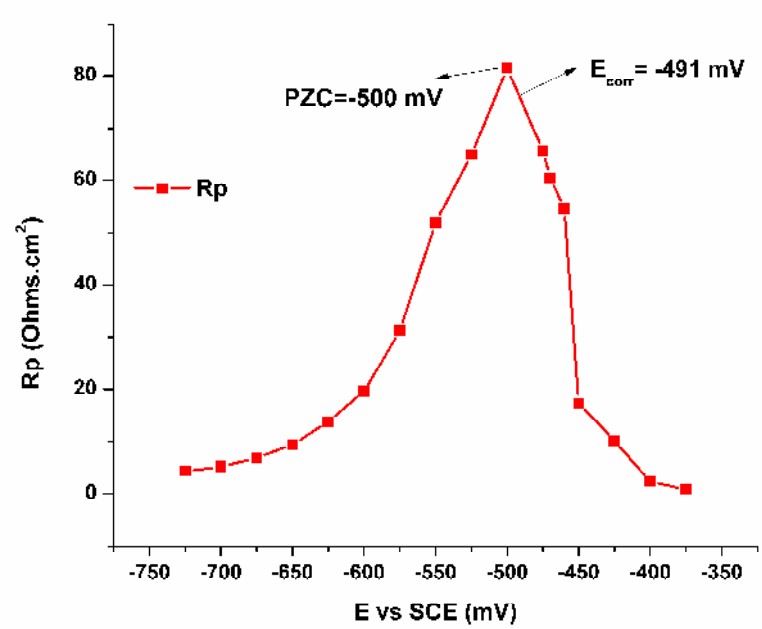

Figure 81 – A plot of Rp versus applied potentials (E vs.SCE) for MS in 1M HCl

4.4.2.2 Behavior of the Chitosan Schiff bases during the temperature studies of the corrosion monitoring techniques:

The basic information about the adsorption of Chitosan Schiff bases on the metal surface was provided by the adsorption isotherm and the thermodynamic parameters of adsorption. From the chapters explained earlier, all the Chitosan Schiff bases were found to

be obeying the Temkin adsorption isotherm which is the preliminary proof for the chemisorptive adsorption of these inhibitors on the metal surface.

Chitosan Schiff bases possess functional groups like –CH=N, OH and also Chitosan repeating unit with $–NH_2$ and OH (since 100% substitution is not possible). Tthese groups can be present in the inhibitor can exist as protonated form in acidic solution. It is assumed that, at least in first few minutes of the contact between the substrate and the inhibitor solution, these cationic forms of Chitosan and Chitosan Schiff bases may be preferentially adsorbed due to the coloumbic interaction (physical adsorption) between the cationics and the metal surface. This adsorption will be further strengthened due to the presence of the imine groups (-HC=N) and –OH groups with lone pair of electrons that can be adsorbed on to the anodic sites of the metal surface. In this case, besides the physisorption, chemisorption will be more pronounced due to the chemical interaction of the lone pairs of electrons with the empty vacant d- orbitals of the metal atom. Moreover, the π-electrons present in the aromatic ring of the substituted aldehydes can also interact with the mild steel surface by sharing electrons with the metal atom. The thermodynamic parameters of adsorption calculated and discussed in previous chapters revealed the chemisorption of the Chitosan Schiff bases on the mild steel surface. This is supported by the values of ΔG which is above -40 KJ mol^{-1} for all the Chitosan Schiff bases studied.

4.4.2.3 Supporting evidences for the proposed mechanism:

The foresaid plausible mechanism of inhibition of Chitosan was further supported by surface analytical techniques. The nature of the metal surface and its modification in the morphology after the addition of Chitosan Schiff bases is more important in proposing the mechanism. FTIR technique of surface analysis of mild steel surface was explained in detail in Phase - III. Some of the conclusions drawn from the technique are briefed as follows:

- The presence of strong peak at 442 cm^{-1} due to Fe-N stretching confirmed the formation of coordinate bond between the nitrogen atom present in the inhibitors and the Fe^{2+} ions present on the metal surface.
- Shifting of the absorption peaks of stretching vibration of -HC=N imine group from the range of 1631-1649 cm^{-1} to 1726 cm^{-1} confirmed that the coordination of Chitosan Schiff bases through nitrogen atom with Fe^{2+}.
- Shifting of C=C absorption peak of vibration of aromatic system also revealed the interaction between the aromatic π electrons and the Fe substrate.

It is evident that Chitosan Schiff bases have successfully interacted with the metal surface by means of all possible adsorption ways.

EDX technique:

The results of the composition of the Chitosan Schiff bases deposited metal surface showed the presence of carbon and nitrogen and also sulphur in the case of ChTSB is quite another confirmation for the chemisorbed protective layer on the metal surface.

XPS characterization technique:

From the XPS technique, the presence of nitrogen species on the steel surface such as –HC=N and C-O-C linkage of Chitosan chain corroborated for the formation of Chitosan Schiff base film on the metal surface. The peak N-Fe confirmed that the investigated ChSSB was chemisorbed on the steel surface.

Quantum chemical investigation:

The detailed information about the active sites and reactivity parameters for the inhibiting performance of the Chitosan Schiff bases was also confirmed by theoretical studies. The important conclusions obtained from the theoretical results are:

- Both semi-empirical and DFT methods confirmed the presence of HOMO orbitals on the imine and hydroxyl groups of Chitosan Schiff bases and LUMO orbitals on the substituted aldehydes - This indicates that the inhibition may be achieved by the interaction between the unshared electron pairs in nitrogen with d-orbitals of iron atoms and also due to the interaction of substituted molecule in the Chitosan chain with the metal surface
- Presence of Mulliken charges on the nitrogen atoms of the Chitosan Schiff bases could augment for the donation of its lone pair of electrons to unoccupied orbital of the metal atom thereby inhibiting the metal surface by donor-acceptor reaction.

Thus the Chitosan Schiff bases inhibit the mild steel surface by chemical adsorption by forming coordinate bond between the active sites and vacant d-orbitals of mild steel surface. The schematic representation of the inhibitive action of the Chitosan Schiff bases is shown in Figure 82.

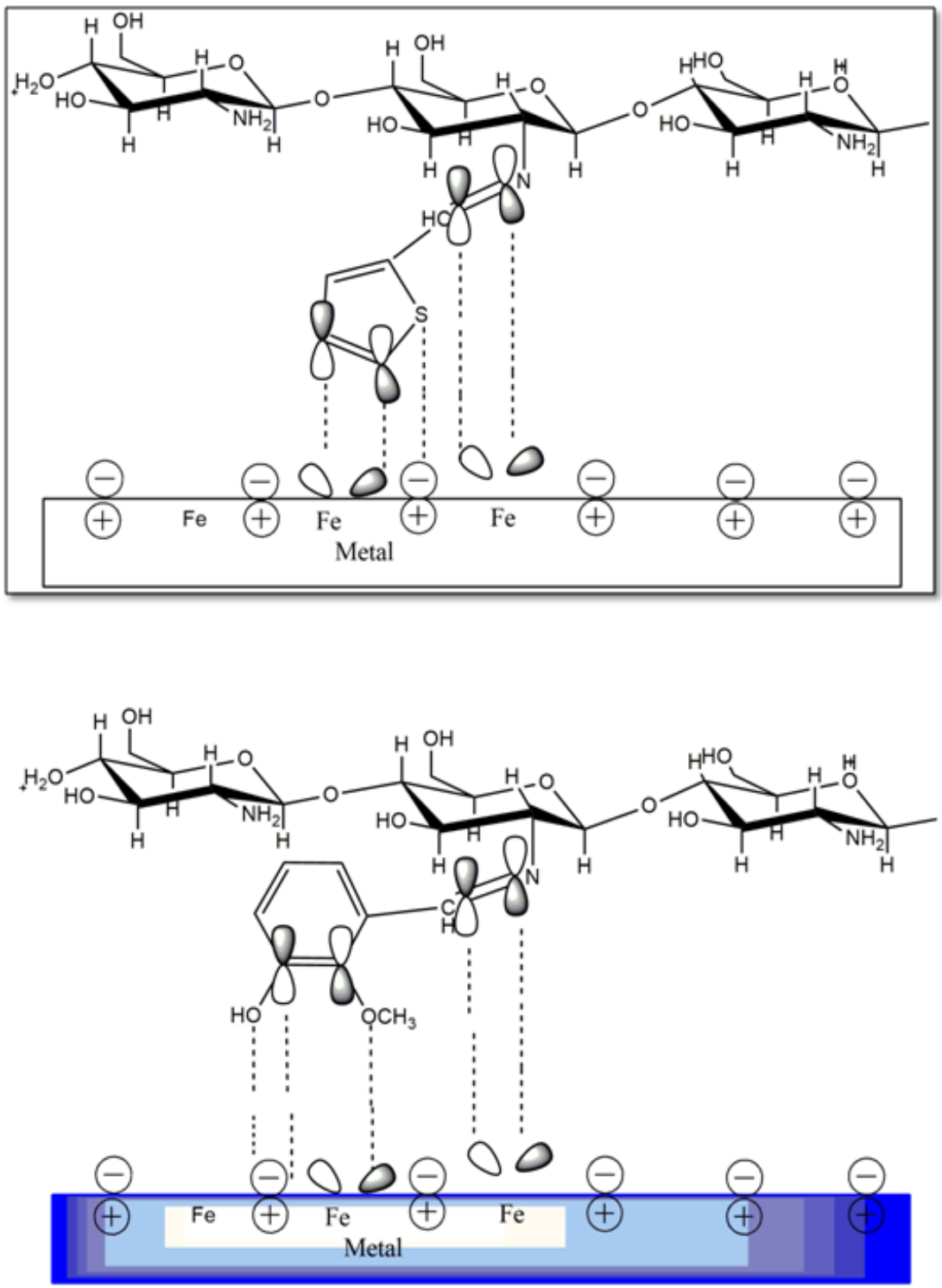

Figure 82 – Schematic representation of Plausible Mechanism proposed for the inhibition action of Chitosan Schiff bases

Phase - V

4.5 Testing the efficacy of prepared Chitosan Schiff bases as $CaCO_3$ scale inhibitor

Scale - Introduction

The formation of mineral scales is a persistent and expensive problem in different facets of industrial processes and domestic installations. Scale formation on heat transfer surfaces is a severe problem widely occurring in numerous industrial processes including batch precipitation, power generation, water transport and oil or gas production (**Demadis *et al*., 2007; El Dahan and Hegazy, 2000; Gu *et al*., 2012; Suharso *et al*., 2011**). The presence of a scale layer can cause a series of problems, such as impedance of heat transfer, increase of energy consumption, and unscheduled equipment shutdown in the industry sectors. Scaling is a phenomenon of precipitation or simple adhesion of calcium carbonate on the walls in contact with water containing calcium and magnesium salts. During scaling the precipitate will bond on the surface of materials and form relatively stable bond with the matrix. In other words, scale is an assemblage of inorganic mineral deposits that cake perforations, casing, production tubing, valves, pumps, down-hole completion equipment, thereby clogging the wellbore and preventing fluid flow. Undesirable scale deposits can cause numerous technical and economical problems in operational industries. In nuclear plants, the power produced is often restricted by the formation of scales in cooling towers. In Great Britain, the cost of around 6000 million pounds per year was estimated as non-productive expenses in connection with scaling problems. Hence the losses due to scale formation are high and it is very important to establish appropriate methods and effective ways to prevent it.

Calcium carbonate ($CaCO_3$) –major component of scaling

Scaling is essentially linked to the formation of calcium carbonate ($CaCO_3$). Scaling may contain other residues such as algae, calcium sulfate, clays and the brucite $Mg(OH)_2$. But formation of calcium carbonate is more predominant since it precipitates easily because of the low solubility. Calcium carbonate ($CaCO_3$) is one of the main components of scale that is commonly encountered in chemical industries, cooling water system and oilfield water injection system. The calcium carbonate scale often grows extensively on equipment and parts, causing major operational difficulties (**Muryanto *et al*., 2014**). Calcium carbonate scale has a significantly bad influence on heat transfer for cooling water system and normal oil field production (**Cai *et al*., 2007**). The main reason for the calcium carbonate precipitation is due to high carbonate hardness and excessive salinity of cooling water. Salts that are dissolved in the water get condensed as water evaporation proceeds and usually precipitate when the

solubility product gets exceeded. The process runs in the heat exchanger (and in cooling installations) make an advantageous environment for the beginning of solid phase crystallization. Scale deposits that forms in cooling water systems are polycrystalline porous substances with amorphous inclusions.

In oil- field industries also, calcium carbonate scale is considered to be main problem in operational process viz., water injecting, oil extracting, demulsification and so on (**Luo *et al*., 2015**). They also cause a significant loss in industries like mining, water supply and pulp/paper. $CaCO_3$ scale cause a drastic effect on equipments such as boilers, steam generators, evaporators, distillation units, heat exchangers, cooling tower fill, engine jackets, etc. (**Demadis *et al*., 2007**).

Forms of Calcium carbonate scale

Generally amorphous calcium carbonate forms first, crystallizes and dehydrates to form crystal structures. Calcium carbonate crystallizes in three different polymorphs, namely calcite, aragonite and vaterite (**Sawada, 1997**). Calcite is known to be the stable form of calcium carbonate crystals (**Nancollas *et al*., 1981**). In contrast, aragonite and vaterite are thermodynamically unstable and given appropriate conditions they could eventually transform into calcite (**Muryanto *et al*., 2014**). Many factors affect the formation of calcium carbonate precipitation viz., pH, temperature, concentration of reactants, and duration of precipitation.

The chemical reaction of $CaCO_3$ precipitation is:

$$Ca^{2+} + HCO^-_3 + OH^- \rightarrow CaCO_3\,(s) + H_2O$$

4.5.1 Scale control methods

Calcium carbonate scale deposition can be prevented by physical, chemical and biological methods. These prevention methods fit into three main categories ie., affecting the solubility, altering the growth mechanisms of the crystals and the change in potential of a surface to foul.

Physical methods like antiscale magnetic treatment (**Alimi *et al*., 2006**), water treatment in electric fields or the use of sonic waves (**Limpert and Raber, 1985**) are used but the results of these methods are yet questionable (**Baker and Judd, 1996**).Also the mechanism of the physical methods are not so clear, therefore their practical application is very limited. Chemical methods consist of acid injection, quantitative complexation method using chelating agents for complexing Ca^{2+} ions. But these methods are very expensive and they do cause severe consequences to the environment (**Ketrane *et al*., 2009**).

Threshold inhibition is considered to be appropriate and the best method to control scale crystal growth (**Shakkthivel *et al*., 2006**). The base of "threshold treatment" of scale can be explained as: the presence of impurities of some metal ions and organic molecules in solution can influence the rate of precipitation and the crystal structure. Also these impurities present at very low concentrations may adsorb onto the crystal surface and block the energetically favouring growth positions of the flow surface thus completely inhibiting further precipitation (**Meyer, 1984**). Similarly, the addition of scale inhibitors can affect the growth of scales on the surface.

Scale inhibitor:

A scale inhibitor is a chemical that can retard or reduce the formation of calcium carbonate crystal and scales. The most effective and widely used technique for controlling scaling problems is using chemical additives that are able to inhibit growth of scale and weaken its adherence to a flow surface. These chemical additives may act as a barrier for scale formation to protect a system from various operational problems. Most commonly used commercial antiscalants are derived from three families: polyphosphates, polyphosphonates and polycarboxylic acid. Many inorganic metallic compounds such as chromates, zinc compounds and some non metallic ones such as phosphates, nitrites and azoles have also been applied as scale inhibitors. But due to some disadvantages like toxicity, low stability and selective protective action of these inhibitors have turned the researchers to the application of organic compounds with multifunctional groups as potential scale inhibitors.

In this regard, a large number of polymers and non-polymeric descaling chemicals have been reported. **Chew and Mat, 2015** have tested the efficacy of calcium carbonate scale inhibition using commercially available scale inhibitors such as Polymaleic Acid (PMA), Polyamino Polyether Methylene Phosphonic Acid (PAPEMP) and Acrylic Acid-Maleic Anhydride (AA/MA). **Todd *et al*., 2012** reported the phosphorous functionalized polymers for scale inhibition. **Li *et al*., 2015** studied the effect of six kinds of commercially scale inhibitors on calcium carbonate precipitation and the results showed better inhibition efficacy on the growth of calcium carbonate scale. Many polymeric compounds such as Polyaspartic acid (**Zhenhua *et al*., 2008**), polyacrylic acid and 2-phosphonobutane-1,2,4-tricarboxylic acid (**Yang *et al*., 2001**) been tested as scale inhibitors.

Biodegradable and eco-friendly scale inhibitors

The use of polymeric compounds as scale inhibitors have satisfactorily inhibited the scale formation, the main drawback is the residual disposal of these compounds. Some of phosphorous based polymers which can serve as nutrients leading to eutrification difficulties (**Hasson *et al*., 2011**). The discharge of the residues of the undegraded polymers has a strong impact on the environment. Increasing environmental concerns and discharge limitations have caused scale inhibitor chemistry to move towards "green antiscalants" that readily biodegrade and have low impact on environmental concerns. Hasson and co-authors reviewed and discussed the exploitation of biodegradable scale inhibitors. Recently, many researchers are focusing on environment friendly scale inhibitors. **Zeng and Yan, 2013** have studied the scale inhibiting efficiency of Chitosan along with poly acrylic acid and benzotriazole and reported as ecofriendly scale inhibitor. Another inhibitor poly aspartic acid also reported to be green scale inhibitor by **Zhenhua *et al*., 2008.** Poly aspartic acid/Chitosan graft copolymer has been evaluated for the scale and corrosion inhibition performance by **Zhang *et al*., 2015. Nayunigari *et al*., 2014** along with co workers developed antiscalant of dual polymer system composed of poly (aspartic acid- citric acid) for water systems. **Liu *et al*., 2016** evaluated β-cyclodextrin–polyethylene glycol as green scale inhibitor for calcium carbonate formation.

Synthesized Chitosan Schiff bases with imine groups along with aldehydeic moiety and hydroxyl groups in the Chitosan matrix can help in incorporating and chelating the Ca^{2+} ions within them. Moreover, these compounds are biodegradable and environmental friendly; their disposal will not affect the environment. Bearing all these facts, an attempt was made to test the efficacy of synthesized Chitosan Schiff bases for calcium carbonate scale removal.

4.5.2 Analysis of Scale inhibiting effect of Chitosan Schiff bases

Effect of inhibitor dosage

The brine solutions with and without the Chitosan Schiff bases were evaluated for static scale inhibition tests at different test conditions and the supernatant solution after the precipitation of $CaCO_3$ scale was titrated using EDTA solution. The effect of inhibitor dosage of Chitosan Schiff bases (ChSSB, ChVSB, ChTSB, ChPSB) for $CaCO_3$ scales was determined and its inhibition performance is shown in Figure 83.

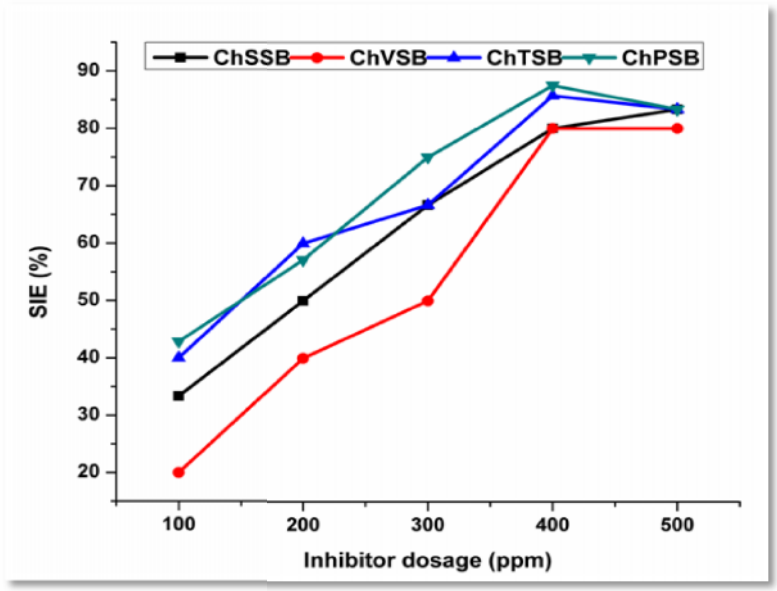

Figure 83 - Scale inhibition efficiencies of Chitosan Schiff bases at different inhibitor dosage

From the Figure 83, it is clear that the inhibition efficiency increases with the increase in the inhibitor dosage for all investigated Schiff base polymers. The trend of the inhibition rate of Schiff bases is found to be same. All the polymers show an increase in inhibition efficiency after the inhibitor dosage of 100ppm and reach a maximum inhibition percentage at 400ppm except ChSSB which exhibit maximum inhibition rate at 500ppm (83.34%).The other polymers show better inhibition rate by following the order, ChPSB>ChTSB>ChVSB with their respective inhibition efficiency as 87.5% > 85.71% > 80. Further increasing the dosage of these polymers slightly dropped the efficiency in ChPSB and ChTSB whereas in the case of ChVSB the efficiency remains stable. The reason for the inhibition can be explained by the active groups present in the Chitosan Schiff bases. They contain more number of hydroxyl groups in their parent matrix, imine group and oxygen atoms in the anchoring groups with the lone pair of electrons. These active groups effectively adsorb on the surface which reduce the growth rate of $CaCO_3$ scale and delay the formation of precipitation (**Zeng *et al.*, 2015**). The bonding strength disordered the normal lattice structure of $CaCO_3$ crystals which helps in dissolving the Ca^{2+}ions (**Zhang *et al.*, 2015**). Moreover, these groups have the tendency to interact with Ca^{2+}ions in the solution; therefore with increase in the inhibitor dosage obviously more number of Ca^{2+}ions can be chelated (**Liu *et al.*, 2016**) and thus exhibiting good inhibition performance.

Effect of bath time

The scale inhibition efficiency of Chitosan Schiff bases at optimum concentration with different bath time was evaluated for static scale inhibition test and the performance of the Chitosan Schiff bases with respect to bath time is shown in Figure 84.

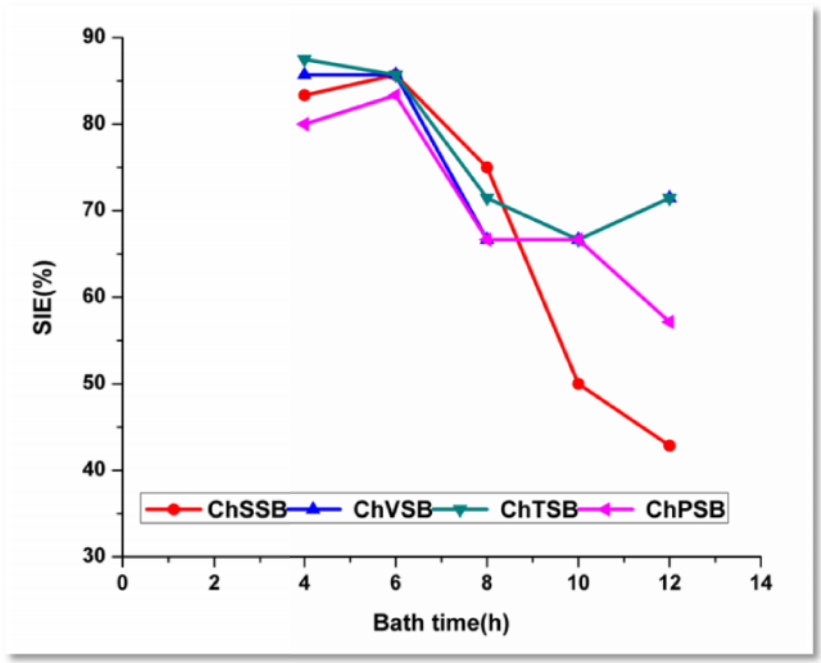

Figure 84 - Scale inhibition efficiencies of Chitosan Schiff bases at different bath time

Results indicate that the performance of Schiff base polymers is very effective on calcium carbonate scale formation at different bath time ranging from 4-12 h. All the polymers exhibited the highest inhibition efficiency at 6 h of bath time. The high SIE of the polymers may be due to the assumption of sufficient interaction of the inhibitor with Ca^{2+} ions in the static system. As the bath time increases, it is seen that the Schiff base polymers have a significant slowdown effect against $CaCO_3$ scale and decrease in SIE is observed at prolonged bath time. The drop in SIE after the bath time of 6 h might be due to the destabilization of the Schiff base polymers or increase in decomposition of chelated molecules (**Liu *et al.*, 2016**). The decrease in the SIE for longer bath time may be due to the weak interaction of Schiff base polymers and calcium ions. This weak interaction accompanied with adsorption-desorption equilibrium, so desorption might have occurred at longer bath time at constant temperature thus resulting in reduction of SIE (**Luo *et al.*, 2015**).

Effect of bath temperature

It is well known that temperature has great influence on the formation of calcium carbonate scale. Generally, the solubility of the calcium carbonate scale is inversely proportional to the solution temperature. The solubility –temperature studies suggested that the scaling tendency will be higher at the heat exchanger than at the normal parts of the recirculating water systems (**Amjad, 1997**).The influence of temperature on the scale inhibiting efficiency of optimum concentrations of Schiff base polymers at constant bath time of 6 h was evaluated and the results are shown in Figure 85.

The SIE declined with increasing the bath temperature. The highest SIE of 83.34% was obtained for ChVSB at the bath temperature of 70 ^{o}C while ChTSB and ChPSB exhibited SIE of 88.9% and ChSSB showed 87.5% of SIE at 65 ^{o}C bath temperature. The decrease in the SIE at higher temperatures may be attributed to the fact that the high temperature makes the calcium carbonate to form easily and becomes thicker, so the amount of calcium carbonate scale will be more at higher temperatures. The inhibitor dosage may not be sufficient to reduce the growth rate of calcium or to chelate with calcium ions. On the whole, extra dosage of inhibitor may be needed to maintain a high inhibition rate of calcium carbonate control (**Luo *et al*., 2015**).

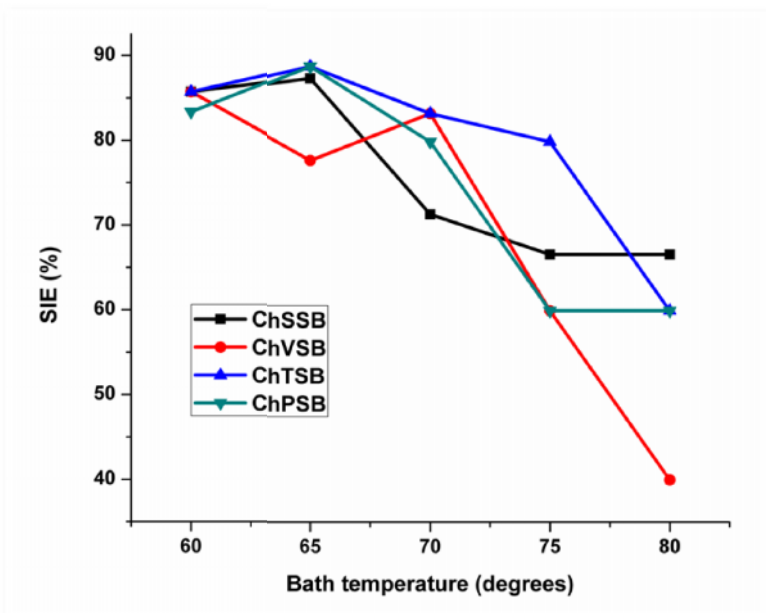

Figure 85 - Scale inhibition efficiencies of Chitosan Schiff bases at different bath temperature

4.5.3 Characterization of calcium carbonate scale- SEM analysis

The effect of the Chitosan Schiff bases on the growth and morphology changes of $CaCO_3$ crystals in absence and presence of the optimal scale inhibitors were characterized by SEM analysis. Based on the appearance of the calcium carbonate crystals provided by SEM, the crystalline forms of the $CaCO_3$ may be identified. The scanning micrographs of $CaCO_3$ crystals are shown in Figure 85. From the Figure, it could be seen that the crystals of $CaCO_3$ in absence of Schiff base scale inhibitors (Figure 86) have a regular and compact structure. The major regular structures are of hexagon, rhombohedron (**Chew and Mat, 2015**) and cubic crystals which correspond to calcite (**Ketrane *et al.*, 2009**). Calcite is the most thermodynamically stable form of $CaCO_3$ crystals. Moreover, long strips or cylindrical corresponding to aragonite crystal form also seen.

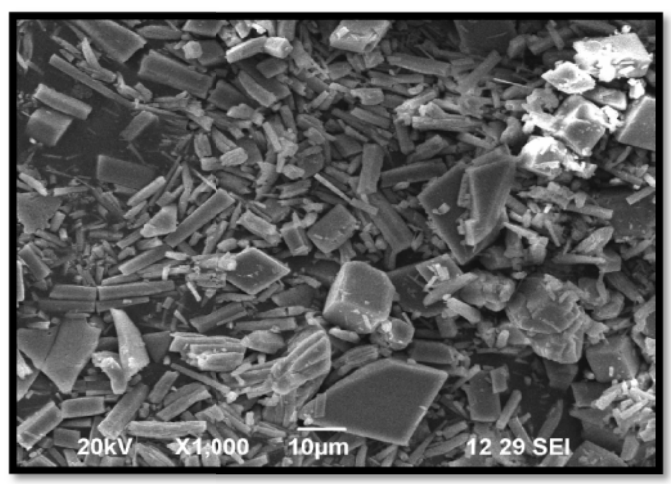

Figure 86 – SEM images of $CaCO_3$ precipitation in absence of Chitosan Schiff bases

The crystal shape of $CaCO_3$ loses its distinctive sharp edges and morphology of the crystals has been visibly modified or altered in presence of Chitosan Schiff bases as shown in Figures 86 & 87. The morphology of crystal in presence of inhibitors was changed to vaterite with non- crystal spherical particles.

Generally, all the scales in presence of inhibitors seem to be soft scale which will be difficult for the scales to contact with surface equipment firmly, and can be easily washed away by water. More specifically, the morphology of ChSSB (Figure 87a) exhibit high irregularity in shape and in magnified view the crystals were embedded on the polymer matrix. The SEM micrograph of $CaCO_3$ in presence of ChVSB, the crystal lattice twists to form some bigger and anomalistic non-crystal spherical particulates, which are loose and can be washed away by flow water easily.

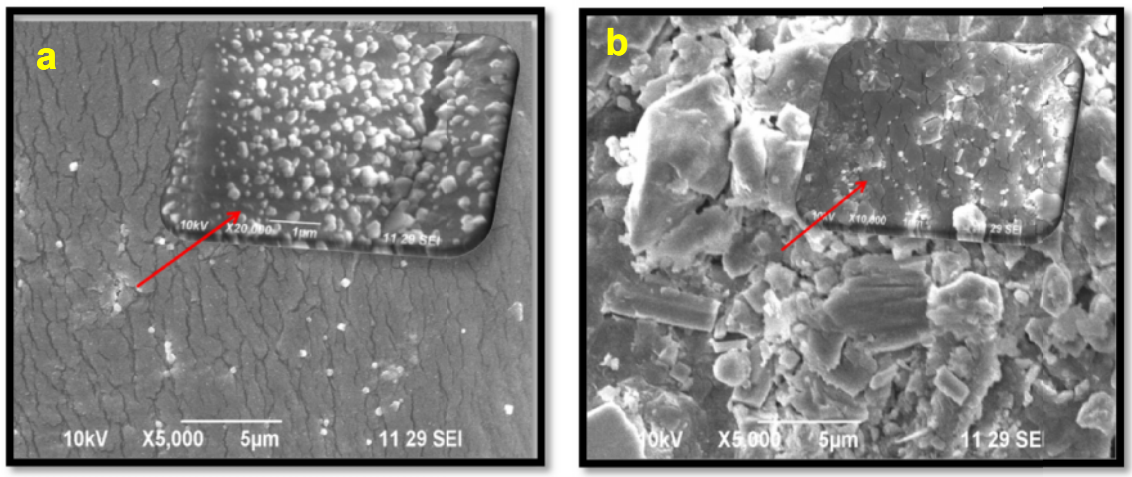

Figure 87 – SEM images of $CaCO_3$ precipitation in presence of a)ChSSB and b)ChVSB

The SEM image of $CaCO_3$ crystal in presence of ChTSB and ChPSB exhibit the distorted crystalline forms due to internal stress that leads to crystal fractures and deposition of microcrystals. Thus the crystal structure was highly affected by the addition of Schiff base polymers and these structures will have the difficulty of adhering to the surface of the equipment.

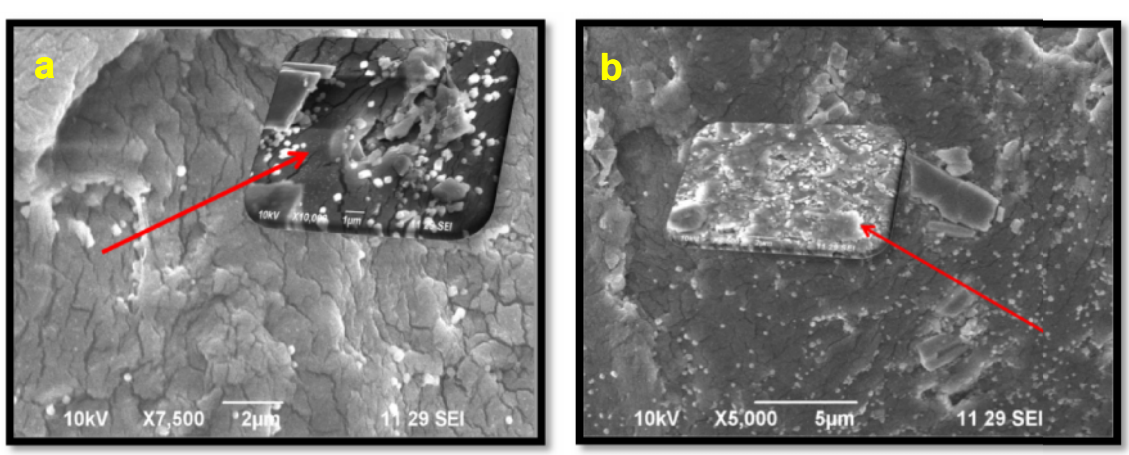

Figure 88 – SEM images of $CaCO_3$ precipitation in presence of a) ChTSB and b)ChPSB

During $CaCO_3$ crystal growth in presence of scale inhibitors, the inhibitor molecules or ions are adsorbed in a different concentration onto the various types of crystal faces, since each type of face has a different surface lattice structure and thus a different distribution of adsorption sites, different degree of growth retardation of each type of crystal results in different morphology (**Yang *et al.*, 2001**). On the basis of SEM analysis, we speculate that the functional groups such as hydroxyl group, imine groups had chelating and dispersing

abilities to the calcium ions which interfered with the regular formation of crystal lattices and appeared to be loose structures.

4.5.4 Thermal analysis of the calcium carbonate scale:

In order to further investigate the thermal changes occurred in the $CaCO_3$ crystals with and without the scale inhibitors was subjected to thermal analysis using TGA. The TGA curves for $CaCO_3$ formation in the solution of absence and presence of Chitosan Schiff base polymers are shown in Figure 89.

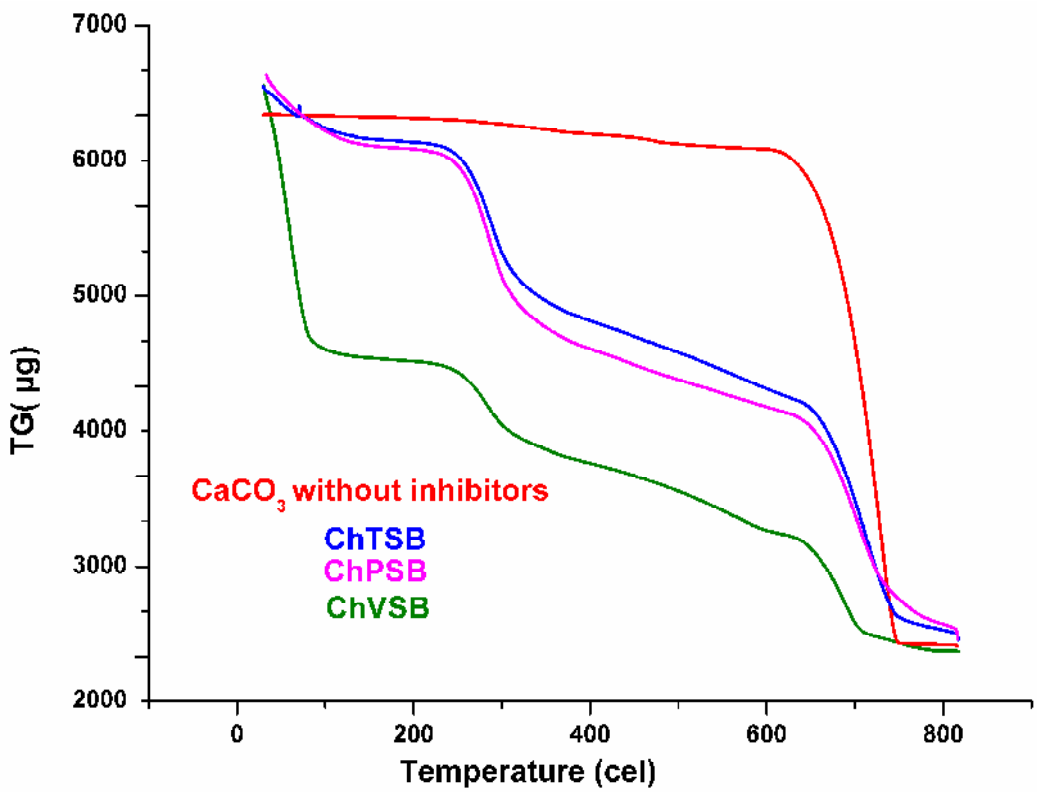

Figure 89 – TGA curves of the $CaCO_3$ crystal formed in the absence and presence of scale inhibitors

The TGA curves of the blank $CaCO_3$ and $CaCO_3$ with scale inhibitor polymers are compared and their weight losses provided new and important findings. The thermal decomposition of $CaCO_3$ occurs at two stages viz. 612 ^oC and 724 ^oC which is consistent with the literature reports (**Liu *et al*., 2016, Xie *et al*., 2006, Filip *et al*., 2013**). But the thermal decomposition of the $CaCO_3$ scale formed in presence of Chitosan Schiff base polymers shows distinctively multiple stages which may be due to the chelation of Schiff base polymers into the $CaCO_3$ crystal lattice. The first two peaks approximately around the region 230 ^oC and 320 ^oC for Schiff base polymers inhibited $CaCO_3$ scale can be assigned to the

decomposition of the Schiff base polymers on the sample surface. While the last two peaks at the regions around 630°C and 710 °C can be assigned to the degradation of $CaCO_3$ particles. $CaCO_3$ crystals were completely decomposed at the temperature of 710 °C which is lower than the classic decomposition temperature of $CaCO_3$. These phenomenal changes may be attributed to the embedding of polymers in the crystal structure, making the crystal lattice distortion.

4.5.5 Probable Mechanism of adsorption and scale inhibition

Calcium carbonate crystallization consists of two stages: nucleation and growth. The inhibition of scale formation was supposed to be offered by the adsorption of inhibitor molecules by interfering with the two processes involved in crystal formation. During the nucleation period, crystal growth takes place on the many small particles (**Tao *et al*., 2005**). This suggests that the inhibition mechanism can be described by inhibitor adsorption on the earlier particles formed during the nucleation stage, hence the active crystal growth sites will be blocked (**Lin and Singer, 2005**). The threshold effect of inhibitors also occurs apparently by interfering with early crystal growth. In the crystal growth stage, the inhibitor molecules retard the scale growth when some inhibiting species are preferentially adsorbed on active sites. Most inhibitor compounds possess large ions and are presumed to require a relatively large crystal surface coverage for effective crystal growth retardation. After adsorption, scale deposit structure can be significantly distorted and weakened. Since the Chitosan Schiff bases are macromolecules they do retard the scale formation in the growth stage.

According to crystal growth theory, crystal growth has the habit effect of growing in same shape in same external conditions. Crystal growth is influenced by the factors of internal structure, in addition external environmental factors such as temperature, supersaturation, impurities also have impact on it. When other factors are same, impurities have significant impact on the relative growth rate of each crystal face of crystal, which results in different crystals different from the original crystal form. In supersaturated solution along with scale inhibitors, inhibitors molecules that have the same effect as impurities are adsorbed to the crystal growth point, and then inhibit or slow the growth of crystals, so that the supersaturated solution is in a stable state temporarily. However the slowly growing surface in the absence of inhibitors absorbed has a certain growth in the period of induction, which can cover the inhibitors molecules adsorbed on the active site, so that the crystal can grow again, but orientation (habit) of crystal growth is destroyed, the crystal state is also distorted and skewed. So before and after adding inhibitors the structure of crystal changes and the lattice is distorted.

From the results of SEM analysis, it is clear that morphology of scale can be changed to different extents by different scale inhibitors and crystal forms in calcium carbonate vary according to scale inhibitors exhibiting different inhibition efficiencies. The more efficient the scale inhibitor is, the more vaterite appears in scale. This trend is in correspondence with the effect of inhibitor on morphology of scale. So it can be concluded that apparently scale morphology is modified in the presence of scale inhibitor, and essentially crystal forms are altered. Based on the change of crystal form, the inhibition effect of inhibitor on scale formation can be proved.

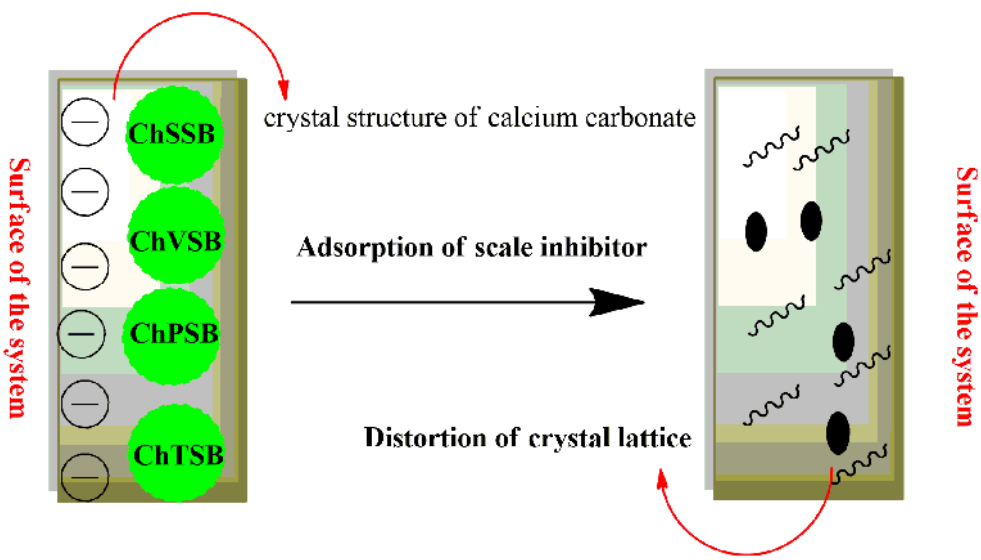

Figure 90 - Schematic representation of adsorption of scale inhibitors